This is to certify that the
dissertation entitled

EFFECT OF CYCLIC AMP IN MODULATING CELL DIFFERENTIATION AND SURVIVAL BEHAVIORS

presented by

LINXIA ZHANG

has been accepted towards fulfillment
of the requirements for the

Doctoral	degree in	Materials Science and Engineering & Biochemistry and Molecular Biology

Major Professor's Signature

8/25/10

Date

MSU is an Affirmative Action/Equal Opportunity Employer

EFFECT OF CYCLIC AMP IN MODULATING CELL DIFFERENTIATION AND SURVIVAL BEHAVIORS

By

LINXIA ZHANG

A DISSERTATION

Submitted to
Michigan State University
in partial fulfillment of the requirements
for the degree of

DOCTOR OF PHILOSOPHY

Materials Science and Engineering &
Biochemistry and Molecular Biology

2010

ABSTRACT

EFFECT OF CYCLIC AMP IN MODULATING CELL DIFFERENTIATION AND SURVIVAL BEHAVIORS

By

LINXIA ZHANG

Mesenchymal stem cells (MSCs), originally identified from bone marrow, have gained popularity due to their multilineage differentiation capability and promising results from preclinical and clinical applications. In addition to their well established differentiation routes to mesodermal lineage cells, such as osteoblasts, adipocytes and chondrocytes, MSCs are also capable of differentiating into neural lineage cells. The ubiquitous messenger cyclic adenosine monophosphate (cAMP) has been used frequently to induce neural lineage differentiation in MSCs. However, a clear understanding of how cAMP induces MSCs into functional neurons is lacking. Ongoing research employing *in vitro* pre-differentiated MSCs to treat neuronal diseases, including the combinatorial therapy of cAMP and MSCs for spinal cord injury repair, necessitate a better understanding of cAMP induced differentiation of MSCs to neural lineages. Accordingly, the goal of the current study is to determine the role of cAMP in MSC differentiation to neural lineages. We assessed if cAMP can enable MSCs to gain neuronal function and investigated a potential mechanism by which cAMP regulates MSC differentiation to neural cells. The results suggested that cAMP initiated neuron-like morphological changes early and induced neural marker expression much later. These two processes are regulated differentially downstream of protein kinase A (PKA). The early-phase neuron-like morphology is the result of cell shrinkage, which gradually decreased with cAMP

treatment, whereas the expression of neural markers increased with exposure time. In addition to neural marker expression, cAMP also enabled MSCs to gain some neuronal function, namely inducing a calcium rise upon stimulation by neuronal activators. Further studies suggested that cAMP response element binding protein (CREB) plays a critical role in mediating the calcium rise upon stimulation by the neuronal activators. While CREB exerts a positive affect on calcium signaling, it appears to negatively impact the adoption of a neuron-like morphology, since a dominant negative CREB promoted the appearance of a neuron-like morphology.

In addition to differentiation, cAMP also participates in various other important cellular processes, such as cell death and survival. In a separate study we found that saturated free fatty acids (FFAs), i.e., palmitate, initiated cell death in hepatocellular carcinoma cells (HepG2) cells. cAMP has been shown to be protective of liver cells from cell death due to various insults. Therefore, we also investigated the role of cAMP in palmitate-induced cell death of HepG2 cells. However, we found that cAMP enhanced palmitate-induced cell death of HepG2 cells. cAMP enhanced palmitate-induced mitochondrial fragmentation and mitochondrial reactive oxygen species (ROS) generation. Mitochondrial fragmentation precedes mitochondrial ROS generation and may contribute to the mitochondrial ROS overproduction. Fragmentation of mitochondria also facilitated the release of cytotoxic proteins from the mitochondria and subsequent activation of caspases. However, the cell death induced by palmitate and cAMP was caspase-independent and predominantly necrotic.

DEDICATED TO MY FAMILY

ACKNOWLEDGEMENTS

Many people have helped me in different ways during my doctoral study at Michigan State University in these years. I owe my deepest gratitude to all these people, although I may not be able to thank each of them individually here.

I am heartily thankful to my advisor, Prof. Christina Chan. I am grateful that she took me as her student and patiently guides me to learn and grow. Without her continuous guidance, support and encouragement, this dissertation would be simply impossible. In addition, she is always enthusiastic about research, accessible, and willing to help, which has helped me to become a better researcher and person, and also has turned into a lifelong fortune for me.

I would like to thank Prof. Pat Walton, for providing valuable suggestions and discussions to my research over all these years. I am also grateful to Prof. Bill Henry, Prof. Sarat Dass and Prof. David Arnosti, to be on my committee and give me insightful suggestions. I feel lucky to have these brilliant people on my committee and learn from them.

My current and former lab members made it a great place to work. It is hard to put down all of their names, because there are so many of them. I was delighted to interact with my lab members. The interactions and discussions in the lab inspired me both in research and life. Their support, and more importantly, their friendship in the past six years, has meant so much to me. Thanks. In particular, I would also like to thank the three undergraduate students who worked with me, Linsey Seitz, Amy Abramczyk, and

Kendell Paweleck. They helped me with the experiments, and helped improve my oral English.

My deepest gratitude goes to my parents and my sister, for always being there for me and giving me constant support and love. I am also deeply grateful to my husband, Yuxin Zhang, for his encouragement, support, love and the joy he brings to me.

Last but not least, I would like to thank the Department of Chemical Engineering and Materials Science, the College of Engineering, and Michigan State University, and the funding sources from Quantitative Biology and Modeling Initiative (QBMI) at MSU, National Science Foundation and National Institutes of Health. They made my doctoral study and research life smooth and rewarding.

TABLE OF CONTENTS

LIST OF TABLES

LIST OF FIGURES

(Images in this dissertation are presented in color)

LIST OF ABBREVIATIONS

AC: adenylyl cyclase

ACSF-HEPES: artificial cerebral spinal fluid with HEPES

ActD: actinomycin D

AKAP: A-kinase anchoring protein

AMPA: α-amino-3-hydroxy-5-methyl-4-isoxazole-propionate

Arp2/3: actin-related protein 2/3

ATF: activating transcription factor

BDNF: brain-derived neurotrophic factor

bFGF: basic fibroblast growth factor

BHA: butylated hydroxyanisole

BME: β-mercaptoethanol

β-NGF: nerve growth factor beta

CaMK: Ca^{2+}/calmodulin dependent kinase

cAMP: cyclic adenosine monophosphate

CCND1: cyclin D1

CDK: cyclin-dependent kinases

CHX: cycloheximide

CKI: CDK inhibitor

CNTF: ciliary neurotrophic factor

CRE: cAMP response element

CREB: cAMP response element binding protein

CRF: corticotropin-releasing factor

Cu-DIPS: Copper (II) 3,5-diisopropylsalicylate

D1, D2, D3, D4 and D5: dopamine receptors 1, 2, 3, 4 and 5

db-cAMP: dibutyryl-cAMP

DCFDA: dichiorofluorescin diacetate

DMSO: dimethylsulfoxide

DMU: N, N'-dimethylurea

DRIP: dopamine receptor interacting proteins

EGF: epidermal growth factor

EPAC: exchange protein directly activated by cAMP

ER: endoplasmic reticulum

ERK: extracellular-regulated kinase

ESC: embryonic stem cell

FFA: free fatty acid

FI: forskolin and IBMX

GFAP: glial fibrillary acidic protein

GLAST: glutamate/aspartate transporter

GLP-1: glucagon-like peptide-1

GLT-1: glutamate transporter-1

GPCR: G-protein coupled receptor

$G_i\alpha$: inhibitory G protein α-subunit

$G_s\alpha$: stimulating G protein α-subunit

GSK3β: glycogen synthase kinase 3β

HepG2: hepatocellular carcinoma cells

hiPSC: human induced pluripotent stem cell

HSC: hematopoietic stem cell

IBMX: isobutylmethylxanthine

iGluR: ionotropic glutamate receptor

IL-6: interleukin-6

KID: kinase inducible domain

KIX: interacting domain

LDH: lactate dehydrogenase

M1-CREB: CREB with serine 133 site mutated to alanine

MAP2: microtubule-associated protein 2

MEK: mitogen-activated protein kinase kinase

mGluR: metabotropic glutamate receptor

MMP: mitochondrial membrane permeabilization

MSC: mesenchymal stem cell

MSK: mitogen and stress activated kinase

NeuroD: neurogenic differentiation

NeuN: neuronal nuclei

NF: neurofilament; including light (L), medium (M) and heavy (H) chain

NMDA: N-methyl-d-aspartate

NO: nitric oxide

NSC: neural stem cell

NSE: neuron-specific enolase

OB: olfactory bulb

Op18: oncoprotein 18

PDE: phosphodiesterase

PDGF: platelet-derived growth factor

PGE2: prostaglandin E2

PI: propidium iodide

PI3K: phosphatidylinositol 3-kinase

PKA: protein kinase A

PLC: phospholipase C

PMP-22: peripheral myelin protein-22

Ptx: Paclitaxel

RA: retinoic acid

Rb: retinoblastoma protein

ROS: reactive oxygen species

RSK2: ribosomal S6 kinase 2

RT-PCR: reverse transcription-polymerase chain reaction

SHP2:(SH)2-containing phosphotyrosine phosphatase

Smac: second mitochondria-derived activator of caspase

SVZ: subventricular zone

TNF-α: tumor necrosis α

TrkA: neurotrophic tyrosine kinase receptor type 1

Tuj1: β-III tubulin

Shh: sonic hedgehog

VA: valproic acid

CHAPTER 1. INTRODUCTION

Signaling initiated by external stimuli can greatly influence intracellular events and impinge on cell fate choices. The ubiquitous messenger cyclic adenosine monophosphate (cAMP) has been extensively studied due to its diverse roles in various important cellular processes. Ongoing research continues to reveal more aspects of cAMP that have not been appreciated before. For example, a recent study suggested that cAMP is a crucial component for maintaining human induced pluripotent stem cells (hiPSCs) in a previously undefined pluripotent state [1]. In contrast to this relatively new role in maintaining pluripotency in hiPSCs, cAMP has long been indicated to exert a role on differentiation, especially in neural lineage differentiation [2, 3]. While research using cAMP as a component for neural differentiation has been on-going for over three decades, its application of neural induction of mesenchymal stem cell (MSC) differentiation is less than a decade old [4]. The underlying mechanism leading to neural differentiation by cAMP in MSCs remains elusive. Given the emerging use of MSCs as a source for treating neuronal diseases, such as Parkinson's disease and spinal cord injury [5, 6], a better understanding of the cellular behavior to external stimuli, such as agents that induce cAMP production is necessary. Despite its frequent use, the effect cAMP may exert on MSCs with respect to different functions, i.e., proliferation, apoptosis and functional differentiation, has not been extensively examined or investigated. Therefore, a major focus of this thesis is to study the effect and the underlying mechanism of cAMP-induced neural differentiation in MSCs. In addition, cAMP culminated in apoptosis during its induction of neural lineage differentiation in MSCs. A similar pro-apoptotic effect of cAMP was observed in hepatocellular carcinoma cells (HepG2) treated with

palmitate. Given that cAMP is primarily protective in hepatocytes and islet cells according to the literature [7-14], we sought to determine the potential mechanism by which cAMP could be potentiating palmitate-induced cell death in HepG2 cells.

1.1 Components of the cAMP signaling pathways

The universal second messenger cAMP is recognized as an important player in mediating a plethora of cellular processes including metabolism, differentiation, apoptosis and immune responses [15-17]. Generation of cAMP is mainly achieved through adenylyl cyclases, which convert ATP into cAMP [16] (Figure 1.1). At least nine adenylyl cyclases exist, and they are mainly regulated by G-protein coupled receptors (GPCRs) [18, 19]. While all the adenylyl cyclases (ACs) are activated by the stimulating G protein α-subunit ($G_s\alpha$), many of them are negatively regulated by the inhibitory G protein α-subunit ($G_i\alpha$) [19]. Apart from regulation by GPCRs, calcium can also regulate the AC isoforms, either positively or negatively [20, 21]. In addition to being regulated by ACs, intracellular cAMP levels can also be controlled by phosphodiesterases (PDEs), which terminate cAMP signaling by hydrolysis of the 3' cyclic phosphate bond [22] (Figure 1.1).

The most common downstream effector of cAMP is protein kinase A (PKA), a tetrameric holoenzyme consisting of two catalytic (C) subunits and two regulatory (R) subunits [23]. Two types of PKA holoenzymes exit: the type I holoenzyme, which contains the RI (RIα, RIβ) subunits and the type II holoenzyme, which contains the RII (RIIα, RIIβ) subunits. The R subunit dimers associate with and inhibit the activation of the C subunits (Cα, Cβ, Cγ) [24]. Binding of cAMP to the R subunits releases the R

subunits from the C subunits and thereby enables the activation of the C subunits [16] (Figure 1.1). Regulation of PKA activity is also highly coordinated by the A-kinase anchoring proteins (AKAPs), which target PKA to distinct subcellular locations [25]. AKAPs serve as scaffolding proteins for the formation of multiple protein complexes including kinases, phosphatases and PDEs [26]. Such compartmentalization facilitates the generation of spatiotemporal PKA signaling as well as integration of multivalent signaling events [25, 26].

One of the most important PKA targets is the transcription factor cAMP response element binding protein (CREB) [16, 27] (Figure 1.1). CREB is one of the CREB/activating transcription factor (CREB/ATF) family transcription factors that binds to the concensus palindromic CRE sequence TGACGTCA and the half CRE sequence CGTCA/TGACG [28]. Activation of CREB is mediated by phosphorylation at the serine 133 site in its kinase inducible domain (KID) by various kinases, such as PKA, Ca^{2+}/calmodulin dependent kinase (CaMK), ribosomal S6 kinase 2 (RSK2) and mitogen and stress activated kinase (MSK) [29, 30]. Phosphorylation of CREB at serine 133 helps the interaction of the KID domain with the KID interacting domain (KIX) on the transcription coactivators CBP/p300, which in turn facilitates the recruitment of the basal transcription machinery [31-33]. Transcriptional activation of CREB culminates in expression of genes involved in various events including differentiation, proliferation and survival [34, 35].

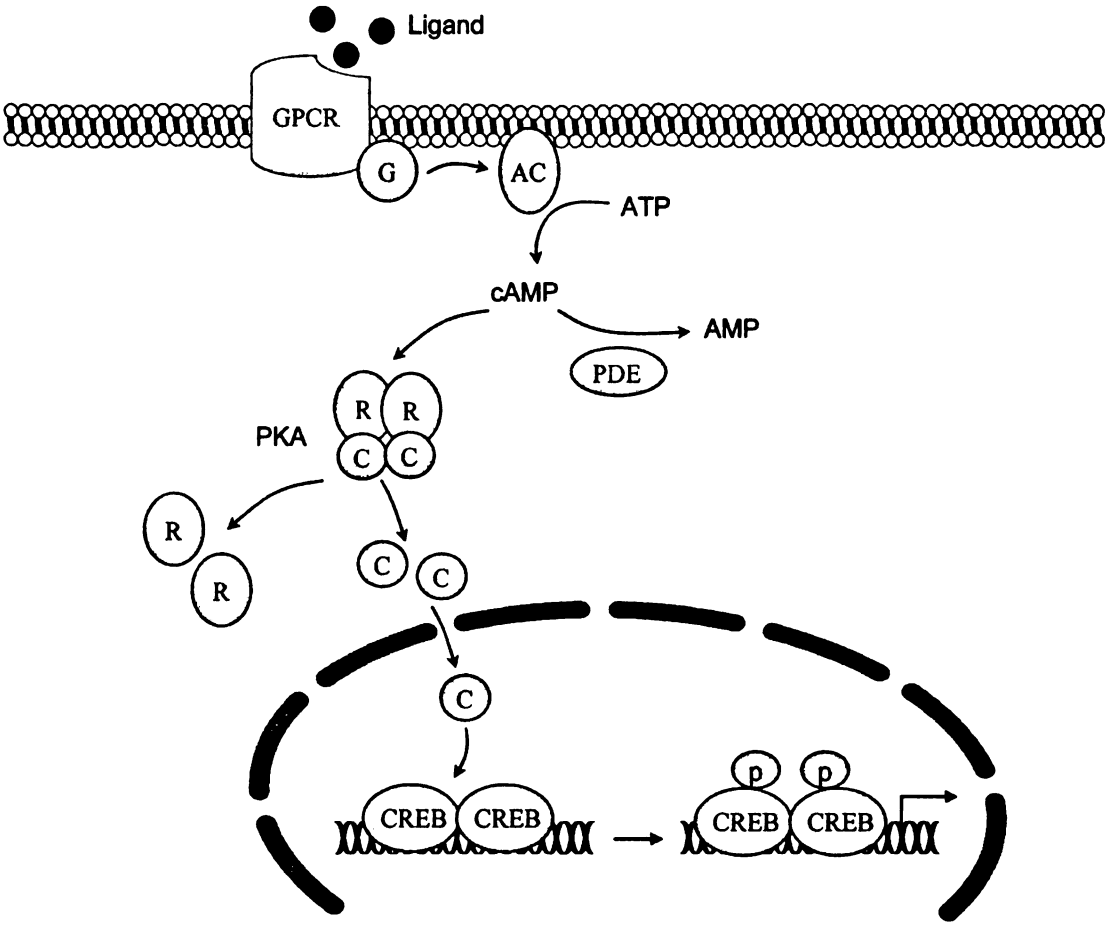

Figure 1.1 Components of the classical cAMP signaling pathway.

1.2 cAMP in cell death and survival

The ability of cAMP to influence cell death and survival has been implicated in various cell systems. Whether cAMP protects cells from cell death or promotes cell death differs in different systems and the mechanism remains elusive. cAMP has been indicated to be protective in the survival of various types of neurons, such as sympathetic and sensory neurons [36], spinal motor neurons [37] and cerebellar granule neurons [38]. Further studies indicate that cAMP-mediated survival in neurons may be related to the phosphorylation of glycogen synthase kinase 3β (GSK3β), whose proapoptotic ability is

reduced upon phosphorylation [39]. Several studies indicated that cAMP delays apoptosis in neutrophils [40-42], which nevertheless have a short life span and will eventually die by apoptosis [43]. Introducing cAMP to pancreatic cancer cells [44] or pancreatic β-cells [14] also protected these cells from apoptosis. In hepatocytes, elevation of cAMP protected them from bile acid-induced apoptosis [7-10], which may involve both PKA-dependent and independent mechanisms [9]. cAMP also suppressed tumor necrosis factor α (TNF-α) [11, 12] and Fas-induced apoptosis in hepatocytes [13]. Physiological stimuli that trigger cAMP production, such as prostaglandin E2 (PGE2) and glucagon, are also reported to promote cell survival in many systems [45-47]. Moreover, the protective role of cAMP was observed in hematopoietic stem cells (HSCs) [48], HSCs-derived megakaryocytes [49], epithelial cells [50], endothelial cells [51], vascular smooth muscle cells [52], thyroid follicular cells [53] and leukemia cells [54, 55].

While the majority of the studies suggest a positive role of cAMP on cell survival, a negative impact of cAMP on cell survival has also been reported. Raising cAMP levels was shown to promote apoptosis [56] and potentiate glucocorticoid induced apoptosis in thymocytes [57], enhance Fas-mediated apoptosis in T lymphocytes [58], trigger apoptosis in B-cells [59] and enhance glucocorticoid stimulated apoptosis in lymphoblastic leukemia cells [60, 61]. Although a protective effect of cAMP has been observed in many different cell types, a deleterious effect of cAMP has been reported predominantly in immune response related cells, to which MSCs are closely related.

1.3 cAMP in proliferation and differentiation

While cAMP stimulates proliferation in some cells, it is generally considered to be growth inhibitory in most cells, especially in cells of mesenchymal origin [62]. A large body of evidence indicates that cAMP induced growth inhibition can be mediated through regulation of cell cycle regulators [63-69]. Cell cycle regulators, such as cyclins, cyclin-dependent kinases (CDKs), CDK inhibitors (CKIs) and retinoblastoma protein (Rb), act in a concerted manner to control cell progression. CDK activity is positively regulated by cyclins and negatively regulated by CKIs [70]. Activation of CDK4/6 phosphorylates Rb and thereby relieves the inhibitory effect of Rb on the E2F transcription factors, promoting S phase entry [71]. The proliferation inhibitory effect of cAMP has been demonstrated to be related to the down-regulation of cyclin D1 [66, 68], upregulation of CKIs such as $p27^{kip1}$ and $p21^{cip1}$ [63, 67], and dephosphorylation of Rb [64, 67]. It is believed that the proliferation inhibitory effect of cAMP is related also to the down-regulation of the Ras/Raf-1/MEK1/2/ERK signaling cascade [72-76], which can be directly or indirectly mediated by PKA [75, 77-79].

cAMP not only affects proliferation, it also influences differentiation, especially of neural lineage cells such as neurons and glias. Early studies that showed cAMP can induce neuronal differentiation were performed in murine neuroblastoma cell lines and normal neuronal cells [80]. One of the most well characterized models for studying neuronal differentiation is the rat pheochromocytoma PC12 cells [81]. cAMP is reported to induce neuronal differentiation of PC12 cells through PKA-dependent [82] and – independent [83] mechanisms. Regulation of cAMP induced neuronal differentiation of PC12 cells has also been suggested to be mediated by PI3K [82], p38 [84] and ERK [83]. Elevated intracellular cAMP levels also promote morphological differentiation in human

neuroblastoma cells [85, 86], human neuronal progenitor cells [87] and neural stem cells [88]. Moreover, the cAMP signaling pathway has been demonstrated to be critical in estrogen-induced differentiation of midbrain dopaminergic neurons [89] and corticotropin-releasing factor (CRF)-induced differentiation of catecholaminergic immortalized neurons [90].

cAMP not only mediates differentiation of neurons, it also regulates differentiation of glia cells, i.e., oligodendrocytes, Schwann cells, astrocytes and microglias, which are important components of the nervous system [91]. Elevation of cAMP led to astrocytic differentiation of cortical precursor cells [92, 93] and rat glioma cells [94, 95], mediated perhaps by interleukin-6 (IL-6) [96]. The glial lineage differentiation induced by cAMP is not limited to astrocytes; reports have suggested that cAMP can also induce differentiation of progenitor cells into oligodendrocytes [97, 98] and schwann cells [99]. Taken together, these results show that cAMP is a critical component for inducing neuronal or glial tumor cell lines as well as differentiating neural progenitor cells into neurons or glias.

1.4 Mesenchymal stem cells and neural lineage differentiation

Mesenchymal stem cells (MSCs) were first identified by Friendenstein and co-workers in the 1960s. When cultured in plastic culture dishes, these adherent fibroblast-like cells formed colonies that can differentiate into osteoblasts or chondrocytes [100, 101]. This worked was later extended by other researchers in the 1980s [102, 103]. Since then, MSCs has been actively investigated and can reportedly be obtained from various

sources, including bone marrow, umbilical cord, adipose tissue, skeletal muscle, synovium and postnatal organs and tissues [104-106].

Characterization of MSCs is usually based on expression of surface markers, such as Stro1, CD29 (also known as β1-integrins), CD44, CD71, CD73 (also known as SH3/4), CD90 (also known as Thy1), CD105 (also known as SH2), CD106 (also known as vascular cell adhesion molecule-1 [VCAM-1]) and CD271 (also known as low-affinity nerve growth factor receptor) [107-110]. While MSCs express the aforementioned markers, they do not express HSC-specific markers, such as CD34 and CD45 [108].

As adult stem cells, MSCs have the multipotency to differentiate into various different cell lineages [111], including osteoblasts [112-114], adipocytes [113] and chondrocytes [115, 116] (Figure 1.2). Besides these cell types, MSCs are also capable of differentiating into hepatocytes [117], myocytes [118] and neural cells [4, 119, 120].

In addition to their multipotent differentiation ability, MSCs can secret a plethora of growth factors that favor tissue repair and regeneration [121]. Moreover, MSCs have immunosuppressive features and, when used allogenically, show minimal immune rejection [122, 123]. As such, a number of studies have reported the promising use of MSCs in treating bone defects [124, 125], coronary artery disease [126], osteogensis imperfecta [122, 127], hematpoietic recovery [128], myocardial infarction [129] and graft-versus-host disease [130].

Besides the potential therapeutic applications mentioned above, the ability of MSCs to give rise to neural lineage cells also makes them a promising source for treating neuronal diseases such as Parkinson's disease [5]. Both *in vitro* and *in vivo* studies showed that MSCs can differentiate into neural lineage cells, including neurons [131-

139], astrocytes [131, 136, 138, 140] and oligodendrocytes [141]. The motivation to induce MSCs to differentiate into neural lineage cells *in vitro* before transplantation is desirable for two reasons: 1) pre-differentiation may enhance the functional integration of differentiation cells into the lesion site and may also enhance efficacy, and 2) pre-differentiation restricts the differentiation potential of MSCs and therefore reduces the possibility of tumor formation [142]. Various protocols have been applied to induce MSCs to differentiate into neural lineage cells *in vitro*. A list of these studies is summarized in Table 1.1. In particular, some studies suggest that *in vitro* pre-differentiated MSCs can survive and migrate to the lesion sites in animal models of Parkinson's disease [143]. Moreover, others have suggested that transplantation of *in vitro* pre-differentiated MSCs improves behavioral recovery in a rat model of Parkinson's disease [144] and facilitates nerve regeneration in rat models of spinal cord injury [145, 146]. Therefore, MSCs appears to be a promising source for treating neuronal diseases and a better understaning of their ability to differentiate into neural lineage cells will help further their application in cell-based therapies.

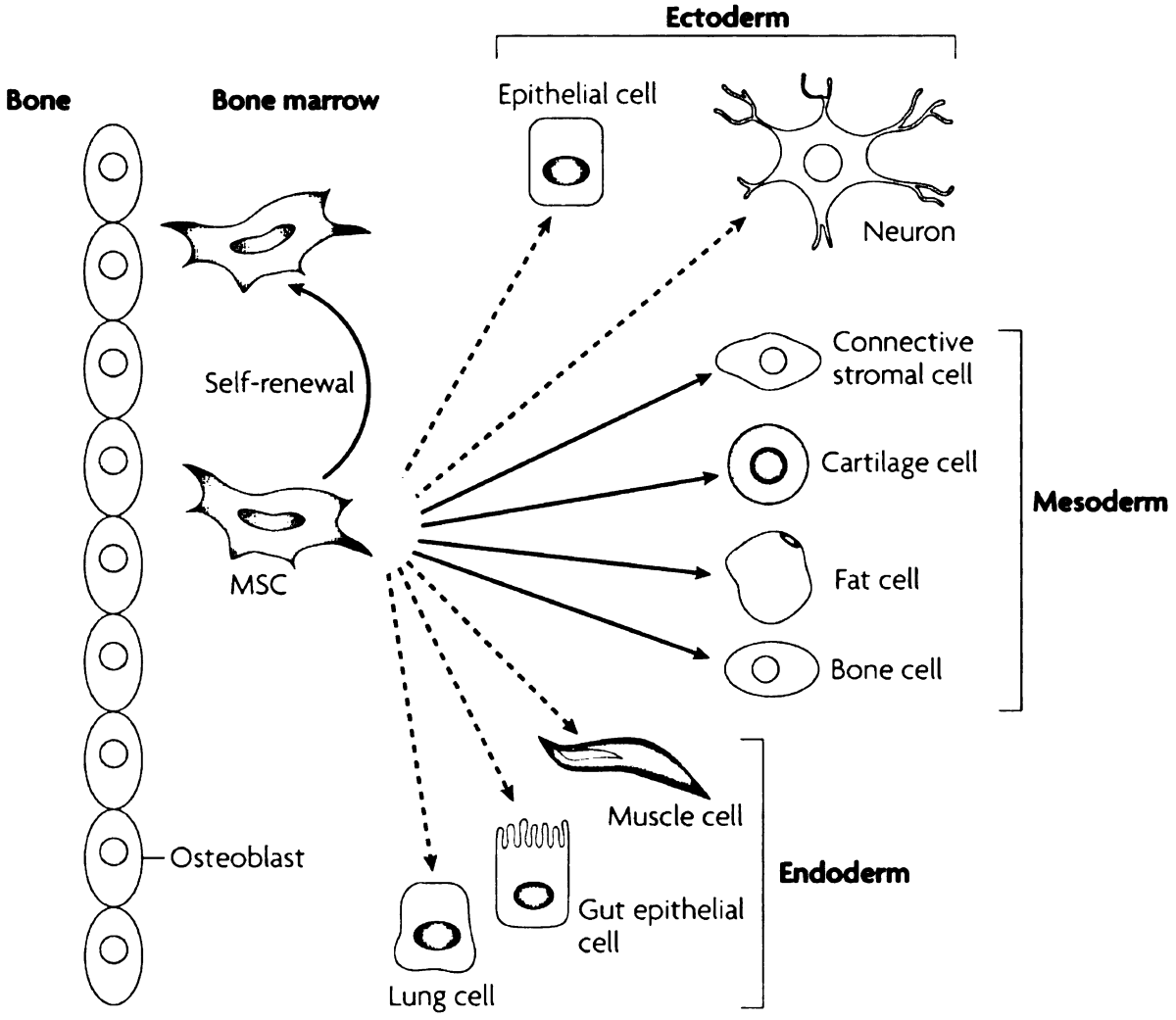

Figure 1.2 Self-renewal and multilineage differentiation ability of MSCs. MSCs primarily differentiate into mesodermal lineages such as fat cells and bone cells. Transdifferentiation of MSCs into ectodermal and endodermal lineage cells are also reported (dashed lines). (Uccelli, A. et.al., Nat Rev Immunol (2008) 8, 726-736. [111]).

Table 1.1 *In vitro* studies regarding neural lineage differentiation in MSCs. Please refer to 'Abbreviations' for the acronyms.

Reference	Source cell	Treatment	Phenotype verification	Functional assay
Woodbury 2000 [139]	rMSCs and hMSCs	β-mercaptoethanol (BME) + dimethylsulfoxide (DMSO) + butylated hydroxyanisole (BHA) + valproic acid (VA) + forskolin + KCl	Neuron-like morphology; expression of NSE, NF-M, tau and NeuN by immunostaining.	N/A
Sanchez-Ramos 2000 [138]	mMSCs and hMSCs	retinoic acid (RA) + brain-derived neurotrophic factor (BDNF)	Neuron-like morphology; expression of nestin, NeuN and GFAP by immunostaining; expression of nestin by RT-PCR.	N/A
Deng 2001 [4]	hMSCs	3-isobutyl-1-methylxanthine (IBMX) + dibutyryl-cAMP (db-cAMP)	Neuron-like morphology; expression of vimentin and NSE by western blotting.	N/A
Jin 2003 [147]	mMSCs	basic fibroblast growth factor (bFGF) + epidermal growth factor (EGF) + RA + nerve growth factor beta (β-NGF)	Neuron-like morphology; expression of neural markers such as NeuN, MAP2 and Tuj1 by immunostaining and western blotting.	N/A
Wisket-Gendebien 2003 [119]	rMSCs	Nestin-positive neurospheres formed by rMSCs were cocultured with mouse neural stem cells (mNSCs).	Expression of astroglial markers GFAP and GLAST by immunostaining.	N/A
Levy 2003 [148]	mMSCs	BHA + db-cAMP + IBMX + RA	Neuron-like morphology;	N/A

Table 1.1 (cont'd)

			expression of NeuN by western blotting and immunostaining.	
Munoz-Elias 2003 [149]	rMSCs	Used induction media as in [139]	Neuron-like morphology; expression of tau, NSE and NeuN by immunostaining.	N/A
Rismanchi 2003 [150]	rMSCs	Used induction media as in [139] and [4]	Neuron-like morphology; expression of NeuN and GFAP by immunostaining.	N/A
Dezawa 2004 [144]	rMSCs and hMSCs expressing Notch intracellular domain (NICD)	Forskolin + bFGF + ciliary neurotrophic factor (CNTF)	Neuron-like morphology; expression of MAP2ab, NF-M and Tuj1 by immunostaining; expression of MAP2ab by western blotting.	Voltage-clamp for K^+ currents.
Hermann 2004 [151]	hMSCs cultured in neurosphere-like structures	RA + BDNF for neuronal induction; RA + platelet-derived growth factor (PDGF) for glial induction	Neuron-like morphology; Expression of neuronal or glial markers such as Tuj1 and GFAP by RT-PCR and immunostaining.	Whole-cell patch- clamp showed K^+ currents after glial induction.
de Hemptinne 2004 [152]	rMSCs	bFGF + CNTF with or without RA	Expression of glial markers such as GLT-1 and GLAST by RT-PCR and immunostaining; glutamate transporters-mediated aspartate uptake.	N/A
Jori 2005 [153]	rMSCs	Forskolin + BHA + DMSO	Neuron-like morphology;	N/A

Table 1.1 (cont'd)

			expression of trkA, NSE and Id2 by RT-PCR; expression of NF by immunostaining.	
Yaghoobi 2005 [154]	rMSCs	Used protocol as described in [139]	Neuron-like morphology; expression of markers such as NeuroD by RT-PCR and immunostaining.	N/A
Kondo 2005 [155]	mMSCs	bFGF + forskolin + IBMX + BDNF + sonic hedgehog (Shh) + RA	Neuron-like morphology; expression of pan neural markers such as NSE and tau; expression of sensory neuron markers such as P2X3 by RT-PCR and immunostaining.	N/A
Chu 2006 [156]	KP-hMSCs (immortalized hMSCs)	IBMX	Neuron-like morphology ; expression of markers such as NeuN and Gal-C by western blotting and immunostaining.	N/A
Krampera 2006 [157]	hMSCs	BHA + forskolin + KCl + valproic acid (VA)	Neuron-like morphology; expression of neural markers such as PMP-22, GFAP and NeuN by immunostaining.	N/A
Trople 2006 [158]	mMSCs	bFGF	Neuron-like morphology; expression of NF-L and Tuj1 by immunostaining and RT-PCR.	Ca^{2+} signalling

1.5 Specific aims of the current study

The use of MSCs in therapeutic applications for treating neuronal diseases necessitates a better understanding and identification of intracellular events involved in regulating the induction of MSCs into neural lineage cells. While cAMP is frequently used for *in vitro* induction of MSCs towards the neural lineage cells, little is known regarding whether cAMP can turn MSCs into functional neurons or how cAMP elicits neural differentiation. Therefore, two of the specific aims are:

1. Investigate the effects of cAMP on MSC neural differentiation and determine whether cAMP can turn MSCs into functional neurons.

   Previous studies suggested that cAMP is one of the best inducers for differentiating MSCs into neural lineages [153]. However, such evidence mostly relied on the appearance of neuron-like morphology, which may be an artifact rather than true differentiation as suggested with BHA/DMSO induced neural lineage differentiation of MSCs [159]. We observed that cAMP initiated neuron-like morphology changes quickly, which decreased with treatment time, while expression of neural lineage markers increased more gradually, which led to our first hypothesis that these two events may be differentially regulated. Therefore, the first part of this specific aim characterizes the effect of cAMP on the neuron-like morphology and neural marker expression. The second part of the aim determines if cAMP is able to induce MSCs to achieve some neuronal function along with neural marker expression. This is discussed in Chapter 2.

2. Identify the intracellular signaling components that play a major role in cAMP- initiated neural differentiation of MSCs.

The results of specific aim 1 suggested that cAMP enabled MSCs to obtain some neuronal function in terms of calcium signaling in response to neuronal activators, dopamine, glutamate and KCl. Preliminary results indicated that the cAMP activated transcription factor CREB may be a critical regulator of this process. Therefore, we hypothesized that CREB is involved in regulating calcium signaling during cAMP-induced neural differentiation of MSCs. In this specific aim, overexpression and down-regulation of CREB was performed to determine its role in calcium signaling upon stimulation by the neuronal activators. This is discussed in Chapter 3.

The effect of cAMP is not limited to differentiation but also has been shown to protect many cell types from apoptosis [7-13, 36-55]. We observed that the cAMP level was down-regulated in palmitate-treated HepG2 cells, and palmitate-induced cell death. Given that the results gathered from the literature suggested cAMP is anti-apoptotic in HepG2 cells [7-13], we set out to determine if cAMP can protect HepG2 cells from palmitate-induced apoptosis and, if so, the potential mechanisms involved. Specific aim 3 is:

3. Characterize the effect of cAMP on palmitate-induced cell death in HepG2 cells.

Saturated free fatty acid (FFA) palmitate is lipotoxic and induces cell death in a variety of cell types [160-162]. cAMP is primarily protective in hepatocytes according to the literature, since it reduces bile acid [7-10], TNF-α [11, 12] and Fas induced apoptosis [13]. We observed that palmitate but not the unsaturated FFAs oleate or linoleate, down-regulated intracellular cAMP levels [163]. Thus we hypothesize that cAMP may attenuate palmitate-induced cell death in HepG2 cells. However, the effect of cAMP on death and survival may differ depending on what other stimuli are occurring. For example, while cAMP reduced surface antibody-induced apoptosis in thymocytes [47], it potentiated glucocorticoid-induced apoptosis in thymocytes [57]. Therefore, it is likely that even though cAMP protectes hepatocytes from bile acid [7-10], TNF-α [11, 12] and Fas-induced apoptosis [13], it may not necessarily ameliorate the toxicity exerted by palmitate. As such, we aim to characterize the effect of cAMP on HepG2 cell survival during palmitate treatment and identify the potential mechanisms involved. This is discussed in chapter 4.

CHAPTER 2. cAMP INITIATES EARLY PHASE NEURON-LIKE MORPHOLOGICAL CHANGES AND LATE PHASE NEURAL DIFFERENTIATION IN MESENCHYMAL STEM CELLS

This work is in press of Cellular and Molecular Life Science:
Zhang, L., Seitz, L.C., Abramczyk, A.M. and Chan, C. cAMP initiates early phase neuron-like morphology changes and late phase neural differentiation in mesenchymal stem cells. Cell Mol Life Sci (2010) [Epub ahead of print].

2.1 Abstract

The intracellular second messenger cAMP is frequently used in induction media to induce mesenchymal stem cells (MSCs) into neural lineage cells. To date, an understanding of the role cAMP exerts on MSCs and whether cAMP can induce MSCs into functional neurons is still lacking. We found cAMP initiated neuron-like morphological changes early and neural differentiation much later. The early-phase changes in morphology were due to cell shrinkage, which subsequently rendered some cells apoptotic. While the morphological changes occurred prior to the expression of neural markers, it is not required for neural marker expression; and the two processes are differentially regulated downstream of cAMP activated protein kinase A. cAMP enabled MSCs to gain neural marker expressions with neuronal function, such as, calcium rise in response to neuronal activators, dopamine, glutamate and potassium chloride. However, only some of the cells induced by cAMP responded to the three neuronal activators and these cells further lack the neuronal morphology, suggesting that although cAMP is able to direct MSCs towards neural differentiation, they do not achieve terminal differentiation.

2.2 Introduction

Mesenchymal stem cells (MSCs) are adult stem cells with multipotency to differentiate into mesodermal lineage cells such as osteoblasts [114], adipocytes [113] and chondrocytes [115]. Studies also suggested that these cells have the potential to transdifferentiate into other lineages, such as hepatocytes [117], cardiomyocytes [164], neurons [165] and astrocytes [131]. Several recent studies indicated that the shape of the cell [166] guided by surface cues [167], and matrix elasticity [168] can influence the lineage commitment of stem cells. Thus, these studies suggest that the surface is as important, if not more so, in directing cell lineage and guiding function to follow form. In contrast, we found that cyclic adenosine monophosphate (cAMP) induced the function but not the form.

cAMP is a soluble, biochemical cue that is frequently used either alone [4] or in combination with other factors [144, 153, 169] to induce neural differentiation of MSCs. cAMP initiated transient neuron-like morphological changes that lasted only a few hours. These morphological changes were the result of cell shrinkage and did not contribute to the later-phase neural differentiation. Similarly, studies using β-mercaptoethanol (BME), dimethylsulfoxide (DMSO) and butylated hydroxyanisol (BHA) to induce neural differentiation of MSCs have attributed the neuron-like morphology to an artifact of cell shrinkage rather than neurite outgrowth [159]. However, unlike BME, which induced changes in morphology for up to 24 hours [159], cAMP initiated a transient change in morphology for up to 3 hrs that decreased over time.

The classical cAMP signaling pathway involves activation of PKA, which is composed of two catalytic subunits, PKAc, and two regulatory subunits, PKAr [16]. Binding of cAMP to the regulatory subunits dissociates PKAr from PKAc, thereby enabling the activation of PKAc [34]. Signaling events initiated by PKAc plays important roles in regulating cell death and survival [170, 171], cell movement and structure [172] as well as differentiation [173, 174]. We investigated whether PKA is involved in regulating both the morphological changes and neural differentiation and function and whether neural differentiation is contingent upon the changes in morphology.

Although cAMP has been shown to induce neural marker expression [4, 153], we show cAMP also induced a calcium rise, an indicator of neural function, that persisted for at least one week. We found MSCs showed differential responses to neural activators (i.e., dopamine) despite the lack of neuron-like morphology, thus cAMP is able to facilitate neural differentiation but by itself is not sufficient to induce MSCs to terminally differentiated neurons.

2.3 Materials and methods

2.3.1 Materials

Forskolin (Sigma) and isobutylmethylxanthine (IBMX) (Sigma) were used to increase intracellular cAMP levels at concentrations of 10 μM and 100 μM, respectively. H89 (Sigma) and Rp-cAMPS (Sigma) were used as PKA inhibitors at concentration of 2.5 μM and 10 μM. Actinomycin D (ActD) (Sigma) was used to

inhibit transcription at concentration of 1 μg/ml. Cycloheximide (CHX) (Sigma) was used to inhibit translation at concentration of 10 μg/ml. Paclitaxel (Ptx) (Sigma) was used to stabilize microtubules at concentration of 0.4 μM. The three neuronal activators used during calcium imaging were: 100 μM dopamine (Sigma), 100 μM glutamate (Sigma) and 50 mM KCl (J.T.Baker).

2.3.2 Cell isolation and culture

All procedures in the cell isolation were approved by the Institutional Animal Care and Use Committee at Michigan State University. Bone marrow mesenchymal stem cells were isolated from 6-8 week old Sprague-Dawley female rats as described in Appendix 1. In brief, femurs and tibias from 6-8 week old rat were dissected and the two ends were cut open. The marrow was flushed out with DMEM using a needle and syringe. The cell suspension was filtered through a 65μm nylon mesh to remove bone debris and blood aggregates. Cells were cultured in DMEM (Invitrogen) supplemented with 10% fetal bovine serum (Invitrogen), 100 μg/mL streptomycin (Invitrogen) and 100 U/mL penicillin (Invitrogen) and placed in an incubator with a humidified atmosphere containing 5% CO_2 at 37 ^{o}C. Non-adherent cells were removed on the second day after plating. Media was replaced every 3 to 4 days until the cells reach 80~90% confluence. Confluent cells were detached by 0.25% trypsin-EDTA (Invitrogen) and plated for further experiments.

Primary cortical neurons were isolated as described in [175]. In brief, animal heads were decapitated from 1-day old Sprague-Dawley rat pups. Cortical neurons

were obtained from the brain and cultured on poly-L-lysine coated plates in cortical media [DMEM (Invitrogen) supplemented with 10% horse serum (Sigma), 2 mM glutamine (Invitrogen), 100 μg/mL streptomycin (Invitrogen) and 100 U/mL penicillin (Invitrogen)] in an incubator with a humidified atmosphere containing 5% CO_2 at 37 °C. Cells were used within 3 days after isolation.

2.3.3 Live cell imaging

Cells were cultured in 4-well Chambered glass bottom plate (Thermo Fisher Scientific). Before taking images, media was changed to 0.5 ml Leibovitz (Liz) media (Sigma). The plate was mounted in a temperature controlled chamber set at 37 °C on the microscope station. 0.5 ml Liz media containing 20 μM forskolin and 200 μM IBMX was added to the chambered well to achieve a final concentration of 10 μM forskolin and 100 μM IBMX. Phase contrast images were captured by confocal microscope Olympus FluoView 1000 at intervals of 5 minutes.

2.3.4 cAMP assay

Intracellular cAMP levels were measured by a competitive immunoassay from Assay Designs (Assay Designs) according to the manufacturer's instructions. In brief, cells were lysed with 0.1M HCl and the supernatant collected. The cAMP in the samples or standards was allowed to bind to a polyclonal cAMP antibody in a competitive manner with alkaline phosphatase-conjugated cAMP. Cleavage of a substrate by the alkaline phosphatase is inversely proportional to the cAMP level in

the samples or standards. Colorimetric readings were taken by SPECTRAmax plus384 from Molecular Device at 405 nm. All the readings were normalized to protein levels (μg/ml) by Bradford assay.

2.3.5 Caspase 3 activity assay

Caspase 3 activity was measured by a kit from BIOMOL (BIOMOL) according to the manufacture's instructions. Briefly, cell extracts were incubated with substrate Ac-DEVD-AMC. The cleavage of the substrate generates fluorescence which is proportional to the concentration of active caspase 3 in the cell extracts. Fluorescence was measured by Spectra MAX GEMINI EM plate reader at excitation of 360 nm and emission of 460 nm. All the readings were normalized to protein levels (μg/ml) by Bradford assay.

2.3.6 Western blot

Whole cell extracts lysed with CelLytic (Sigma) were assayed for protein concentrations by Bradford assay (Bio-Rad). 15-30μg protein samples were separated by 10% Tris-HCl gel and transferred to nitrocellulose membrane. Membranes were then blocked in 5% milk and 0.05% Tween 20-TBS (tris buffered saline) (USB corporation) for one hour and incubated with primary antibodies, NSE (neuron-specific enolase) (BIOMOL), Tuj1 (βIII-tubulin) (Millipore), GFAP (Glial fibrillary acidic protein) (DAKO), GAPDH (Cell signaling), PKAc (R&D Systems), pPKAc (Cell Signaling) and ser133 phosphorylated CREB (pCREB) (EMD Chemicals)

overnight at 4 °C. Anti-mouse or anti-rabbit HRP-conjugated secondary antibody (Thermo Scientific) were added the second day after primary antibody incubation. The blots were incubated for one hour and then washed three times with 0.05% Tween 20-TBS. The blots were then visualized by SuperSignal west femto maximum sensitivity substrate (Thermo Scientific).

2.3.7 Immunocytochemistry

For staining against Tuj1, cells were fixed in PBS containing 3.7% formaldehyde for 15 minutes and permeabilized with 0.5% Triton X-100 (Research Products Internationals) for 20 minutes at room temperature. After washing with PBS three times, cells were blocked in 1% BSA (bovine serum albumine) (US Biological) for 20 min and incubated with Tuj1 (Millipore) antibody at room temperature for one hour. Cells were then washed with PBS three times and incubated with Alexa Fluor 488-conjugated anti-mouse IgG secondary antibody (Invitrogen) for one hour at room temperature. Stained glass coverslips were washed three times with PBS and mounted in ProLong Gold (Invitrogen). Fluorescence images were taken by confocal microscope Olympus FluoView 1000.

Triple staining for actin filaments, microtubules and nucleus was performed as previously described [176]. In brief, actin filaments were stained with Texas Red-X phalloidin (Invitrogen), microtubules were stained with α-tubulin (Invitrogen) primary antibody followed by Alexa Fluor 488-conjugated anti-mouse IgG secondary antibody (Invitrogen), and the nucleus was stained with DAPI (4', 6-diamidino-2-

phenylindole) (Invitrogen). Stained glass coverslips were mounted in ProLong Gold (Invitrogen). Fluorescence images were taken using an Olympus FluoView 1000 confocal microscope.

2.3.8 Annexin *V* and PI (propidium iodide) staining

Apoptosis and necrosis were measured by the annexin *V* and PI (propidium iodide) staining kit (Invitrogen), respectively, according to the manufacturer's instructions. In brief, cells were stained with Alexa Fluor 488 conjugated annexin *V* and PI in 1X annexin binding buffer for 15 minutes at room temperature and then subjected to flow cytometry analysis by BD FACSVantage. Early apoptotic cells were identified as those stained by Alexa Fluor 488 but not PI, late apoptotic cells were those stained by both Alexa Fluor 488 and PI, and necrotic cells were those stained by PI but not Alexa Fluor 488.

2.3.9 Calcium imaging

Calcium imaging was performed according to the protocol described in [158]. Cells were cultured in 4-well chambered cover-glass (Thermo Fisher Scientific). After the desired treatment, the cells were loaded with 4 μM Fluo-4 (Invitrogen) in ACSF-HEPES (artificial cerebral spinal fluid with HEPES: 119 mM NaCl, 2.5 mM KCl, 1.3 mM $MgCl_2$, 2.5 mM $CaCl_2$, 1 mM NaH_2PO_4, 26.2 mM $NaHCO_3$, 11 mM dextrose, 10 mM HEPES, pH=7.4) for 30 min at 37 °C. Excess dye was removed by washing cells with PBS twice placing into a 37 ℃ chamber on the stage of Olympus FluoView

1000. 0.5 ml ACSF-HEPES was added to the well to begin imaging. Images were captured every 1.137 seconds and fluorescence intensity is represented by a spectral table (warmer colors represent higher intensity whereas cooler colors represent lower intensity). After 15~20 images, 0.5 ml ACSF-HEPES buffer containing the following drugs were added: 200 μM glutamate (final concentration 100 μM), 200 μM dopamine (final concentration 100 μM), 100 mM KCl (final concentration 50 mM), or 200 μM ATP (final concentration 100 μM). A total of 200~300 images were recorded and the data was analyzed by the FluoView 100 software. Changes in the fluorescence intensity of the Ca^{2+} signal are represented as F/F_0. The percent of responsive cells is calculated as the number of cells with a F/F_0 signal greater than 20% divided by the total number of cells.

2.3.10 Cell counting

Cells were trypsinized by 0.25% trypsin-EDTA (Invitrogen) and an equal volume of media was added to inactivate the trypsin. Number of cells was determined by diluting the cell suspension 1:1 with 0.4% trypan blue (Sigma) and then counted on a hemocytometer.

2.3.11 Stable cell line expressing dominant negative CREB

MSC were transfected with the empty control pCMV vector containing neomycin resistance and the dominant negative CREB mutant (serine 133 mutated to alanine) M1-CREB (a kind gift from Dr. David Ginty) using lipofectomine 2000 (Invitrogen).

24 hours after transfection, cells were trypsinized and replated at low density in media containing 500 μg/ml geneticin (Invitrogen) for selection. The geneticin-containing media was replaced every 3 days for two weeks. Colonies formed from surviving cells were isolated by cloning cylinders (Sigma) and maintained in culture media containing geneticin.

2.3.12 Statistical analysis

All experiments were performed at least three times and results were shown as mean ± standard deviation. Statistical analysis were carried out by an unpaired, two tail Student's T-test. * indicates $p<0.05$, ** indicates $p<0.01$ and *** indicates $p<0.001$.

2.4 Results

2.4.1 cAMP induces early-phase neuron-like morphological changes

Deng et al. showed that upon exposure of human MSC to cAMP elevating agents, 1 mM dibutyryl-cAMP (db-cAMP) and 0.5 mM IBMX, for two days, the cells exhibit neuron-like morphology [4]. However, we found the neuron-like morphology occurred much earlier than previously reported. Uninduced MSCs exhibited flat-like morphology (Figure 2.1A), whereas MSCs induced with 10 μM forskolin and 100 μM IBMX (abbreviated as FI) showed neuron-like morphology within an hour of induction (Figure 2.1B). These MSCs isolated from rat were characterized as described previously [177]. They have the ability to self-renew as well as undergo

multilineage differentiation to other cell lineages such as adipocytes and osteoblasts (Appendix figure 2.1). A recent study attributed the morphological changes to an artifact of cell shrinkage rather than neurite outgrowth [159]. We imaged live cells to determine whether the neuron-like morphology induced by cAMP was also a result of cell shrinkage. As the induction time increase, the cytoskeleton progressively retracts towards the cell center (Figure 2.1C-F). Microtubules and actin filaments staining confirmed the reorganization and retraction of the cell body towards the cell center. The retraction appears incomplete, with partial disruption of the cytoplasm in some of the cells (Figure 2.1B and Appendix figure 2.2, arrows). As with the previous study, the cAMP-induced neurite-like structure is due to a disruption in the cytoskeleton and cell shrinkage rather than neurite outgrowth.

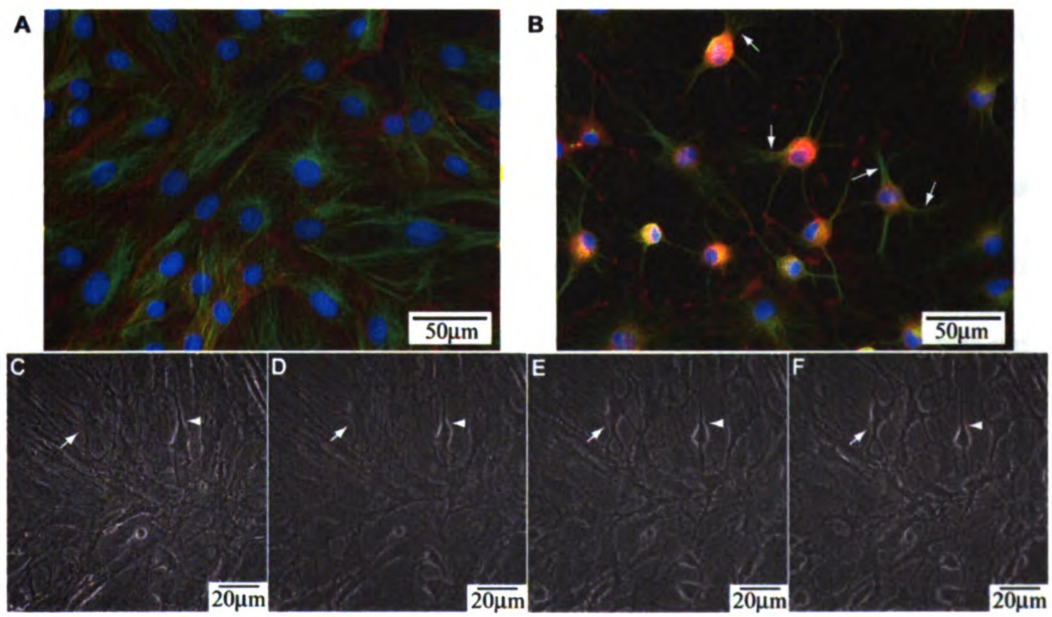

Figure 2.1 Morphological changes upon cAMP induction. (A) Morphology of uninduced MSCs. Green: microtubules; red: actin filaments; blue: nucleus. (B) Morphology of MSCs treated with 10 μM forskolin and 100 μM IBMX (FI) for 1 hr. (C-F) Live cell images of cells treated with FI for 15 minutes (C), 30 minutes (D), 45 minutes (E) and 60 minutes (F).

2.4.2 Neuron-like morphology decreases along time

A large percentage of cells developed neuron-like morphology within an hour after FI treatment (Figure 2.2A, denoted by the arrow head), with an appreciable number still showing neuron-like morphology three hours later (Figure 2.2B and 2.2K). However, unlike the previous study with BME which showed continuous changes in morphology [159], the population of cells with altered morphology decreased with increasing treatment time (Figure 2.2K), with fewer cells showing neuron-like morphology 6 (Figure 2.2C), 12 (Figure 2.2D) and 24 hrs (Figure 2.2E) after FI treatment. By the second day, even with fresh induction media, essentially no change in morphology was observed (Figure 2.2F-G and Figure 2.2K), suggesting that the neuron-like morphology cannot be re-induced by FI. Similar neuron-like morphology was initiated by the apoptosis inducer staurosporine (Appendix figure 2.3), therefore we evaluated whether the morphological changes induced by FI treatment were due to apoptosis. However, the rise in apoptotic cells did not occur within the first 3 hrs after FI treatment (Figure 2.2L), during which maximal changes in morphology resulted (Figure 2.2K), suggesting the change in morphology was not likely due to apoptosis.

Figure 2.2 Time-dependent morphological changes and cell death induced by cAMP. (A-J) Morphology of MSCs induced with 10 μM forskolin and 100 μM IBMX (FI) for different amount of time. Cells with changed morphology appear as green dots (as indicated by the arrows) at the magnification noted. (A-E) On day 1, cells treated with FI for 1, 3, 6, 12 and 24 hours, respectively. (F-J) One day after FI treatment, cells treated again with FI for 1, 3, 6, 12 and 24 hours, respectively. (K) Percentage of cells with changed morphology (n=3). (L) Apoptotic and necrotic labeling by PI and Alexa Fluor-488 conjugated annexin *V*, respectively, of cells treated with FI for 1, 3, 6, 12 and 24 hours. *Early apoptotic cells:* PI^- annexin V^+ cells; *late apoptotic cells*: PI^+ annexin V^+ cells; *necrotic cells*: PI^+ annexin V^- cells (n=3). **: $p<0.01$.

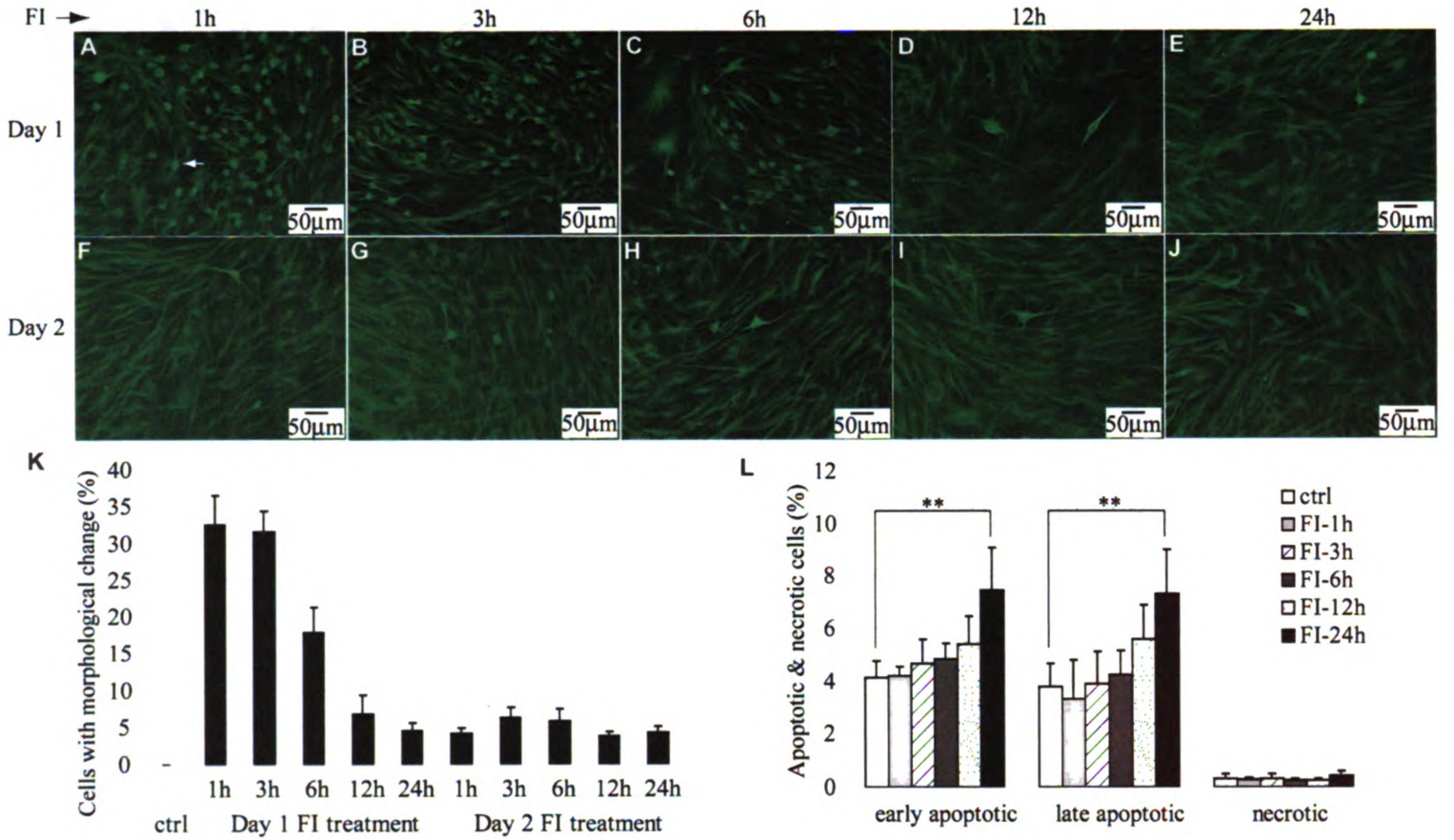
FI
1h
3h
6h
12h
24h
Day 1
Day 2
A
B
C
D
E
F
G
H
I
J
50μm
K
Cells with morphological change (%)
40
35
30
25
20
15
10
5
0
ctrl
1h 3h 6h 12h 24h 1h 3h 6h 12h 24h
Day 1 FI treatment
Day 2 FI treatment
L
Apoptotic & necrotic cells (%)
12
10
8
6
4
2
0
**
**
ctrl
FI-1h
FI-3h
FI-6h
FI-12h
FI-24h
early apoptotic
late apoptotic
necrotic

2.4.3 Morphological changes are correlatd with apoptosis

Changes in cell morphology and cytoskeletal structure can switch cells from surviving to apoptotic [178, 179]. Disruption of the cytoskeletal structure can lead to cell rounding and even detachment, which can result in anchorage-dependent apoptosis called anoikis [180]. Since cAMP elevation induced a disruption of the cytoskeletal structure in the MSCs (Appendix figure 2.2), we assessed whether the morphological changes led to apoptosis. Initially, FI treatment disrupted the cytoskeletal structure in a large number of cells (Figure 2.2A-C). However, most of the cells with changes in morphology remained attached and apoptosis or necrosis was not observed within the first few hours (Figure 2.2L). As FI treatment continued, some cells that underwent morphological changes began to round up (Appendix figure 2.4, arrows) and detach from the surface, likely due to a loss in their ability to anchor (Appendix figure 2.4, arrow head). The cells that round up (Figure 2.3A, arrows) also showed positive staining against annexin *V* (Figure 2.3B-C, arrows), indicating that they have become apoptotic. The number of detached cells increased after 12 hours, with cells floating after 24 hours of treatment (data not shown), corresponding to the time at which the cells stained for apoptosis (Figure 2.2L). Apoptosis increased significantly after 24 hours (Figure 2.2L) and was further enhanced after 48 hours of FI treatment (denoted as day 2), albeit not statistically (Figure 2.3D). Since additional morphological changes did not occur on the second day of FI treatment (Figure 2.2K), i.e., very few cell rounding and detachment, correspondingly increases in apoptosis were not observed (Figure 2.3D).

Concomitantly, caspase-3 activity, another indicator of apoptosis, increased significantly upon FI treatment but remained constant during the second day of treatment (Figure 2.3E). Accordingly, these results suggest that a disruption of the cytoskeletal structure, induced upon cAMP elevation, may have resulted in subsequent apoptosis of ~ 10% of the MSCs.

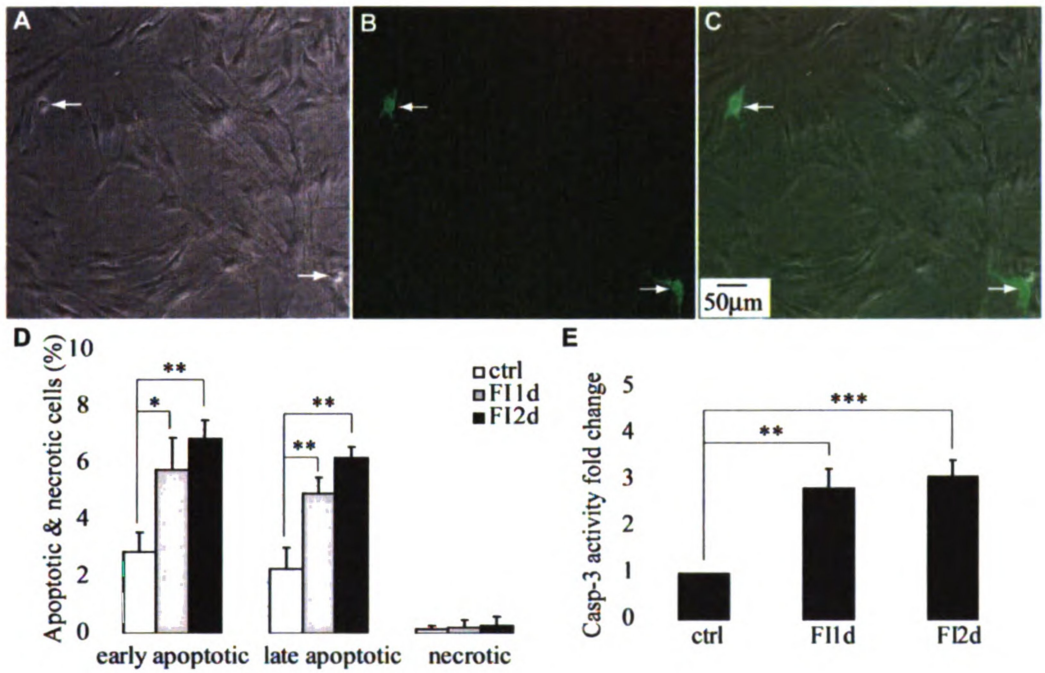

Figure 2.3 cAMP induced apoptosis in MSCs. (A-C) Phase contrast and fluorescence images of apoptotic cells labeled with Alexa Fluor-488 conjugated annexin *V*. Cells were treated with 10 μM forskolin and 100 μM IBMX (FI) for 24 hours. (A) Phase contrast image of MSCs treated with FI for 24 hours. (B) Apoptotic staining with Alexa Fluor-488 conjugated annexin *V*. (C) Overlay image of (A) and (B). (D) Apoptotic and necrotic labeling by Alexa Fluor-488 conjugated annexin *V* and PI (propidium iodide), respectively, of control cells and cells treated with FI for 1 day and 2 days. *Early apoptotic cells:* PI^- annexin V^+ cells; *late apoptotic cells*: PI^+ annexin V^+ cells; *necrotic cells*: PI^+ annexin V^- cells (n=3). (E) Caspase-3 activity of control cells and cells treated with FI for 1 day and 2 days. *: $p<0.05$, **: $p<0.01$, ***: $p<0.001$.

2.4.4 cAMP induces late-phase neural differentiation

Unlike the early-phase changes in morphology which occurred quickly, neural differentiation took much longer. A previous study using DMSO/BHA to induce neural differentiation of MSCs did not observe an increase in mRNA level of neuron-specific enolase (NSE) [159], while we observed an increase in both mRNA (Appendix figure 2.5) and protein levels (Figure 2.4A) of neural markers. FI treatment increased the expression of neuron markers, NSE and neuron-specific class β-III tubulin (Tuj1), as well as astrocytic marker, glial fibrillary acidic protein (GFAP) (Figure 2.4A and 2.4C), but not within the first 6 hours (Figure 2.4B and 2.4D), whereas the changes in morphology peaked within the first 3 hours (Figure 2.2K). An increase in the expression of NSE and Tuj1 was detected 12 hours after FI treatment (Figure 2.4D) whereas an increase in GFAP was not detected until well after 12 hours (Figure 2.4A), suggesting that neural marker expression is a late-phase response as compared with the morphological changes. Immunostaining for the neuronal marker Tuj1 further support the gradual increase in the neural marker expression. Untreated cells do not express Tuj1 (Figure 2.4E), but a few cells gained Tuj1 expression after two days of FI treatment (Figure 2.4F), with more cells expressing Tuj1 a week after FI treatment (Figure 2.4G). Nonetheless, the cells that expressed Tuj1 look distinctly different from primary neurons (Figure 2.4H).

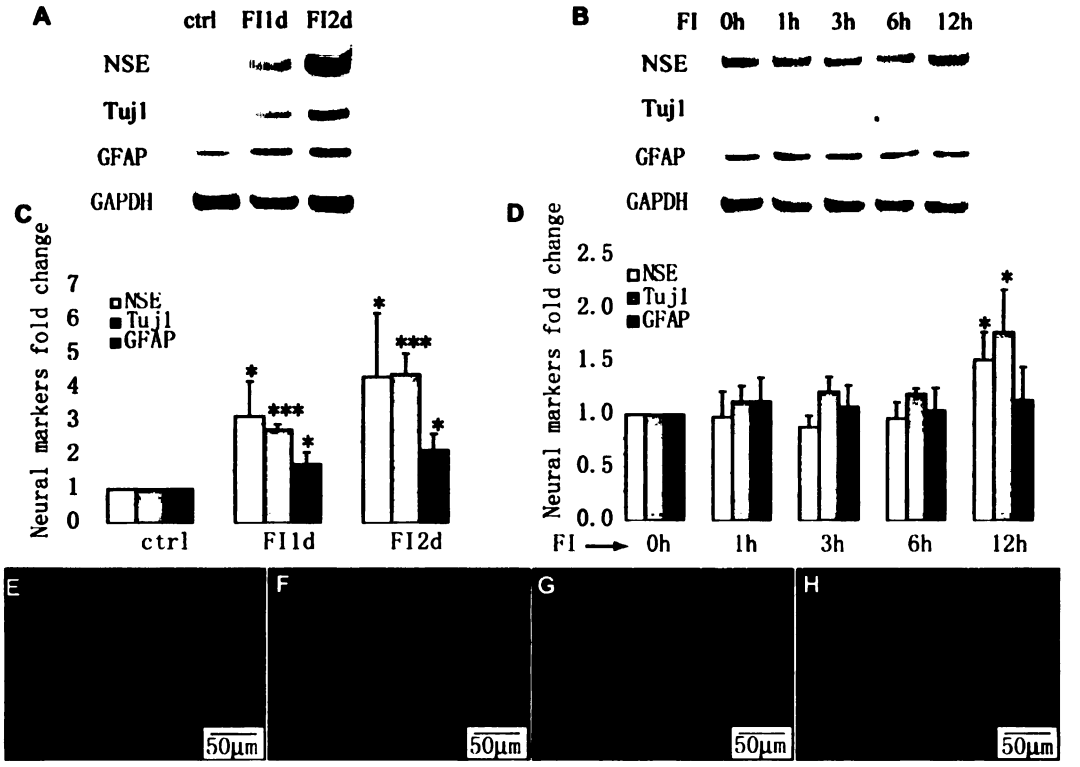

Figure 2.4 Expression of neural markers, NSE, Tuj1 and GFAP. (A) Protein levels of NSE, Tuj1, GFAP and GAPDH of uninduced cells (ctrl), cells treated with 10 μM forskolin and 100 μM IBMX (FI) for 1 day (FI1d) and 2 days (FI2d). (B) Protein levels of NSE, Tuj1, GFAP and GAPDH of cells treated with FI for 0, 1, 3, 6 and 12 hours. (C) Quantification of NSE, Tuj1 and GFAP levels of the blots shown in (A) (n=3). (D) Quantification of NSE, Tuj1 and GFAP levels of the blots shown in (B) (n=3). *: $p<0.05$; ***: $p<0.001$. (E-H) Tuj1 staining of uninduced MSCs (E), MSCs treated with FI for 2 days (F) and 7 days (G) and primary neurons (H).

The induced cells also gained some neuronal function despite their distinct lack of neuronal morphology and features. Neuronal function was assessed with several neuronal activators, 1) dopamine, which stimulates Ca^{2+} signal through the dopamine receptors [181] or through potentiation of the N-methyl-D-aspartic acid (NMDA) receptors [182], 2) KCl, which stimulates Ca^{2+} signal through voltage-gated ion channels [183], and 3) glutamate, which induces Ca^{2+} signal through the glutamate receptors [184]. Figures 2.5A-D are representative images of FI treated cells upon

stimulation with 100 μM dopamine, with time-dependent fluorescence intensity profiles of four individual cells shown in Figure 2.5B. Intracellular Ca^{2+} levels remained fairly constant before stimulation (Figure 2.5A and 2.5E, position denoted by A). Shortly after dopamine supplementation (Figure 2.5E, arrow), some cells showed a Ca^{2+} signal within 10 seconds, and others peaked more slowly, taking up to 34 seconds (Figure 2.5E). The pattern of Ca^{2+} signaling also varied, with some cells responding with a single Ca^{2+} peak (Figure 2.5E, Cell-1 and Cell-3) and other cells being repeatedly excited (Figure 2.5E, Cell-2 and Cell-4). Uninduced cells and cells treated with FI for 1, 2 and 7 days were quantified for their neuronal function upon stimulation by dopamine, KCl and glutamate (Figure 2.5F). Around 40% of the uninduced MSCs showed a response to dopamine, which increased to 60% after one day and 80% after 7 days of FI treatment (Figure 2.5F). Only 12% of the uninduced MSCs responded to KCl stimulation, which increased to 40% after FI treatment (Figure 2.5F). Few uninduced cells responded to glutamate, with about 20% of the cells glutamate responsive after a week of FI induction (Figure 2.5F). These results suggest that FI induction enabled MSCs to gain some neuronal function. However, the heterogeneity in their response to neuronal activators (Figure 2.5F), and the lack of neuronal morphology (Figure 2.4G) indicate that the cells are not terminally differentiate

Figure 2.5 Calcium imaging in response to the neuronal modulators, dopamine, glutamate and KCl. (A-D) MSCs induced with 10 μM forskolin and 100 μM IBMX (FI) for 1 day and stimulated with 100 μM dopamine. Fluorescence images represented by a spectral table; warmer colors indicate higher fluorescence intensities and cooler colors indicate lower fluorescence intensities. Images were captured before dopamine stimulation or 12, 34 and 82 seconds after dopamine stimulation. (E) Fluorescence intensity profiles of four selected cells shown in (B) over time. Arrow indicates the point of dopamine addition. Annotation of A, B, C, D corresponds to the images in (A-D). (F) Quantification of the percentage of uninduced MSCs, FI induced MSCs for 1 day, 2 days and 7 days that respond to 100 μM dopamine, 100 μM glutamate and 50 mM KCl (n=4). **: $p<0.01$, ***: $p<0.001$.

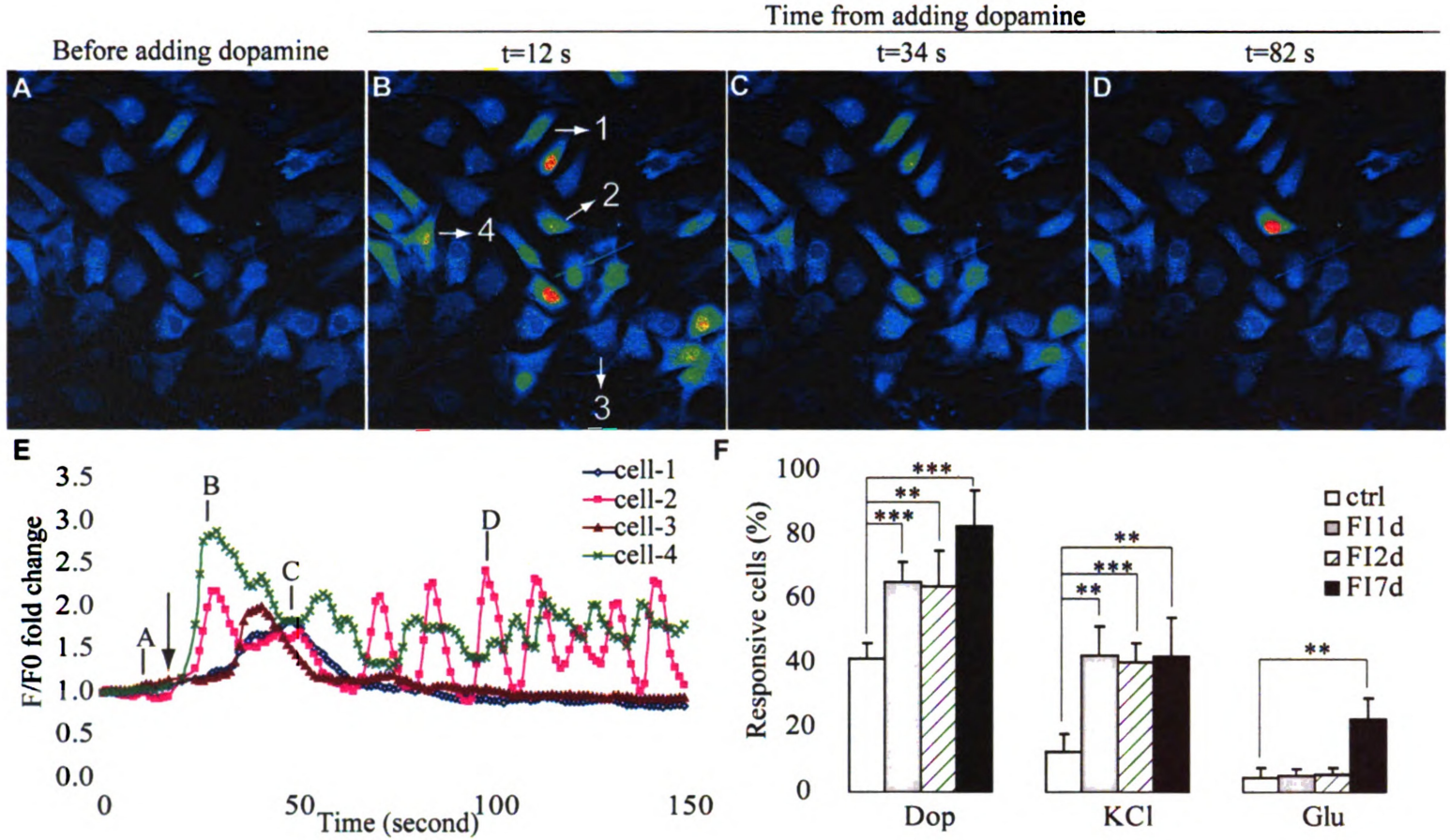
Time from adding dopamine
Before adding dopamine
t=12 s
t=34 s
t=82 s
A
B
C
D
1
2
3
4
E
F/F0 fold change
Time (second)
cell-1
cell-2
cell-3
cell-4
A
B
C
D
F
Responsive cells (%)
ctrl
FI1d
FI2d
FI7d
Dop
KCl
Glu

2.4.5 PKA regulates both the changes in morphology and neural marker expression

As shown above, the percentage of cells with changes in morphology peaked an hour after FI treatment and decreased with treatment time (Figure 2.2K). The intracellular cAMP levels paralleled the changes in morphology, peaking also an hour after FI treatment and decreasing over the next few hours to a constant level that was maintained for the next 12 hrs (Figure 2.6A). Although fresh media containing FI was added on the second day, the intracellular cAMP level did not increase (Figure 2.6A), perhaps, because of desensitization of the agonist-induced receptor [185]. Since cAMP can trigger a variety of intracellular events through the activation of the classical downstream component protein kinase A (PKA) [16], we therefore assessed whether PKA activation is involved in regulating the changes in morphology and neural marker expressions. The activity of PKA can be determined by the level of phosphorylation of threonine 197 on the PKA catalytic subunit (PKAc) [186, 187]. Upon FI treatment, phosphorylated PKA (pPKAc) increased transiently and then returned to below basal level, whereas the total PKAc level dropped continuously, with both remaining stable after one day (Figure 2.6B-C). Inhibiting PKA activity with H89 prevented the FI-induced morphological changes (Figure 2.6D-E) as well as the neural marker expressions (Figure 2.6F-G). Similar results were obtained using another PKA inhibitor Rp-cAMPS (Appendix figure 2.6), suggesting that PKA mediates the onset of both the morphological changes and neural marker expression.

Figure 2.6 PKA regulates both morphological changes and neural markers expressions. (A) Intracellular cAMP levels of control MSCs, MSCs induced with 10 μM forskolin and 100 μM IBMX (FI) for 1, 3, 6, 12 and 24 hours (Day 1), and MSCs induced again with FI for 1, 3, 6, 12 and 24 hours, following a 24-h FI induction period (Day 2) (n=3). (C) Western blotting results of PKAc and pPKAc levels of control MSCs, MSCs induced with FI for 1, 3, 6, 12 and 24 hours, and MSCs induced with FI for 1, 6 and 24 hours following a 24-h FI induction period. (C) Quantification of PKAc and threonine 197 phosphorylated PKAc (pPKAc) levels as in (B) (n=4). *: $p<0.05$, **: $p<0.01$, ***: $p<0.001$ as compared with the corresponding control condition. (D) Phase contrast image of MSCs induced with FI for 1 hour. (E) Phase contrast image of MSCs induced with FI in the presence of 2.5 μM PKA inhibitor H89 for 1 hour. (F) Quantification of NSE, Tuj1 and GFAP expression for control MSCs, MSCs induced with FI for 1 day in the absence or presence of PKA inhibitor H89 (n=3). (G) Expression of neural markers, NSE, Tuj1 and GFAP, for control MSCs, MSCs induced with FI for 1 day in the absence or presence of H89.

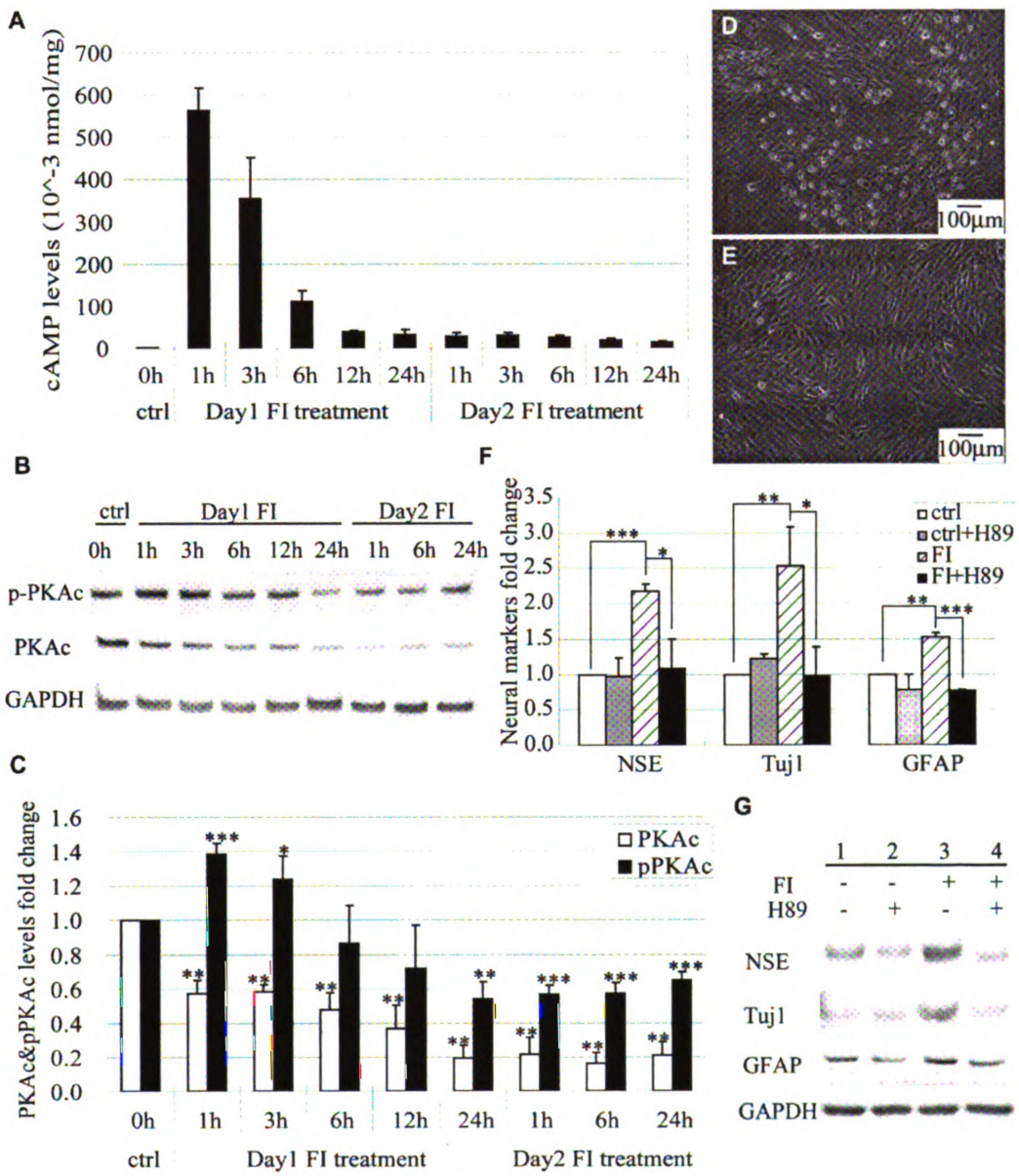
A
cAMP levels (10^-3 nmol/mg)
700
600
500
400
300
200
100
0
0h 1h 3h 6h 12h 24h 1h 3h 6h 12h 24h
ctrl
Day1 FI treatment
Day2 FI treatment
D
100μm
E
100μm
B
ctrl
Day1 FI
Day2 FI
0h 1h 3h 6h 12h 24h 1h 6h 24h
p-PKAc
PKAc
GAPDH
F
Neural markers fold change
3.5
3.0
2.5
2.0
1.5
1.0
0.5
0.0
ctrl
ctrl+H89
FI
FI+H89
NSE
Tuj1
GFAP
C
PKAc&pPKAc levels fold change
1.6
1.4
1.2
1.0
0.8
0.6
0.4
0.2
0.0
PKAc
pPKAc
0h 1h 3h 6h 12h 24h 1h 6h 24h
ctrl
Day1 FI treatment
Day2 FI treatment
G
1 2 3 4
FI - - + +
H89 - + - +
NSE
Tuj1
GFAP
GAPDH

2.4.6 Morphological changes and neural marker expression are differentially regulated

Although the changes in both morphology and neural marker expression are regulated by PKA, the neuron-like morphology occurs early and very quickly, whereas the neural marker expressions appear much later and more slowly. Since the morphological changes appear prior to changes in neural marker expression (Figure 2.1 and Figure 2.4), we assessed whether the morphological changes are required and thus precede the gain of neural marker expression. The microtubule stabilizer paclitaxel (Ptx) was used to inhibit the changes in morphology. Microtubules are dynamic polymers that undergo polymerization and depolymerization powered by energy from GTP hydrolysis [188]. Binding of Ptx to the microtubules prevents the depolymerization and stabilizes the microtubules [189]. Since dynamic polymerization and depolymerization are required for the assembly of the mitotic spindles, applying Ptx may inhibit mitosis and cause subsequent apoptosis [190, 191]. To minimize the toxicity induced by Ptx while still inhibiting the onset of morphological changes, the cells were treated with FI in the presence of 0.4 μM Ptx for only 3 hours and the media was subsequently changed to FI media for another 21 hours. Stabilized cytoskeletal structure was maintained upon removal of Ptx from the FI media (Appendix figure 2.7). This could be due to the inability of the media to initiate another intracellular cAMP peak (Appendix figure 2.8A) required for regulating the morphological changes (Figure 2.2K and 2.6A). The number of viable cells 21 hours after replacing the induction media (a total of 24 hrs including the 3

hour pretreatment) remained constant, thus Ptx exposure did not adversely affect cell viability (Appendix figure 2.8B). Although Ptx inhibited changes in morphology (Figure 2.7A-B), it did not prevent the increase in neural marker expression (Figure 2.7C-D), suggesting neuron-like morphology is not required for neural markers expression.

The morphological changes occur very quickly (beginning minutes after FI treatment), thus is unlikely that gene or protein synthesis is required for this event. Indeed, inhibiting transcription with actinomycin D (ActD) and translation with cycloheximide (CHX) did not impact the morphological changes (Figure 2.7E-F), but did reduce the neural marker expression upon treatment with FI (Figure 2.7G-H). Thus transcription and translation are required for neural marker expression. ActD and CHX affect transcription and translation on a global level and treatment for a long period may cause cell death. Therefore as with the paclitaxel treatment, the media supplemented with ActD or CHX was replaced after 3 hours and the viability of the cells was assessed after 24-hours of treatment. Supplementing the FI treatment with ActD or CHX did not significantly change the total number of viable cells (Appendix figure 2.8B).

Figure 2.7 Morphological changes and neural markers are differentially regulated. (A) Appearance of neuron-like morphology of MSCs induced with 10 μM forskolin and 100 μM IBMX (FI) for 1 hour. (B) Cell morphology of MSCs induced with FI in the presence of 0.4 μM microtubule stabilizer paclitaxel (Ptx) for 1 hour. (C-D) Expression of neural markers, NSE, Tuj1 and GFAP, in control cells, cells induced with FI for 1 day in the absence or presence of Ptx (n=3). For the FI treatment, cells were treated with FI or FI plus Ptx for 3 hours and then changed to fresh FI media to reduce toxicity from Ptx treatment. (E) Appearance of neuron-like morphology of MSCs induced with FI for 1 hour in the presence of 1 μg/ml Actinomycin D (ActD). (F) Appearance of neuron-like morphology of MSCs induced with FI for 1 hour in the presence of 10 μg/ml Cycloheximide (CHX). (G-H) Expression of neural markers, NSE, Tuj1 and GFAP, in control cells, cells induced with FI for 1 day, in the presence or absence of ActD or CHX. For the FI treatment, cells were treated with FI or FI plus ActD/CHX for 3 hours and then changed to fresh FI media to reduce toxicity from ActD/CHX treatment. *: $p<0.05$, **: $p<0.01$, ***: $p<0.001$.

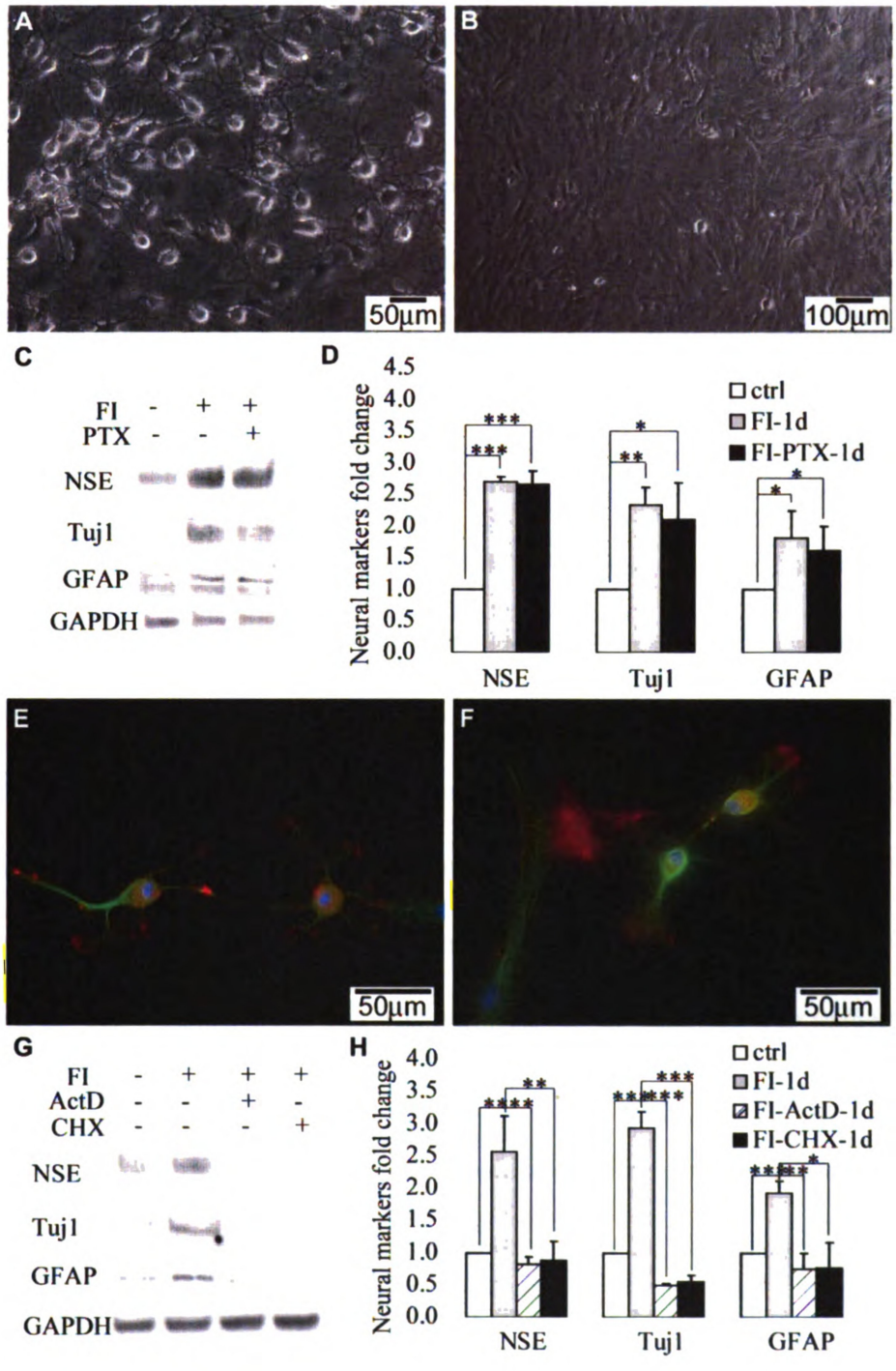
A
50μm
B
100μm
C
FI - + +
PTX - - +
NSE
Tuj1
GFAP
GAPDH
D
Neural markers fold change
4.5
4.0
3.5
3.0
2.5
2.0
1.5
1.0
0.5
0.0
ctrl
FI-1d
FI-PTX-1d
NSE
Tuj1
GFAP
E
50μm
F
50μm
G
FI - + + +
ActD - - + -
CHX - - - +
NSE
Tuj1
GFAP
GAPDH
H
Neural markers fold change
4.0
3.5
3.0
2.5
2.0
1.5
1.0
0.5
0.0
ctrl
FI-1d
FI-ActD-1d
FI-CHX-1d
NSE
Tuj1
GFAP

Taken together, the early-phase neuron-like morphological changes do not rely on gene and protein synthesis whereas the late-phase neural marker expressions do. Correspondingly, changes in morphology occur prior to but are not required for the expression of neural markers. Therefore, although both the morphological changes and the neural marker expressions are regulated by PKA, they are differentially regulated downstream of PKA.

2.5 Discussion

cAMP has been shown to play a positive role in the regeneration of the central nervous system (CNS) [36, 192, 193]. Decrease in neuronal cAMP level has been associated with loss in neuronal regenerative capacity [192], whereas an increase in cAMP levels can promote axonal regeneration [194]. In addition to directly stimulating neuronal regeneration for neuronal repair, cAMP also can indirectly facilitate neuronal repair by inducing adult stem cells, such as MSCs, to differentiate into neural lineage cells [4]. cAMP has been suggested to be one of the best inducers of MSCs neural differentiation [153]. However, the assessment of neural differentiation has been largely based on the appearance of neuron-like morphology and neural marker expression [4, 153]. MSCs treated with cAMP increasing agent (FI) achieved neuron-like morphology (Figure 2.1B) which was due to disruption of the cytoskeleton and cell shrinkage (Figure 2.1C-F) rather than neurite outgrowth. Thus, the morphological changes are not always a reliable assessment of neural differentiation. In contrast to the early onset of changes in morphology, expression of neural markers occurred much later. An increase in the neural markers, such as NSE,

Tuj1 and GFAP became apparent a day after induction (Figure 2.4A and 2.4C) with some degree of neuronal function, i.e. rise in calcium signaling in response to neuronal activators (Figure 2.5). The gain of neuronal function by MSCs upon induction with cAMP alone has not been previously reported. Although our results showed that cAMP enabled MSCs to obtain neuronal function, the cells are at different stages with respect to their ability to respond to the different neuron activators. Some cells show a calcium rise upon stimulation by all three neuronal activators, while others respond to only one or two, or even none of the activators (Figure 2.5F). Since these cells do not show the morphology of primary neurons (Figure 2.4G), cAMP alone is unable to terminally differentiate the MSCs into neural lineage cells. The argument whether MSCs can differentiate into functional neurons *in vitro* and *in vivo* is rarely addressed. A couple of transplantation studies indicated that MSCs can differentiate towards neural lineage cells *in vivo* [131, 134, 195-197] and some of the differentiated cells were able to gain neuronal functionality [197]. However, whether these functional neurons are generated by MSCs through differentiation or fusion of MSCs with existing neurons remains unclear [198].

Our results point to differential regulation of the morphology and neural marker expression downstream of PKA. With respect to morphology, PKA can activate the Src homology domain (SH)2-containing phosphotyrosine phosphatase (SHP2) [199], which can then dephosphorylate the focal adhesion protein paxillin and result in disassembly of the focal adhesion and subsequent loss of actin stress fibers and cell rounding [199, 200]. Alternatively, the cAMP-PKA signaling pathway may disrupt

the cytoskeleton by inhibiting the Rho family GTPases, which play important roles in modulating the cytoskeletal structure. Rho GTPases can promote actin polymerization and stress fiber formation by activating the polymerization factors actin-related protein 2/3 (Arp2/3) and formin, and inhibiting the depolymerization factor cofilin [201]. They can also regulate microtubule stability by inhibiting the microtubule disassembly factor oncoprotein 18 (Op18) and activating the mammalian Diaphanous-related (mDia) formins [201, 202]. cAMP can promote cytoskeleton disruption in melanocytes [203] mediated by RhoA inhibition [204], through phosphorylation of RhoA at serine 188 by PKA [205]. Therefore, the cAMP-PKA pathway could modulate the cytoskeleton by altering the phosphorylation status of focal adhesion proteins or the Rho GTPases.

Signaling events are rapid as compared to gene or protein synthesis. Thus in contrast, expression of neural markers takes longer and requires transcription and translation (Figure 2.7G-H), suggesting that transcription factors activated by the cAMP-PKA signaling pathway may be involved. One such downstream factor is the cAMP response element binding protein (CREB), which can be phosphorylated by PKA at serine 133 [16]. FI treatment transiently increased nuclear PKAc and pCREB levels (Figure 2.8A-B). Phosphorylation of CREB regulates neurogenesis by promoting survival and differentiation of newborn neurons [206, 207]. Over-expressing the dominant negative form of CREB, M1-CREB (the serine 133 residue is mutated to alanine, therefore it can no longer be phosphorylated) in MSCs led to loss in their response to neuronal activators, such as dopamine (Figure 2.8C-D). This

suggests that phosphorylation of CREB plays a critical role in regulating MSC differentiation towards the neural lineage cells. Interestingly, MSCs stably expressing M1-CREB were much smaller than the normal MSCs after a week of FI induction (Figure 2.8D), indicating that activated CREB is an important determinant in regulating cell size. Indeed, mice expressing dominant negative CREB are reduced in size during embryonic development [208]. Therefore, although the early onset of morphology changes induced by FI do not appear to require transcription (Figure 2.7A), the transcription factor CREB is still required for regulating cell shape during MSC differentiation (Figure 2.8D), hinting as possible cross-talk downstream of PKA.

The present study showed that cAMP induced changes in morphology early and neural differentiation and function much later and these events are regulated by cAMP activated PKA, but diverge in their regulation downstream. While the morphological changes are likely due to cell shrinkage, which rendered some cells to be subsequently apoptotic, nonetheless the neural differentiation induced by cAMP enabled the MSCs to gain neuronal function.

Figure 2.8 Transient activation of CREB and regulation of calcium signal by CREB. (A) Nuclear protein levels of PKAc, pCREB (serine 133 phosphorylated CREB) and CREB in control cells and cells treated with 10 μM forskolin and 100 μM IBMX (FI) for 1, 3, 6, 12 and 24 hours. (B) Quantification of nuclear PKAc, pCREB and CREB levels (n=3). *: $p<0.05$; **: $p<0.01$ as compared with the corresponding '0h' conditions. (C) Quantification of responsive cells stimulated with 100μM dopamine. MSCs (expressing control vector) and M1-MSCs (expressing M1-CREB) were either in control media or induced with FI for 7 days (n=3, ***: $p<0.001$). (D) A representative example of calcium signal in response to neuronal activator dopamine. (D-1 to D-4) MSCs (expressing control vector) induced with FI for 1 week and stimulated with 100 μM dopamine. (D-5 to D-8) M1-MSCs (expressing M1-CREB) induced with FI for 1 week and stimulated with 100 μM dopamine

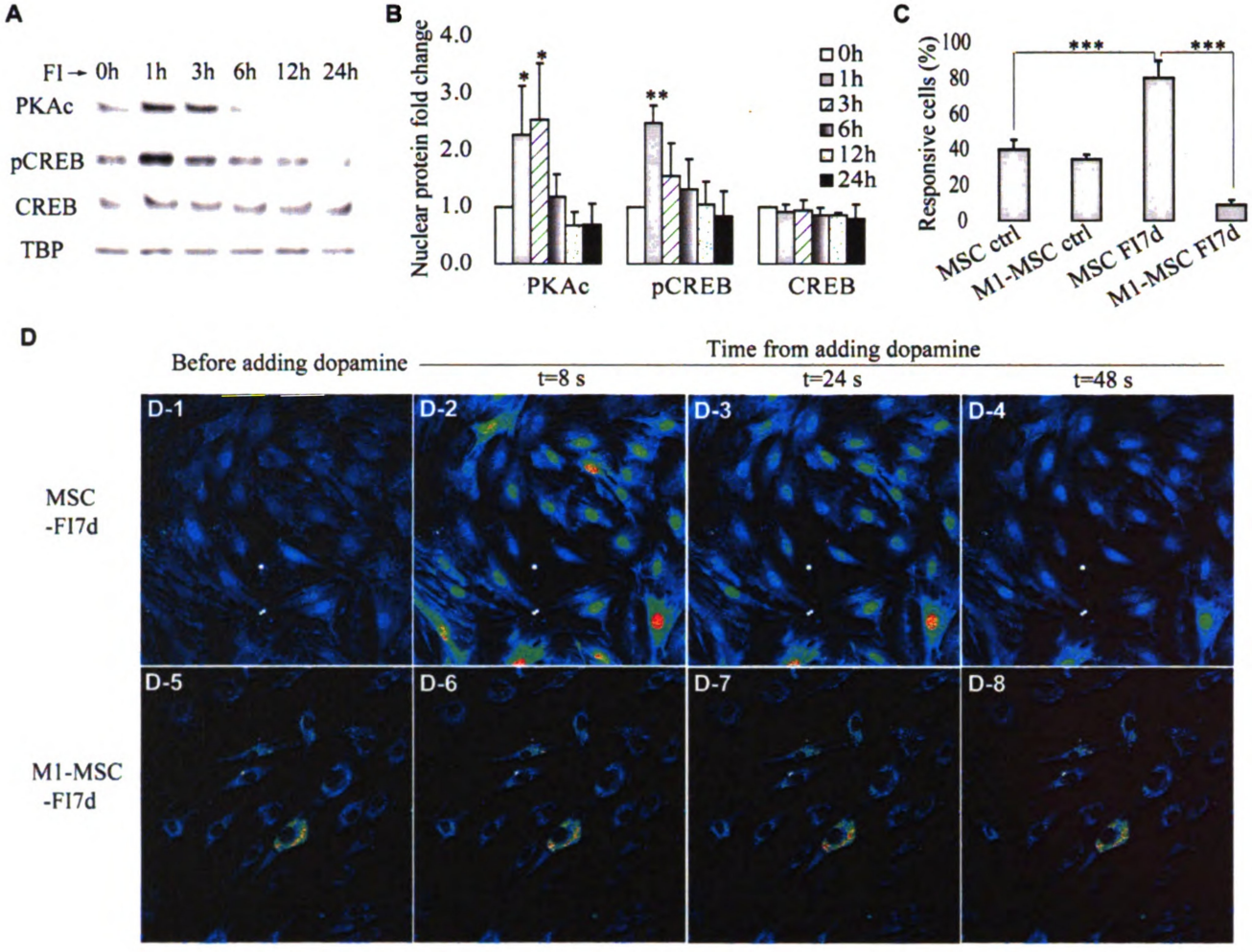
A
FI→ 0h 1h 3h 6h 12h 24h
PKAc
pCREB
CREB
TBP
B
Nuclear protein fold change
4.0
3.0
2.0
1.0
0.0
0h
1h
3h
6h
12h
24h
PKAc
pCREB
CREB
C
Responsive cells (%)
100
80
60
40
20
0
***
***
MSC ctrl
M1-MSC ctrl
MSC FI7d
M1-MSC FI7d
D
Before adding dopamine
Time from adding dopamine
t=8 s
t=24 s
t=48 s
D-1
D-2
D-3
D-4
MSC
-FI7d
D-5
D-6
D-7
D-8
M1-MSC
-FI7d

CHAPTER 3. CREB MODULATES CALCIUM SIGNALING ELICITED BY NEURONAL ACTIVATORS IN MESENCHYMAL STEM CELLS

This work is in review:
Zhang, L. and Chan, C. CREB modulates calcium signaling elicited by neuronal activators in mesenchymal stem cells (In review).

3.1 Abstract

Various studies have suggested that activation of CREB facilitates maturation and survival of immature neurons; however the role of CREB in transdifferentiation of mesenchymal stem cells (MSCs) into neural lineage cells remains unclear. In particular, whether and how CREB affects calcium signaling upon neuronal activator stimulation has not been investigated. In our previous study we observed that cAMP enabled MSCs to generate intracellular calcium signaling in response to several neuronal activators. In an effort to uncover the role of CREB in calcium signaling, we knocked down CREB activity both by siRNA and introducing a dominant negative form of CREB. Our results suggest that knock-down of CREB activity in MSCs greatly reduced or abolished the cAMP-induced calcium response to neuronal activators, whereas reintroducing a constitutively active CREB partially restored the calcium response. The reduction in the calcium response to the neuronal activators appears to involve CREB regulated membrane receptor expression, i.e., dopamine receptor expression. In contrast to the positive effect of CREB on the calcium response, CREB appears to exert a negative effect on the neuron-like morphology, suggesting a complex role of CREB during differentiation of MSCs into neural lineages.

3.2 Introduction

The transcription factor cAMP response element binding protein (CREB) is activated by various extracellular stimuli and serves as a hub for many cellular processes including metabolism, survival, immune response as well as learning and memory [34, 209]. Phosphorylation of CREB at the key serine 133 site by kinases such as protein kinase A (PKA) is required for its transcriptional activity [30, 33]. Recent studies suggest that serine 133 phosphorylated CREB (pCREB) colocalizes in immature neurons of adult hippocampus [206] and enhances maturation and survival of these cells [206, 207]. Activation of CREB was also shown to facilitate the migration of neuronal progenitor cells from the subventricular zone (SVZ) into the olfactory bulb (OB) and enhanced survival of the differentiated neurons in the OB [210]. Nevertheless, understanding how CREB affects neural stem cells function is still at an early stage. The impact of CREB on other stem cells and, in particular, their differentiation towards neural lineages has not been investigated. Although activated CREB appears to co-localize with immature neurons and to be required for neuronal maturation, its role in regulating neuronal functionality such as calcium rise in response to neuronal activators is not known. Elevation of cAMP level, which stimulates CREB activity, has been shown to induce neural stem cells (NSCs) to exhibit neuronal phenotypes [211], and mesenchymal stem cells (MSCs) to differentiate into neural lineages [4]. In a previous study, we observed that cAMP, accompanied by transient activation of CREB, enabled MSCs to produce a calcium rise upon stimulation by several neuronal activators [212]. We set out in this study to

determine the role played by CREB on inducing a calcium rise in cAMP activated MSCs.

Neuronal activators stimulate intracellular calcium rise through voltage-gated ion channels or receptor-gated channels which are predominantly expressed in excitable cells [213]. For example, KCl induces membrane depolarization and calcium influx through voltage-gated calcium channels [214]. Glutamate elicits intracellular calcium rise through ionotropic and metabotropic glutamate receptors [215, 216]. Ionotropic glutamate receptors (iGluRs) are ligand gated ion channels which can be classified into *N*-methyl-D-aspartate (NMDA), α-amino-3-hydroxy-5-methyl-4-isoxazole-propionate (AMPA) and kainate (Ka) receptors [215]. Metabotropic glutamate receptors (mGluRs) are G-protein coupled receptors that signal calcium rise through the generation of second messengers, which includes Group I (mGluR 1, 5), Group II (mGluR 2 and 3) and Group III (mGluR 4, 6-8) mGluRs [216, 217]. The mechanism by which dopamine induces calcium rise is complex and can occur through a variety of mechanisms, such as through binding to the D1-like (including D1 and D5) and D2-like dopamine receptors (including D2, D3 and D4) [218, 219] and through potentiation of NMDA receptors [182].

Previously, we observed that cAMP induction enabled MSCs to produce a calcium rise in response to neuronal activators, dopamine, glutamate and KCl [212]. Although it is well known that CREB activity can be modulated by the Ca^{2+}/calmodulin dependent kinases (CaMKs) [30], to our knowledge, there is no study that has investigated the role of CREB in calcium signaling. Therefore, we set

out to determine if cAMP induced CREB activation is involved in regulating calcium signaling in MSCs. Our results suggested that CREB plays a critical role for MSCs to adopt neuronal function, namely to elicit a calcium rise in response to neuronal activators. In contrast to its role in facilitating the neuronal function, CREB appears to have a negative impact on the production of a neuron-like morphology. Knock-down of CREB activity in a dominant negative CREB cell line promoted the appearance of neuron-like morphology. We also examine if CREB can regulate MSCs proliferation and survival. Our results suggest that while CREB activation, induced by cAMP, does not affect G1 phase lengthening, it is required to protect MSCs from cAMP induced apoptosis. Taken together, CREB regulates several aspects of cellular behavior in MSCs during cAMP induced neural differentiation.

3.3 Materials and methods

3.3.1 Cell culture and materials

All procedures in the cell isolation were approved by the Institutional Animal Care and Use Committee at Michigan State University. Bone marrow mesenchymal stem cells were isolated from 6-8 week old Sprague-Dawley female rats as previously described [177]. In brief, femurs and tibias were taken from the hind legs of 6-8 week old rats. The marrow was flushed out with DMEM and filtered through a 65 μm nylon mesh to remove bone debris and blood aggregates. Cells were cultured in DMEM (Invitrogen) supplemented with 10% fetal bovine serum (Invitrogen), 100 μg/mL streptomycin (Invitrogen) and 100 U/mL penicillin (Invitrogen) and placed in an

incubator with a humidified atmosphere containing 5% CO_2 at 37 °C. Non-adherent cells were removed on the second day after plating. Medium was replaced every 3 to 4 days until the cells reach 80~90% confluence. Confluent cells were detached using 0.25% trypsin-EDTA (Invitrogen) and plated for further experiments.

To induce neural differentiation, forskolin (Sigma) and isobutylmethylxanthine (IBMX) (Sigma) were used to increase intracellular cAMP levels at concentrations of 10 μM and 100 μM, respectively.

3.3.2 Cell cycle analysis

Cell cycle analysis was performed as described previously [177]. In brief, harvested cells were fixed with 70% ethanol on ice for 2 hours. RNA was digested by RNase and then DNA was labeled with PI (propidium iodide) for 30 minutes at room temperature. Labeled samples were analyzed by flow cytometer BD FACSVantage.

3.3.4 Quantitative real time polymerase chain reaction (RT-PCR)

Cells were treated as desired and mRNA was extracted by the RNA extraction kit from Qiagen according to the manufacture's instruction. mRNA was then reverse transcribed to cDNA using the cDNA synthesis kit from Bio-Rad. The primer sets for actin, dopamine receptors D1, D2, D3, D4 and D5 were obtained from Eurofins MWG Operon and are shown in Table 3.1 were used for PCR. Amplification of the cDNA templates were detected by SYBR Green Supermix (Bio-Rad) using Real-

Time PCR Detection System (Bio-Rad). The cycle threshold (CT) values for each condition were determined by the MyIQ software.

Table 3.1 Primer sets for actin, D1, D2, D3, D4 and D5.

Gene	Primer sets	
actin	5'-CTCTTCCAGCCTTCCTTCCT-3'	5'-AATGCCTGGGTACATGGTG-3'
D1	5'-GCCATAGAGACGGTGAGCAT-3'	5'-ATTCCACCAGCCTCTTCCTT-3'
D2	5'-TATGGCTTGAAGAGCCGTGCCA-3'	5'-TACAGCCATGCACACCAGCACA-3'
D3	5'-CAGCCGCATTTGCTGTGACGTT-3'	5'-AGCAAAAGCCAGCACCCACACA-3'
D4	5'-TGCTGCTCATCGGCATGGTGT-3'	5'-AGCCACAAACCTGTCCACGCT-3'
D5	5'-TGGAGCCTATGAACCTGACC-3'	5'-GAAGAAAGGCAACCAGCAAC-3'

3.3.5 Nuclear extraction

Nuclear extraction was carried out according to a protocol described in [220]. In brief, cells were suspended in buffer A (10 mM HEPES (pH=8.0), 1.5 mM $MgCl_2$, 10 mM KCl, protease and phosphatase inhibitor cocktail) and allow to swell on ice for 15 minutes. After swelling, the cells were lysed with a 25-gauge 5/8 inch needle and lysates were spinned down to collect the nuclear pellets. Nuclear pellets were re-suspended in buffer C (20 mM HEPES (pH=8.0), 1.5 mM $MgCl_2$, 25% (v/v) glycerol, 420 mM NaCl, 0.2 mM EDTA (pH=8.0, protease and phosphatase inhibitor cocktails) and incubated on ice for 30min, then centrifuged at 12,000g for 5 minutes to obtain the nuclear extracts.

3.3.6 Western blot

Nuclear extracts or whole cell extracts lysed with CelLytic (Sigma) were assayed for protein concentrations by Bradford assay (Bio-Rad). 15-30 μg protein samples

were separated by 10% Tris-HCl gel and transferred to nitrocellulose membrane. Membranes were then blocked with 5% milk in 0.05% Tween 20-TBS (Tris buffered saline) (USB Corporation) for one hour and incubated with primary antibodies, NSE (neuron-specific enolase) (BIOMOL), Tuj1 (βIII-tubulin) (Millipore), GFAP (Glial fibrillary acidic protein) (DAKO), GAPDH (Cell signaling), CREB (Cell signaling), ser133 phosphorylated CREB (pCREB) (EMD Chemicals), CDK4 (Cell signaling), CDK6 (Cell Signaling), cyclin D1 (Cell Signaling), $p27^{kip1}$ (Cell Signaling), dopamine receptor 1 (D1) (Novus Biologicals), ICER (kinly provided by Dr. Carlose Molina), c-fos (Cell Signaling) and actin (Sigma) overnight at 4 °C. After removing excessive primary antibodies, anti-mouse or anti-rabbit HRP-conjugated secondary antibodies (Thermo Scientific) were added and the blots were incubated for one hour at room temperature. The blots were then washed three times with 0.05% Tween 20-TBS and visualized by SuperSignal West Femto maximum sensitivity substrate (Thermo Scientific).

3.3.7 Immunocytochemistry

Triple staining for actin filaments, microtubules and nucleus was performed as previously described [176]. In brief, actin filaments were stained with Texas Red-X phalloidin (Invitrogen), microtubules were stained with α-tubulin (Invitrogen) primary antibody followed by Alexa Fluor 488-conjugated anti-mouse IgG secondary antibody (Invitrogen), and the nucleus was stained with DAPI (4', 6-diamidino-2-phenylindole) (Invitrogen). Stained glass coverslips were mounted in ProLong Gold

(Invitrogen). Fluorescence images were taken using an Olympus FluoView 1000 confocal microscope.

For staining against dopamine receptor 1, Tuj1 or synapsin, cells were fixed in PBS containing 3.7% formaldehyde for 15 minutes and permeabilized with 0.2% Triton X-100 (Research Products Internationals) for 10 minutes at room temperature. After washing with PBS three times, cells were blocked in 1% BSA (Bovine Serum Albumin) (US Biological) for 20 min and incubated with dopamine 1 receptor (Novus Biologicals) antibody, Tuj1 antibody (Cell Signaling) or synapsin antibody (Cell Signaling) at room temperature for one hour. Cells were then washed with PBS three times and incubated with Alexa Fluor 488-conjugated anti-mouse IgG secondary antibody (Invitrogen) or Rhodamine-conjugated anti-rabbit secondary antibody (Calbiochem) for one hour at room temperature. Stained glass coverslips were washed three times with PBS and mounted in ProLong Gold (Invitrogen). Fluorescence images were taken by an Olympus FluoView 1000 confocal microscope.

3.3.8 Annexin *V* and PI (propidium iodide) staining

Apoptosis and necrosis were measured by the annexin *V* and PI (propidium iodide) staining kit (Invitrogen), respectively, according to the manufacturer's instructions. In brief, cells were stained with Alexa Fluor 488 conjugated annexin *V* and PI in 1X annexin binding buffer for 15 minutes at room temperature and then subjected to flow cytometry analysis by BD FACSVantage. Early apoptotic cells were identified as those stained by Alexa Fluor 488 but not PI, late apoptotic cells were those stained by

both Alexa Fluor 488 and PI, and necrotic cells were those stained by PI but not Alexa Fluor 488.

3.3.9 Calcium imaging

Calcium imaging was performed according to the protocol described in [158]. Cells were cultured in 4-well chambered cover-glass (Thermo Fisher Scientific). After the desired treatment, the cells were loaded with 4 μM Fluo-4 (Invitrogen) in ACSF-HEPES (artificial cerebral spinal fluid with HEPES: 119 mM NaCl, 2.5 mM KCl, 1.3 mM $MgCl_2$, 2.5 mM $CaCl_2$, 1 mM NaH_2PO_4, 26.2 mM $NaHCO_3$, 11 mM dextrose, 10 mM HEPES, pH=7.4) for 30 min at 37 °C. Excess dye was removed by washing the cells twice with PBS and placing them into a 37 °C chamber on the stage of an Olympus FluoView 1000 microscope. 0.5 ml ACSF-HEPES was added to the well to begin imaging. Images were captured every 1.137 seconds and fluorescence intensity is represented by a spectral table (warmer colors represent higher intensity whereas cooler colors represent lower intensity). After 15~20 images, 0.5 ml ACSF-HEPES buffer containing the following compounds were added: 200 μM glutamate (final concentration 100 μM), 200 μM dopamine (final concentration 100 μM), 100 mM KCl (final concentration 50 mM), or 200 μM ATP (final concentration 100 μM). A total of 200~300 images were recorded and the data was analyzed by the FluoView 100 software. Changes in the fluorescence intensity of the Ca^{2+} signal are represented as F/F_0. The percent of responsive cells is calculated as the number of cells with a F/F_0 signal greater than 20% divided by the total number of cells.

3.3.10 Transfection

For siRNA silencing, siRNAs targeting CREB mRNA as well as a scramble siRNA (negative control) were purchased from Ambion. In brief, the transfection reagent Lipofectamine RNAiMAX (Invitrogen) was diluted in Opti-MEM (Invitrogen) reduced media. The siRNAs were also diluted in Opti-MEM and then mixed with RNAiMAX to allow the formation of siRNA-RNAiMAX complex at room temperature for 20 minutes. Cell culture medium was replaced with media without antibiotics. The siRNA-RNAiMAX complexes were then added to the corresponding wells to reach a final concentration of 10 nM siRNA. Medium was replaced after 4~6 hours incubation in a 5% CO_2 incubator at 37 °C. Treatments were performed 24 hours from the start of silencing.

The constitutively active form CREB (VP16-CREB) and the dominant negative form CREB (serine 133 mutated to alanine, named M1-CREB) and the empty vector pCMV are kind gifts from Dr. David Ginty. In brief, cells were transfected with 1.5 μg pCMV, VP16-CREB or M1-CREB using Lipofectamine 2000 (Invitrogen) according to the manufacture's instruction. Medium was replaced after 4~6 hours and cells were incubated in fresh culture medium for up to 24 hours until treatment was carried out. To establish a stable cell line expressing M1-CREB, MSCs that are transiently transfected with M1-CREB for 24 hours were trypsinized and replated at low density in media containing 500 μg/ml geneticin (Invitrogen) for selection. For control, MSCs were also transfected with an empty pCMV vector containing neomycin resistance to establish a control cell line. The geneticin-containing media

was replaced every 3 days for two weeks. Colonies formed from surviving cells were isolated by cloning cylinders (Sigma) and maintained in culture media containing geneticin.

3.3.11 Statistical analysis

All experiments were performed at least three times and results were shown as mean ± standard deviation. Statistical analysis were carried out by an unpaired, two tail Student's t-test. * indicates $p<0.05$, ** indicates $p<0.01$ and *** indicates $p<0.001$.

3.4 Results

3.4.1 CREB regulates expression of some neural markers and dopamine response

CREB has been shown to be an important player in maturation and survival of newborn neurons in the central nervous system [206, 207]. Previously we observed that CREB was transiently activated during cAMP induced neural differentiation of MSCs [212], therefore, we examined whether CREB can regulate neural differentiation of MSCs. Neural induction by forskolin and IBMX (abbreviated as FI, two agents used to increase cAMP levels) increased the expression of neural markers, i.e. neuron-specific enolase (NSE), β-III tubulin (Tuj1) and glial fibrillary acidic protein (GFAP) (Figure 3.1A-B). Silencing of CREB reduced the expression of neuron marker NSE but not the neuron marker Tuj1 or the astrocyte marker GFAP (Figure 3.1A-B), indicating that cAMP-activated transcription factor, CREB, is

involved in regulating some of the neural markers. In addition to neural marker expression, FI also enabled MSCs to gain some neuronal function, such as calcium rise in response to neuronal activators dopamine, glutamate and KCl [212]. It is unclear how cAMP enabled MSCs to gain this function. To determine if CREB plays a role in this process, we silenced CREB in MSCs and assessed their dopamine response. After silencing with either a scramble siRNA (control) or CREB siRNA, MSCs were induced with FI for one day and their calcium rise in response to dopamine was measured as described in [212]. Although the CREB siRNA silenced cells were able to respond to dopamine as compared to the control cells (Figure 3.1C), the response was muted. Quantifying the percentage of dopamine responsive cells suggested that silencing CREB significantly reduced the dopamine response (Figure 3.1D), suggesting that CREB may influence the dopamine response elicited by cAMP.

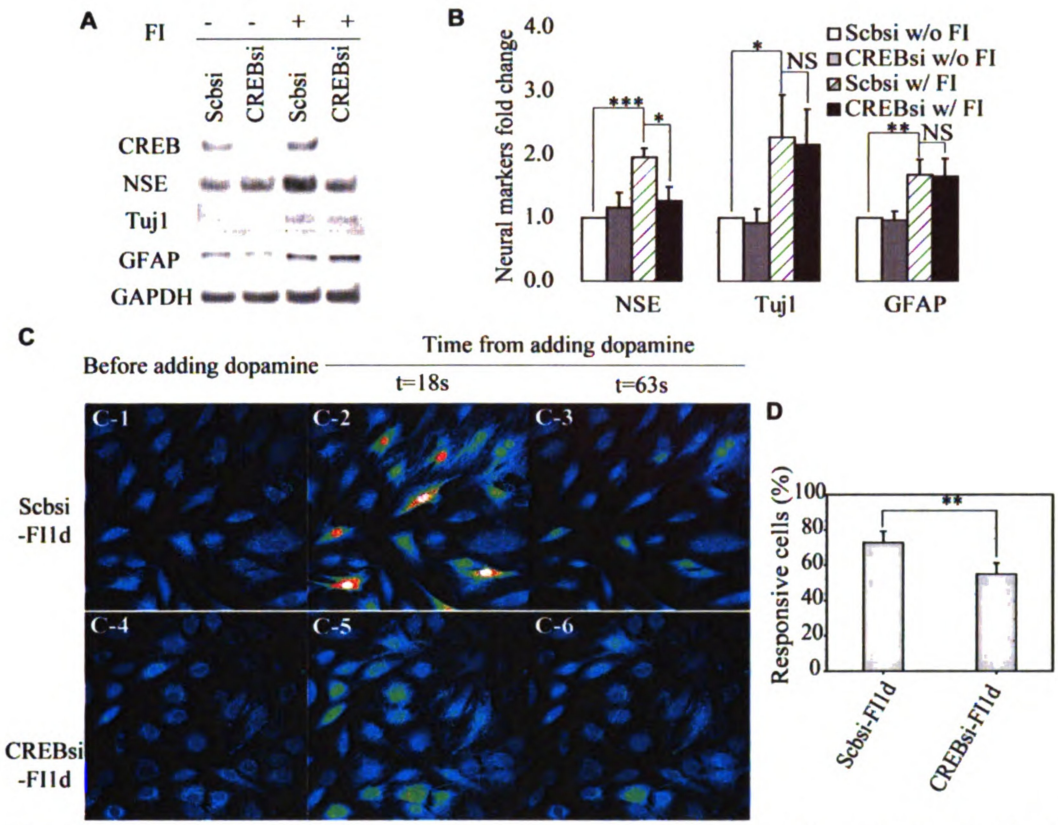

Figure 3.1. Effect of CREB on neural marker expression and calcium rise in response to dopamine. (A) Protein levels of neural markers NSE, Tuj1 and GFAP. MSCs were transfected with the control scramble siRNA or CREB siRNA and incubated in the absence or presence of 10 μM forskolin and 100 μM IBMX (FI) for 1 day. (B) Quantification of protein levels fold change for NSE, Tuj1 and GFAP (n=3). *: $p<0.05$; **: $p<0.01$; ***: $p<0.001$; NS: not significant. (C) Calcium imaging in response to neuronal activator dopamine. (C-1 to C-3) MSCs transfected with a scramble siRNA (control) and induced by FI for 1 day responded upon stimulation with 100 μM dopamine. (C-4 to C-6) MSCs transfected with CREB siRNA and induced FI for 1 day stimulated with 100 μM dopamine. Images were captured before dopamine stimulation or 18 and 63 seconds after dopamine stimulation. Fluorescence images represented by a spectral table; warmer colors indicate higher fluorescence intensities and cooler colors indicate lower fluorescence intensities. (D) Quantification of the percentage of cells responsive to dopamine (n=4). **: $p<0.01$.

3.4.2 CREB regulates calcium rise in response to several neuronal activators

To assess further the long term effect of CREB on neuronal function, we engineered MSCs to stably express the dominant negative form of CREB (M1-CREB, whose serine 133 site is mutated to alanine) and compared their response to MSCs

stably transfected with a control vector that contains neomycin-resistance. MSCs stably expressing M1-CREB, denoted as M1-MSCs, have higher total CREB expression than the control MSCs (Appendix Figure 3.1A). M1-MSCs grew slightly slower as compared with MSCs expressing the control vector (Appendix Figure 3.1B) and are able to form colonies (Appendix Figure 3.1C). To assess for neuronal function, we used three neuronal activators: dopamine, glutamate and KCl as described previously [212]. The response of M1-MSCs to dopamine is similar to MSCs (Figure 3.2A and 3.2C). After FI induction for one week, however, M1-MSCs lost their ability to respond to dopamine as compared to MSCs (Figure 3.2B and 3.2D). Quantification of the results suggests that the uninduced M1-MSCs and uninduced MSCs respond similarly to dopamine, KCl and glutamate (Figure 3.3A). After a week of FI induction however, the response to dopamine, KCl and glutamate dramatically reduced or disappeared in M1-MSCs (Figure 3.3A). When a constitutively active form of CREB (VP16-CREB) was transiently introduced into M1-MSCs, their response to dopamine, KCl and glutamate partially recovered (Figure 3.3A), suggesting a role of CREB in the calcium rise in response to the neuronal activators. Generation of calcium signals can be achieved through both internal and external sources of Ca^{2+} [221]. The influx of external Ca^{2+} into cells is mainly regulated by membrane receptor-operated channels and voltage-operated channels, while release of internal Ca^{2+} from endoplasmic reticulum (ER) can be controlled by second messengers, such as inositol-1,4,5-trisphosphate (IP3) and Ca^{2+} itself [222]. Dopamine, glutamate and KCl can generate Ca^{2+} signals through membrane receptor-

operated channels and voltage- operated channels, and Ca^{2+} influx through these membrane channels can further stimulate the release of calcium from the intracellular ER stores [214-216, 218, 219]. Since the response of M1-MSCs to dopamine, glutamate and KCl was compromised (Figure 3.3A), we determined whether the decrease or loss of response to the neuronal activators is related to a general damage of the membrane receptors and intracellular ER stores. We applied a positive control, ATP, which is able to elicit calcium signals from the external and internal calcium sources through the membrane bound P2X inotropic receptors and P2Y receptor-operated channels [223, 224]. M1-MSCs induced with FI for a week can still respond to ATP (Figure 3.3B), suggesting that the reduction or loss of calcium rise in response to the neuronal activators may not be due to a general damage of the plasma membrane or ER.

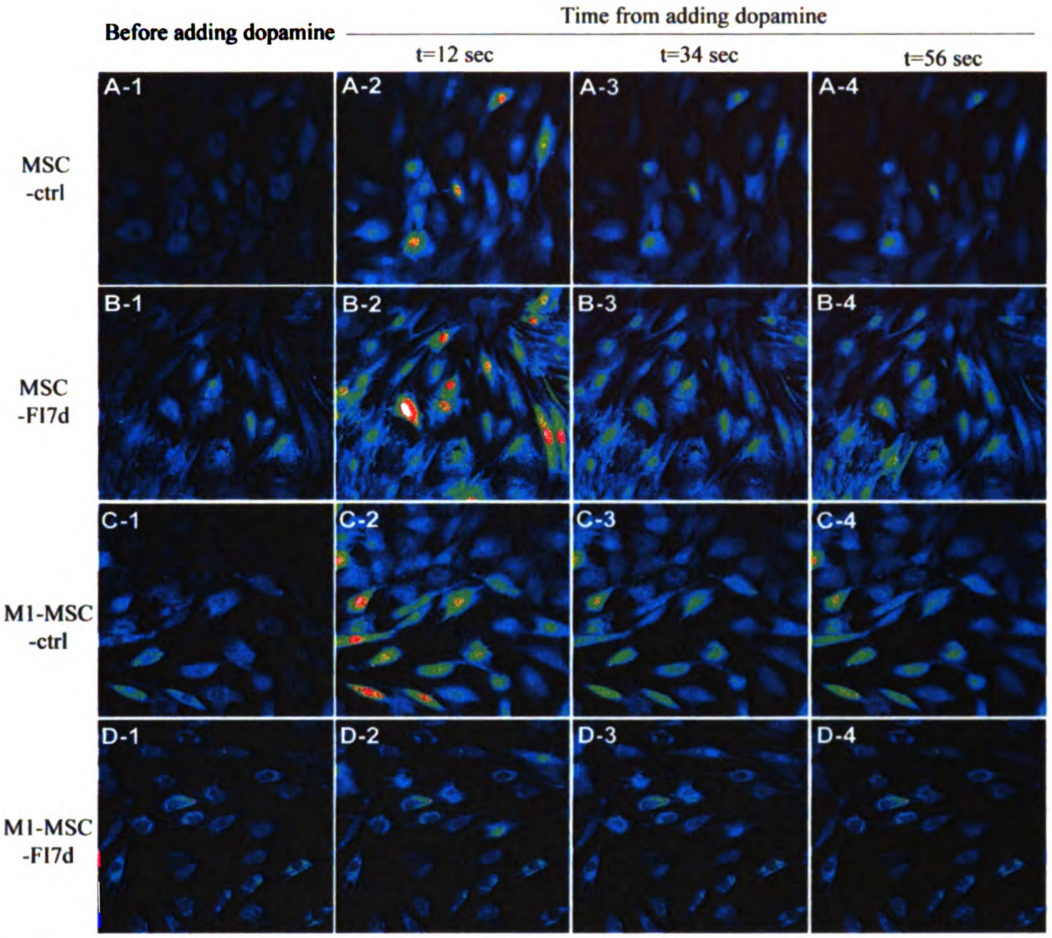

Figure 3.2 Calcium imaging in response to neuronal activator dopamine. (A-1 to A-4) Uninduced MSCs (expressing control vector) before dopamine stimulation and 12, 34 and 56 seconds after 100 μM dopamine stimulation. (B-1 to B-4) MSCs (expressing control vector) induced with 10 μM forskolin and 100 μM IBMX (FI) for 7 days before and after dopamine stimulation. (C-1 to C-4) Uninduced M1-MSCs (expressing M1-CREB) before and after dopamine stimulation. (D-1 to D-4) M1-MSCs induced with FI for 7 days before and after dopamine stimulation. Fluorescence images represented by a spectral table; warmer colors indicate higher fluorescence intensities and cooler colors indicate lower fluorescence intensities.

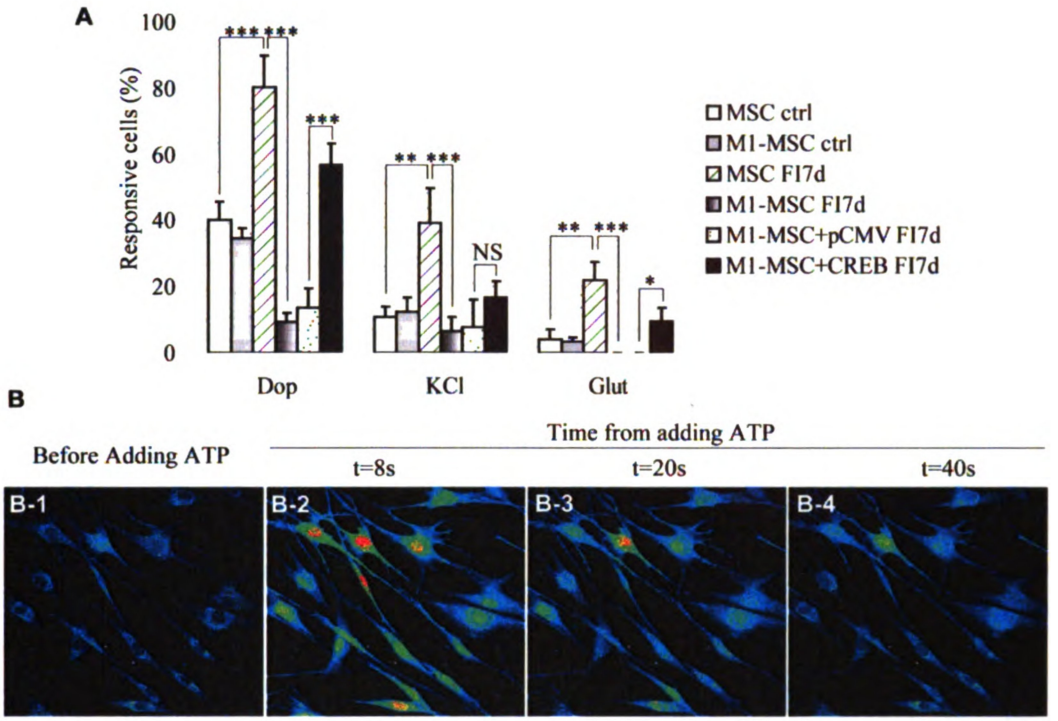

Figure 3.3 Calcium signaling upon stimulation by neuronal activators and ATP. (A) Quantification of the percentage of cells that respond to neuronal activators, dopamine, KCl and glutamate. MSCs (expressing control vector) and M1-MSCs (expressing M1-CREB) were either uninduced or induced with 10 μM forskolin and 100 μM IBMX (FI) for 7 days. To assess whether reintroducing CREB restores the response of the M1-MSCs to neuronal activators, either pCMV or the constitutively active VP16-CREB was introduced and the cellular calcium response was examined (n=4). *: $p<0.05$; **: $p<0.01$, ***: $p<0.001$; NS: not significant. (B) Calcium imaging in response to the positive control ATP for M1-MSCs induced with FI for 7 days. Images were captured before ATP stimulation and 8, 20 and 40 seconds after ATP stimulation. Fluorescence images represented by a spectral table; warmer colors indicate higher fluorescence intensities and cooler colors indicate lower fluorescence intensities.

3.4.3 CREB regulates expression of certain dopamine receptors

To investigate the possibility that CREB modulates the calcium response upon stimulation by the neuronal activator, and since dopamine elicited a robust calcium response in MSCs (Figure 3.3A), we used dopamine. Dopamine modulates calcium signal mainly by binding to the dopamine receptors, which consists of the D1-like (include D1 and D5) and the D2-like (include D2, D3 and D4) families of receptors

[218]. Promoter analysis revealed that these dopamine receptors contained a half CRE sequence (TGACG/CGTCA) [34] and may be regulated by CREB [225]. Thus we hypothesized that CREB modulates the expression of these dopamine receptors to impact calcium signaling. No prior studies examined the expression of all the dopamine receptors in MSCs, and only one study indicated that the expression of D1 is detected in uninduced human MSCs [226]. In this study, we observed that mRNA levels of dopamine receptor D3 and D5 were not affected by CREB silencing (Figure 3.4A), and the expression of dopamine receptor D2 mRNA level was undetectable in MSCs (data not shown). To our surprise, knock down of CREB activity increased rather than decreased mRNA levels of dopamine receptor D1 and D4 after FI induction for one week (Figure 3.4A). While dopamine receptor D1 positively regulates calcium signaling, dopamine receptor D4 can either positively or negatively regulate calcium signaling in a context- and cell type-dependent manner [218]. Moreover, D1 and D2 are the most abundant dopamine receptors in mature brain [227]. Due to a more definitive role of D1 in regulating calcium signaling and its predominant expression in mature brain, we therefore measured D1 protein expression using both immunoblotting and immunostaining. Immunoblotting results suggest that M1-MSCs treated with FI for 7 days have much lower D1 expression than MSCs treated with FI for 7 days (Figure 3.4B). The immunostaining results confirmed the immunoblotting results, i.e. down-regulating CREB activity did not increase but rather decreased the dopamine receptor D1 protein level. Fluorescence intensity of individual M1-MSCs (expressing M1-CREB) appears to be lower than of

the control MSCs (Figure 3.4C-D). Although knock down of CREB activity in the M1-CREB cells increased dopamine receptor D1 mRNA level, it did not translate to an increase in the D1 protein level, but rather to a reduction in the D1 protein level which may contribute, in part, to the reduced dopamine response. The disagreement in mRNA and protein levels of D1 may due to post-transcriptional regulation. Indeed, a previous study showed that an increase in the D1 receptor mRNA level did not result in an increase in the D1 protein level in a mouse neuronal cell line [228]. While a downregulation in the protein level of D1 receptor may play a role in diminishing calcium signaling in M1-CREB cells, this does not preclude other mechanisms that contribute to the CREB-mediated calcium response elicited by dopamine [182, 218].

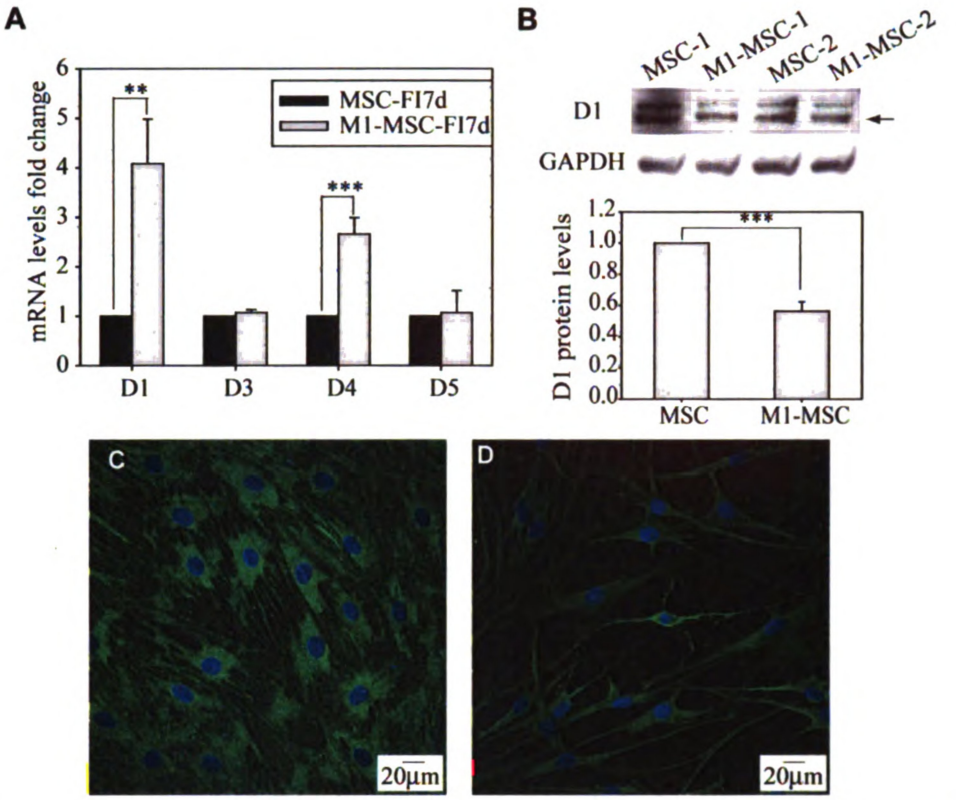

Figure 3.4 Expression of dopamine receptors. (A) mRNA levels of dopamine receptors D1, D3, D4 and D5 for MSCs (expressing control vector) and M1-MSCs (expressing M1-CREB) treated with 10 μM forskolin and 100 μM IBMX (FI) for 7 days (n=3). **: $p<0.01$, ***: $p<0.001$. (B) Protein levels of dopamine receptor 1 (D1) for MSCs and M1-MSCs treated with FI for 7 days (n=3 for quantification). (C) Dopamine receptor D1 staining for MSCs. (D) Dopamine receptor D1 staining for M1-MSCs. Green: D1 staining; blue: nucleus staining.

3.4.4 CREB participates in regulating morphology and survival

Previously, we showed that FI induced neuron-like morphology changes due primarily to cell shrinkage [212]. The neuron-like morphology decreased as the FI induction continued and nearly disappeared after one week of induction (Figure 3.5A). In contrast, one week of FI induction of M1-MSCs appeared to promote a neuron-like morphology with long threads resembling neurites radiating from the cell center (Figure 3.5B). The morphology changed gradually; the M1-MSCs initially appeared similar to the MSCs, but continuous remodeling of the cytoskeleton during FI

induction resulted in neurite-like extensions (Appendix Figure 3.2). However, these neurite-like extensions lack the expression of the pan neuronal marker, Tuj1 (Figure 3.5C, arrow). Immunostaining with the synaptic marker, synapsin, indicates that synapsin is found near the body but not within the neurite-like structures (Figure 3.5C, arrow head). There are a few cells that have Tuj1 staining within the neurite-like structures (Figure 3.5D, arrow); however, they do not stain for synapsin within these structures. These results indicate that although knock-down of CREB promoted the adoption of neurite-like structures, these structures are still quite different from mature neurites. Nevertheless, it is surprising that CREB is required to gain neuronal function yet it appears to prohibit the adoption of a neuron-like morphology. Similar contrasting effects between function and morphology have been reported in retinoid-mediated differentiation of human monoblastic U937 cells, where CREB facilitated functional maturation but inhibited morphological differentiation of these cells [229]. However, it remains a mystery how CREB manages this.

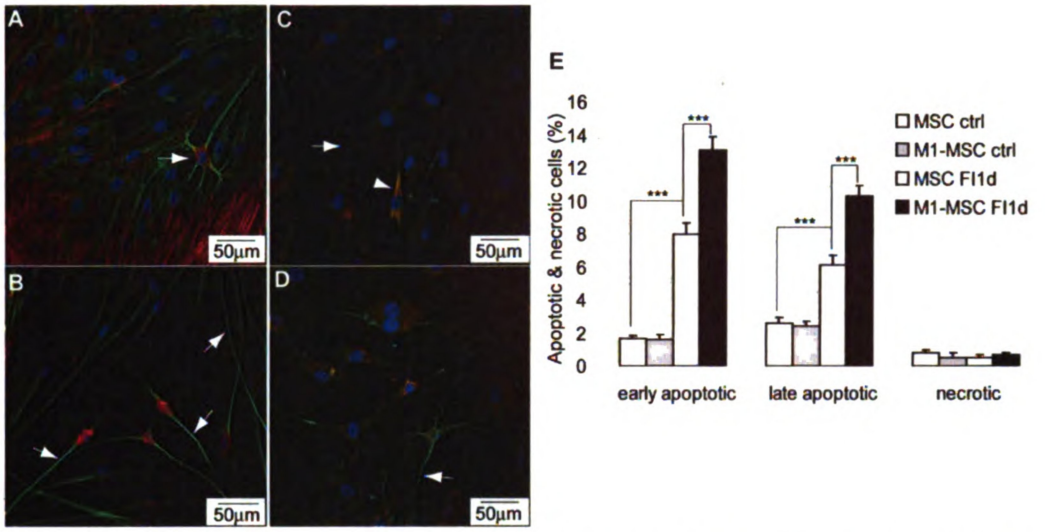

Figure 3.5 CREB affects morphology and apoptosis. (A) Morphology of MSCs (expressing control vector) induced with 10 μM forskolin and 100 μM IBMX (FI) for 7 days. Green: microtubules; red: actin filaments; blue: nucleus. (B) Morphology of M1-MSCs (expressing M1-CREB) induced with FI for 7 days. (C-D) M1-MSCs induced with FI for 7 days stained with antibody against the pan neuronal marker, Tuj1 (green), and the synaptic marker, synapsin (red). Nucleus is counterstained with DAPI. (E) Apoptotic and necrotic labeling by Alexa Fluor-488 conjugated annexin *V* and PI (propidium iodide), respectively, of control cells and cells treated with FI for 1 day and 2 days. *Early apoptotic cells:* PI^- annexin V^+ cells; *late apoptotic cells*: PI^+ annexin V^+ cells; *necrotic cells*: PI^+ annexin *V* cells (n=3). ***: $p<0.001$.

Furthermore, CREB is required for maintaining cell viability. Since fewer M1-MSCs remained attached upon FI induction as compared to the control MSCs (Figure 3.5A-B), we assessed whether knock down of CREB activity caused apoptosis. FI induction itself resulted in significant increases in both early apoptotic and late-apoptotic cells for both M1-MSCs and control MSCs (Figure 3.5E). FI induced apoptosis is not likely due to the concentration of FI used, since 10 μM forskolin and 100 μM IBMX only caused a slight but insignificant increase in toxicity as indicated by lactate dehydrogenase (LDH) release (Appendix Figure 3.3). Knock down of

CREB activity did not increase apoptosis or necrosis in the control medium, however, it greatly enhanced apoptosis upon FI induction (Figure 3.5E), suggesting that CREB plays a protective role against FI induced apoptosis in MSCs.

3.4.5 CREB does not affect G1 phase lengthening

Two important features of stem cells are: unlimited self-renewal to generate daughter stem cells and differentiation into multiple cell lineages [230]. When stem cells differentiate, the G1 phase is lengthened, and proliferation is slowed to allow sufficient time for differentiation [231, 232]. We observed that cAMP rendered MSCs to accumulate in the G0/G1 phase and resulted in a lengthened G1 phase. Uninduced MSCs progressed normally into the S and G2/M phases after release from cell cycle synchronization (Figure 3.6A-C). When MSCs were induced with FI, the cells were retained in the G0/G1 phase without progressing into the S and G2/M phases (Figure 3.6D-F), lengthening the G1 phase or arresting cell cycle in G1. CDK4/6 are the first to be activated during G1/S transition [71], and their activities is positively regulated by cyclin D and negatively by CDK inhibitors (CKIs), such as $p27^{kip1}$ [70]. Although the expression level of CDK4/6 did not changed, the expression level of the positive cell cycle regulator cyclin D1 (CCND1) decreased (Figure 3.6G) while the negative regulator $p27^{kip1}$ increased upon FI treatment (Figure 3.6G). Both down-regulation of CCND1 and up-regulation of $p27^{kip1}$ may contribute to lengthening of the G1 phase and thereby slowing proliferation. In support, a proliferation assay indicated that the

number of cells in the FI treated condition was significantly lower as compared to control, both on day 1 and day 2 (Figure 3.6H).

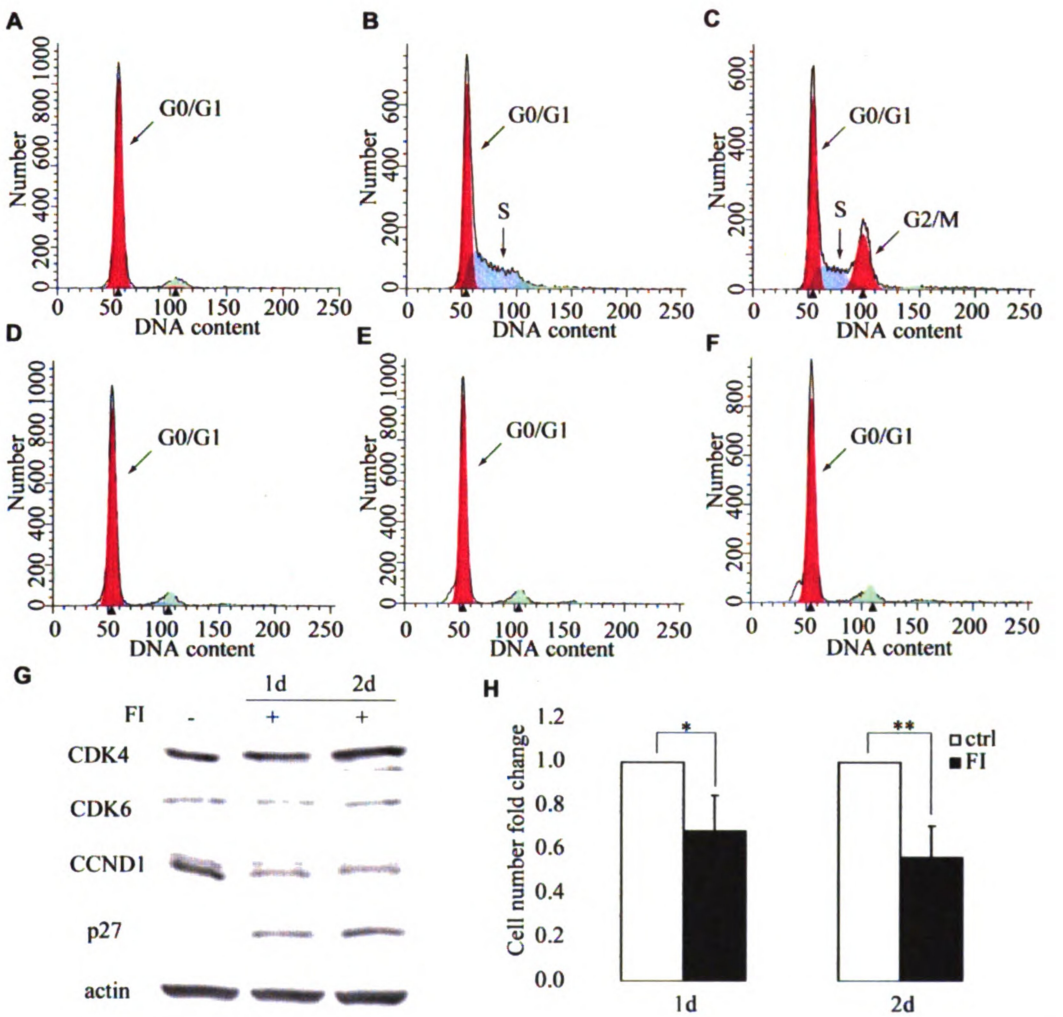

Figure 3.6 Cell cycle progression, cell cycle gene expression and cell proliferation of MSCs and MSCs induced with 10 μM forskolin and 100 μM IBMX (FI). (A-C) MSCs in control media for 5, 15 and 20 hours after release from cell cycle synchronization. (D-F) MSCs induced with FI for 5, 15 and 20 hours after release from cell cycle synchronization. (G) Expression of cell cycle regulators CDK4, CDK6, cyclin D1 (CCND1) and $p27^{kip1}$ of control cells and cells treated with FI for 1 and 2 days. (H) Proliferation of untreated MSCs and cells treated with FI for 1 and 2 days (n=3). *: $p<0.05$, **: $p<0.01$.

Many of the cell cycle regulators are potential CREB target genes. CCND1 is a known CREB target gene [34] while $p27^{kip1}$ is predicted to have half CRE sequences and therefore is a putative CREB target gene [225]. Therefore, we set out to determine if CREB can impact cell cycle progression by regulating genes, such as CCND1 and $p27^{kip1}$, and subsequently contribute to lengthening of the G1 phase. Overexpression of CREB by introducing the constitutively active form of CREB increased expression of the exogenous VP16-CREB protein near 60kD, whereas CREB knock-down by siRNA nearly abolished endogenous CREB protein level (Figure 3.7A). Overexpression of CREB increased CCND1 protein levels significantly in control media, however, it did not increase CCND1 protein significantly in the FI condition (Figure 3.7A-B). Protein level of $p27^{kip1}$ was essentially unaffected by CREB (Figure 3.7A-B). Since the protein levels of CCND1 and $p27^{kip1}$ were affected minimally by FI treatment, it is likely that CREB may not affect G1 phase lengthening induced by cAMP. Indeed, the percentage of cells in the G1/G0 phase was unaffected by CREB overexpression or silencing (Figure 3.8 and Appendix Figure 3.4), suggesting that G1 phase lengthening initiated by cAMP is not regulated by CREB.

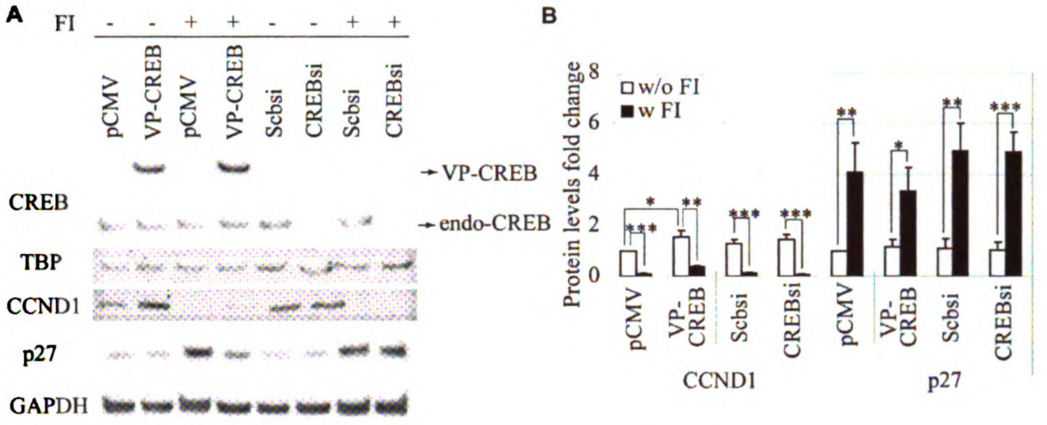

Figure 3.7 Effect of CREB on CCND1 and $p27^{kip1}$ expression. (A) CREB overexpression is achieved by transfection of the constitutively active VP16-CREB and silencing is achieved by CREB siRNA. pCMV and scramble siRNA are used as controls. Transfected cells were incubated in the absence or presence of 10 μM forskolin and 100 μM IBMX (FI) for 1 day. Western blotting is carried out for nuclear extracts and whole cell extracts. TBP and GAPDH are used as loading controls. (B) Quantification of CCND1 and $p27^{kip1}$ protein levels (n=3). *: $p<0.05$; **: $p<0.01$; ***: $p<0.001$.

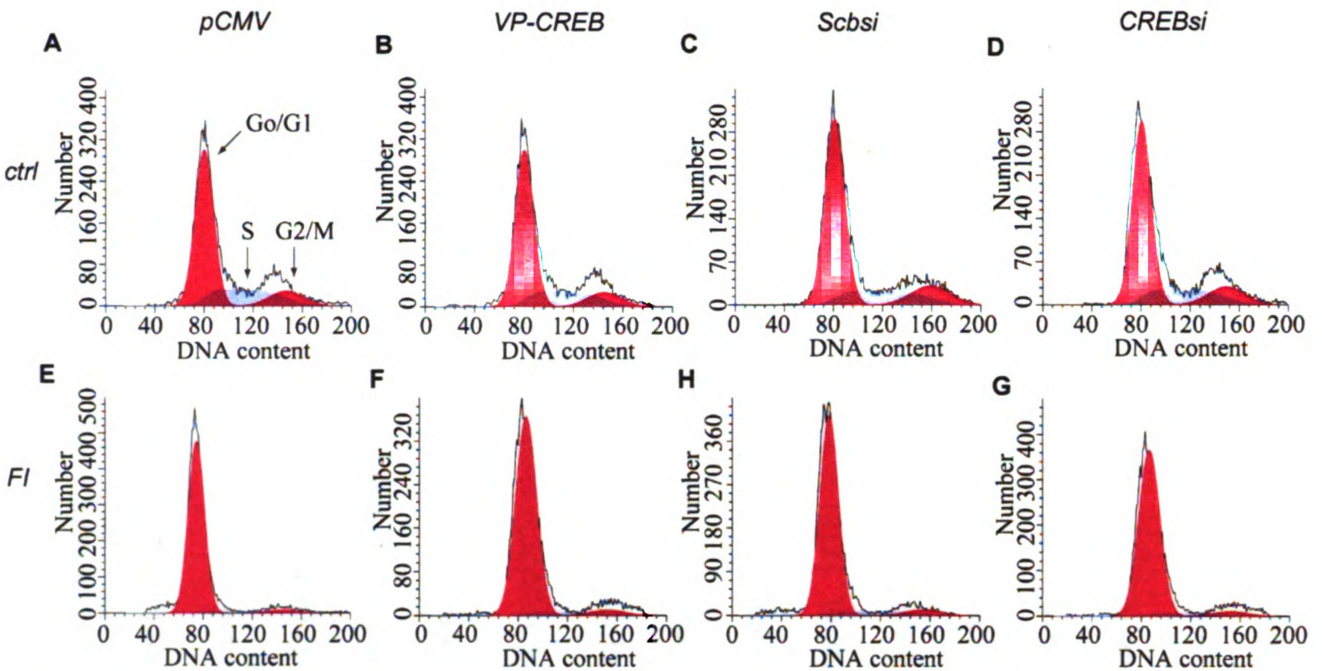

Figure 3.8 Cell cycle distribution for cells overexpressing the constitutively active VP16-CREB and silenced with CREB siRNA. pCMV and scramble siRNA are used as controls. (A-D) Transfected cells in control medium 20 hours after release from synchronization. (E-H) Transfected cells treated with 10 μM forskolin and 100 μM IBMX (FI) for 20 hours after release from synchronization.

3.5 Discussion

cAMP elevating reagents have been widely used in neural induction medium [4, 153, 155, 156], however the intracellular players in the cAMP signaling pathway that initiate neural differentiation in MSCs is unclear. The regulation of neural differentiation initiated by cAMP remains largely unknown. The two studies that attempted to uncover the signaling pathways that lead to neural differentiation relied on morphological changes [153, 156], which we as well as others have shown to be an artifact [159, 212] and are not good indicators of neural differentiation. Apart from the morphological changes, cAMP indeed enabled MSCs to express neural lineage markers and increase calcium response upon stimulation by neuronal activators [212]. In this study, we found that cAMP activated the transcription factor, CREB, which plays an important role in regulating calcium signal induced by the neuronal activators, dopamine, glutamate and KCl. It is well known that CREB activity can be modulated by the calcium activated Ca^{2+}/calmodulin-dependent protein kinases (CaMKs), which can phosphorylate CREB at several serine sites and thereby modulate the transcriptional activity of CREB [30]. However, the impact that CREB may have on calcium signaling is not known. In this study, we observed that both silencing CREB and using a dominant negative CREB (M1-CREB) reduced the calcium signal upon neuronal activator stimulation (Figure 3.1C-D, 3.2 and 3.3A), suggesting that CREB plays a role in regulating calcium signaling. When M1-MSCs (expressing M1-CREB) were induced with FI for one week, the calcium response to dopamine, glutamate and KCl either reduced dramatically or totally disappeared (Figure 3.3A). Reintroducing the constitutively active CREB into the M1-MSCs was able to partially restore the calcium response (Figure 3.3A).

How CREB regulates calcium signaling remains a mystery. Since the calcium response stimulated by the positive control ATP remained intact, we hypothesized that the impaired calcium rise in response to the neuronal activators upon knock down of CREB may be due to downregulation of the membrane receptors that respond to these neuronal activators. Thus, we investigated the effect of CREB on the expression of the dopamine receptors since dopamine elicited the most robust response (Figure 3.3A). Knock down of the CREB activity by M1-CREB did not decrease but rather increased the mRNA level of several dopamine receptors, i.e. dopamine receptor D1 and D4 (Figure 3.4A). Since D1 is the predominant isoform in the brain and the effect of D1 on calcium signaling is more definitive [218, 227], we examined the protein level of D1. M1-MSCs, which express M1-CREB, have lower expression of dopamine receptor D1 as compared to the control MSCs (Figure 3.4B-D). Reduction of dopamine receptors may partially contribute to the reduced dopamine response observed (Figure 3.3A). However, other possible mechanisms cannot be ruled out. The stimulation of calcium signal by dopamine is complex and can be controlled by various mechanisms, including stimulation of phospholipase C (PLC) activity, phosphorylation of calcium channels, regulation of dopamine receptor interacting proteins (DRIPs) and potentiation of NMDA receptors [181, 182, 218]. Therefore, CREB may have both direct as well as indirect impact on the calcium signal elicited by dopamine. Besides dopamine, CREB also modulated the calcium signals generated by glutamate and KCl (Figure 3.3A). CREB has been reported to transcriptionally regulate the AMPA glutamate receptor subunit GluR1 [233, 234]. In addition, a microarray analysis study suggested that CREB may regulate the expression of certain ion channels, such as a sodium channel subunit and a cation channel subunit in

neurons [235]. Therefore, in addition to regulating the membrane receptors, it is also possible that CREB may modulate calcium signal by regulating the expression of ion channels. Since the regulation of the calcium signal by the neuronal activators involves a variety of signaling components [214-216, 218], unraveling the complete mechanism by which CREB regulates calcium signaling remains an important task for the future.

In contrast to the positive affect CREB has on calcium signaling in response to neuronal activators, CREB appears to inhibit the neuron-like morphology. While the control MSCs show a flat morphology one week after FI induction (Figure 3.5A), the M1-MSCs show long neurite-like projections extending from the cell body (Figure 3.5B). These neurite-like projections look very different from the neurite-like projections we observed in our previous study, that resulted from cell shrinkage and are shorter and with dimensions on the size of a cell [236]. Here the neurite-like projections initiated by knocking down CREB are much longer than the dimensions of the cell (Figure 3.4D, 3.5B and Appendix Figure 3.2) and therefore not likely due to cell shrinkage. This suggests CREB may inhibit the neuron-like morphology (Figure 3.4C and 3.5A). This inhibitory affect is removed upon expressing the M1-CREB protein, thereby allowing the cells to adopt a neuron-like morphology (Figure 3.4D and 3.5B). However, the neurite-like extensions mostly lack expression of the neuronal marker, Tuj1, and the synaptic marker, synapsin (Figure 3.5C and 3.5D) and therefore are not likely mature neurites. Nevertheless, CREB appears to have contrasting effects on neuronal function and morphology. Such contrasting effects of CREB on the function and morphology have been observed in a retinoid-mediated differentiation study of human monoblastic U937 cells, whereby CREB promoted functional maturation but suppressed morphological

differentiation [229]. However, it remains unclear how CREB achieved this. The finding that CREB inhibits morphological differentiation of MSCs appears to contradict the previous finding that CREB promotes dendrite growth of newborn neurons in the adult hippocampus [237]. This discrepancy may arise due to the different cell types and cell status in the differentiation process. In our study, MSCs are mesodermal cells and were induced with cAMP to differentiate into ectodermal neural lineage cells. Although cAMP enabled MSCs to transdifferentiate into neural lineage cells, these cells are not truly functional neurons yet [212]. In the study by Fujioka and coworkers, the cells are newborn neurons in the adult hippocampus, which are closer to mature neurons than the neural cells derived from MSCs. The timing of when CREB activity is turned-on and -off may be critical for non-neural originating stem cells to adopt a neural lineage fate that contains both the morphology and function of terminally differentiated cells. A stage-dependent effect on differentiation was reported for the Wnt/β-catenin signaling pathway during cardiac lineage differentiation of embryonic stem cells (ESCs). While early activation of Wnt/β-catenin signaling promotes cardiac lineage of ESCs, late activation of Wnt/β-catenin signaling was shown to inhibit cardiac lineage differentiation [238, 239].

While CREB affects differentiation of MSCs, it does not appear to influence G1 phase lengthening in MSCs. Overexpressing and silencing CREB activity did not significantly affect the cell cycle genes CCND1 and $p27^{kip1}$ (Figure 3.7), nor did it impact G1 phase lengthening (Figure 3.8 and Appendix Figure 3.4), suggesting that CREB does not contribute to cAMP induced G1 phase lengthening. Nevertheless, CREB appears to be required to protect the cells from cAMP induced apoptosis (Figure 3.5E).

In conclusion, we examined the role of CREB in cAMP induced neural differentiation of MSCs. CREB has diverse roles during cAMP induced neural differentiation of MSCs, positively impacting calcium signaling in response to neuronal activators but negatively impacting the adoption of neuron-like morphology.

Chapter 4. Synergistic effect of cAMP and palmitate in promoting altered mitochondrial function and cell death in HepG2 cells

This work has been published in Experimental Cell Research:
Zhang, L., Seitz, L.C., Abramczyk, A.M. and Chan, C. Synergistic effect of cAMP and palmitate in promoting altered mitochondrial function and cell death in HepG2 cells. Exp Cell Res (2010) 316 (5), 716-727.

4.1 Abstract

Saturated free fatty acids (FFAs), e.g. palmitate, have long been shown to induce toxicity and cell death in various types of cells. In this study, we demonstrate that cAMP synergistically amplifies the effect of palmitate on the induction of cell death in human hepatocellular carcinoma cell line, HepG2 cells. Elevation of cAMP level in palmitate treated cells led to enhanced mitochondrial fragmentation, mitochondrial reactive oxygen species (ROS) generation and mitochondrial biogenesis. Mitochondrial fragmentation precedes mitochondrial ROS generation and mitochondrial biogenesis, and may contribute to mitochondrial ROS overproduction and subsequent mitochondrial biogenesis. Fragmentation of mitochondria also facilitated the release of cytotoxic mitochondrial proteins, such as Smac, from the mitochondria and subsequent activation of caspases. However, cell death induced by palmitate and cAMP was caspase-independent and mainly necrotic.

4.2 Introduction

Exposure of non-adipose cells, including β-cells, cardiomyocytes and hepatocytes, to excess free fatty acids (FFAs) has been shown to induce lipotoxicity and cell death [160, 162, 240-246]. While elevated unsaturated FFAs, such as oleate and linoleate, are better tolerated, elevated saturated FFAs, such as palmitate, can cause cellular damage and even cell death [160, 240]. cAMP (cyclic adenosine monophosphate), an important second messenger, has been shown to protect pancreatic β-cells from palmitate induced apoptosis [14, 247]. In addition, cAMP was also reported to protect hepatocytes from bile acid [7, 248], Fas ligand [13, 248] and TNF-α [11, 248] induced apoptosis. Previously we showed that intracellular cAMP levels in HepG2 cells were reduced significantly by palmitate, but not oleate or linoleate [163]. Therefore, we initially hypothesized that the down-regulation of cAMP by palmitate may play a role in the induction of cell death. However, restoring cAMP levels in HepG2 cells did not rescue the cells from palmitate-induced toxicity. Moreover, when cAMP level was increased to a high concentration, it synergized with palmitate to promote cell death. cAMP has been proposed as a potential drug target for type 2 diabetes [249], since it appears to enhance insulin secretion. Given that FFAs, which are elevated in obesity and diabetes [250-252], can induce hepatotoxicity, it warrants evaluating the effect of cAMP in the presence of elevated FFAs. In this study, we assess the effect of cAMP on hepatotoxicity and cell death under elevated levels of FFAs.

Mitochondria serve as an integrator for cell death and survival signals [253, 254], regulating both apoptosis and necrosis. The onset of mitochondrial membrane permeabilization (MMP) releases a number of cytotoxic proteins, such as cytochrome C

and Smac (second mitochondria-derived activator of caspase), from the intermembrane space of mitochondria [255]. Release of these cytotoxic proteins activates both caspase-dependent and -independent cell death [255] and such release can be controlled by mitochondrial morphology. In healthy cells, the mitochondria display an elongated and interconnected structure. When a cell becomes apoptotic, its mitochondrial network is disrupted into short and disconnected structure [256, 257]. Mitochondrial function is also altered in necrosis, manifesting in diminished mitochondrial ATP production [258]. Apoptosis and necrosis can occur simultaneously in the same cell. Cells in late stage apoptosis may contain necrotic features due to the energy loss and permeabilization of the plasma membrane [259].

Regulation of cell death by mitochondria is intimately tied with generation of reactive oxygen species (ROS) in the mitochondria [260]. Superoxide anion ($O_2^{-}\bullet$), which is the precursor of most ROS, is primarily generated at Complex I and III in the mitochondria [260]. $O_2^{-}\bullet$ itself is not a strong oxidant. Dismutation of superoxide by superoxide dismutase (SOD) can produce a stronger oxidant, hydrogen peroxide (H_2O_2), which can be partially reduced to generate one of the strongest oxidants, hydroxyl radical (HO•) [261]. Together these oxidants can damage cellular components, proteins and resulte in cell death [261].

This study aims to evaluate how cAMP and FFAs affect hepatocyte survival and death behavior. Our results suggest that a high cAMP level potentiates mitochondrial fragmentation, mitochondrial ROS generation and necrotic cell death initiated by palmitate.

4.3 Materials and methods

4.3.1 Cell culture and materials

Human hepatocellular carcinoma cell line HepG2 cells were obtained from American Type Culture Collection. Cells were cultured in DMEM (Dulbecco's modified Eagle's medium) (Invitrogen) containing 10% FBS (fetal bovine serum) (Invitrogen) and 2% PS (Penicillin-Streptomycin) (Invitrogen) at 37 ^{o}C in 10% CO_2 atmosphere incubator. Saturated free fatty acid palmitate, monounsaturated free fatty acid oleate and polyunsaturated free fatty acid linoleate were purchased from Sigma in the form of sodium salts. These free fatty acids were prepared in medium containing 4% (w/v) fatty acid free BSA (bovine serum albumin) (USBiologicals) at concentration of 0.7 mM. In this study, we used 0.7 mM FFAs concentration since several studies have reported the physiological plasma FFAs level in obese and diabetic patients is around 0.7 mM [250-252]. For palmitate, concentrations of 0.2 mM and 0.4 mM were also prepared. 4% (w/v) BSA in culture medium (medium/BSA) was used as control. 1 μM or 10 μm Forskolin (Sigma), 100 μM isobutylmethylxanthine (IBMX) (Sigma), 1 μM 8CPT-2Me-cAMP (Sigma) and 100 nM glucagon (Sigma) were used to restore cAMP levels. 25 mM N, N'-Dimethylurea (DMU) (Sigma), 100 μg/ml catalase (Sigma), 5 μM Copper (II) 3,5-diisopropylsalicylate (Cu-DIPS) (Sigma) and 50 μM MnTBAP (Biomol) were used as reactive oxygen species scavengers. 10 μM etomoxir (Sigma) was used to inhibit fatty acid oxidation.

4.3.2 Measurement of cytotoxicity

The cytotoxicity of the treatments was measured by release of LDH (lactate dehydrogenase) into the medium according to the manufacture's instructions (Roche Applied Science) as previously described [162]. Briefly, medium was collected after 24 hours. Cells were lysed in 1% Triton-X100 in PBS at 37 ^{o}C overnight and supernatant was collected. LDH released into medium was denoted as LDH_m, and LDH that was retained in the cells was denoted as LDH_c. LDH activity was measured by the colorimetric assay kit (Roche Applied Science) using plate reader SPECTRAmax plus384 from Molecular Device. Percentage of release was calculated by the following equation: LDH release %= $LDH_m/(LDH_m+LDH_c)*100$.

4.3.3 cAMP assay

Intracellular cAMP levels were measured by a competitive immunoassay from Assay Designs according to the manufacturer's instructions. In brief, cells were lysed with 0.1 M HCl and supernatants were collected. cAMP in the samples or standards was allowed to bind to a polyclonal cAMP antibody in a competitive manner with alkaline phosphatase-conjugated cAMP. Cleavage of the substrate by the alkaline phosphatase is inversely proportional to the cAMP level in the samples or standards. Colorimetric readings were taken by SPECTRAmax plus384 from Molecular Device at 405 nm. All the readings were normalized to protein level (μg/ml) by Bradford assay.

Caspase 3 activity was measured by a kit from BIOMOL according to the manufacture's instructions. Briefly, Cell extracts were incubated with substrate Ac-DEVD-AMC. The cleavage of the substrate will generate fluorescence which is proportional to the concentration of the active caspase 3 in cell extracts. Fluorescence

was measured by Spectra MAX GEMINI EM plate reader at excitation of 360 nm and emission of 460 nm. All the readings were normalized to protein levels (μg/ml) by Bradford assay.

4.3.4 Measurement of reactive oxygen species (ROS)

Cellular ROS levels were measured using a cell-permeable probe 2',7'-Dichiorofluorescin diacetate (DCFDA) (Sigma). Cells were loaded with 10 μM DCFDA in PBS for 30 minutes. After washing cells with PBS twice, fluorescence was measured by Spectra MAX GEMINI EM plate reader at excitation of 495 nm and emission of 525 nm. All the readings were normalized to protein levels (μg/ml) by Bradford assay. Mitochondrial superoxide levels were measured using MitoSOX (Invitrogen) mitochondrial superoxide indicator. Cells were loaded with 2.5 μM MitoSOX for 10 minutes at 37 ^{o}C. After washing cells with PBS twice, fluorescence was measured by Spectra MAX GEMINI EM plate reader at excitation of 510 nm and emission of 580 nm. Mitochondrial superoxide was also detected by confocal microscopy. Similarly, cells cultured in glass-bottom plate (Nunc) were loaded with 2.5 μM MitoSOX for 10 minutes at 37 ^{o}C and then washed with PBS twice. Fluorescence images were taken using an Olympus FluoView 1000 confocal microscope.

4.3.5 Mitochondria extraction

Mitochondria were extracted using a mitochondria extraction kit from Pierce. In brief, cells were harvested and washed with PBS once. Reagent A from the kit was added to swell cells on ice. Two minutes later, reagent B was added to lyze the cells. Lysis was

carried out by vigorously vortexing every one minute for up to five minutes. Then mitochondria were stabilized by reagent C. Cell suspension was spinned at 700 g for 10 minutes at 4 °C to pellet nuclei and cell debris. Supernatant was centrifuged at 12,000 g for 15 minutes at 4 °C to pellet mitochondria. Supernatant was saved as cytosolic fraction, and mitochondria pellets were washed and lysed with SDS-PAGE sample buffer.

4.3.6 Western blot

Mitochondrial-cytosolic extracts were separated by 10% or 16% Tris-HCl gel and transferred to nitrocellulose membrane. Membranes were then blocked in 5% milk in 0.05% Tween-TBS (tris buffered saline) (USB corporation) for one hour and incubated with primary Smac antibody (Cell Signaling), Bcl2 antibody (Cell Signaling) and GAPDH antibody (Cell signaling) overnight at 4 °C. Anti-mouse (Pierce) or anti-rabbit (Pierce) HRP-conjugated secondary antibody were added the second day after primary antibody incubation. The blots were incubated for one hour at room temperature and then washed with 0.05% Tween-TBS three times. The blots were visualized by using SuperSignal west femto maximum sensitivity substrate (Pierce).

4.3.7 DNA content and fragmentation

DNA content was measured by labeling DNA with PI (propidium iodide). In brief, harvested cells were fixed with 70% ethanol on ice for 2 hours. RNA was digested by RNase and then DNA was labeled with PI. Labeled samples were measured for DNA contents by flow cytometer BD FACSVantage. Sub-G1 peak was identified as the peak to the left of G0/G1 peak.

4.3.8 Annexin *V*-PI staining

Apoptosis was measured by the annexin *V*-PI (propidium iodide) staining kit (Invitrogen) according to the manufacturer's instructions. Cells were stained with Alexa Fluor 488 conjugated annexin *V* and PI in 1X annexin binding buffer for 15 minute at room temperature and then subjected to flow cytometry analysis by BD FACSVantage. Apoptotic cells were identified as those stained with Alexa Fluor 488 and showed green fluorescence. Dead cells were those stained with PI but not Alexa Fluor 488 and late apoptotic cells were those stained positive for both Alexa Fluor 488 and PI.

4.3.9 Mitochondria and Smac staining

Mitochondria were labeled using MitoTracker Red (Invitrogen) according to the manufacture's instructions. In brief, cells were incubated with 200 nM MitoTracker Red in warm medium for 30 minutes. Stained cells were washed with warmed PBS and fixed with 3.7% formaldehyde at 37 ^{o}C for 15 minutes. Cell membrane was permeabilized with 2% Triton-X100 for 10 minutes at room temperature. After washing the cells with PBS twice, they were incubated in 1% BSA for 20 minutes at room temperature. Cells were then incubated in anti-mouse Smac primary antibody (Cell Signaling) for 1 hour at room temperature. After washing with PBS three times, cells were incubated in Alexa Fluor-488 conjugated goat anti-mouse secondary antibody for 1 hour at room temperature. Cells were then washed with PBS three times and counterstained with DAPI for 5 minutes. Excess dye was removed by washing and glass coverslips were mounted in ProLong Gold (Invitrogen). Fluorescence images were taken by an Olympus FluoView

1000 confocal microscope. Percentage of cells with fragmented mitochondria was calculated based on three replicates, with two representative images from each replicate.

4.3.10 Determination of mitochondrial mass

Mitochondrial mass was determined by staining mitochondria with MitoTracker Green FM (Invitrogen). Cells were incubated in 200 nM MitoTracker Green FM in warm medium for 30 minutes and then washed with warm PBS three times to get rid of excess dye. Fluorescence was read by Spectra MAX GEMINI EM plate reader with excitation at 490 nm and emission at 516 nm. Fluorescence was normalized to protein levels (μg/ml) which were measured by Bradford assay.

4.3.11 Assessment of triglyceride storage

Triglyceride storage was assessed by Oil Red O staining. Cells were fixed in 3.7% formaldehyde for 30 minutes at room temperature and rinsed with PBS three times (5~10 minutes each time). Cells were rinsed again with water twice. Six parts 0.36% Oil Red O was mixed with four parts deionized water to make Oil Red O working solution. Enough Oil Red O working solution was added into each well and plate was incubated at room temperature for 50 minutes. Excess dye was removed by washing cells with water for three times. Images were taken by Leica RT Color from Diagnostic Instruments. Triglyceride levels were also quantified by an assay from BioVision according to the manufacture's instructions. In brief, samples were collected with 5% Triton-X100. Triglyceride standards and samples were loaded in a 96-well plate. Lipase was then added into each well for 20 minutes at room temperature to convert triglyceride to

glycerol and fatty acids. Glycerol is then oxidized in an enzyme mix reaction to generate a product that reacts with the probe, which can then be detected using the colorimetric methods at 570 nm by SPECTRAmax plus384.

4.3.12 Statistical analysis

Statistical analysis was carried out by an unpaired, two tail Student's T-test. * indicates $p<0.05$, ** indicates $p<0.01$ and *** indicates $p<0.001$.

4.4 Results

4.4.1 Palmitate induced cell death in HepG2 cells

Previous work had ascribed a lipotoxic effect to saturated FFAs, i.e. palmitate [160, 240]. We evaluated the effect of palmitate as well as unsaturated FFAs, oleate and linoleate, on HepG2 cells. The toxicity, as indicated by LDH release, was observed in palmitate-treated but not oleate- and linoleate treated HepG2 cells (Figure. 4.1A). In addition, cell staining with propidium iodide (PI, labels dead cells and late apoptotic cells) and Alexa Fluor 488-conjugated annexin V (labels early and late apoptotic cells) indicated that palmitate treatment significantly increased the necrotic (PI positive and annexin V negative) and late apoptotic cell populations (PI positive and annexin V positive) (Figure 4.1B). Linoleate also increased the necrotic cell population but much less than with palmitate treatment (Figure 4.1B). Palmitate treatment did not affect the population of early apoptotic cells, which was slightly increased in the oleate and linoleate conditions (Figure 4.1B).

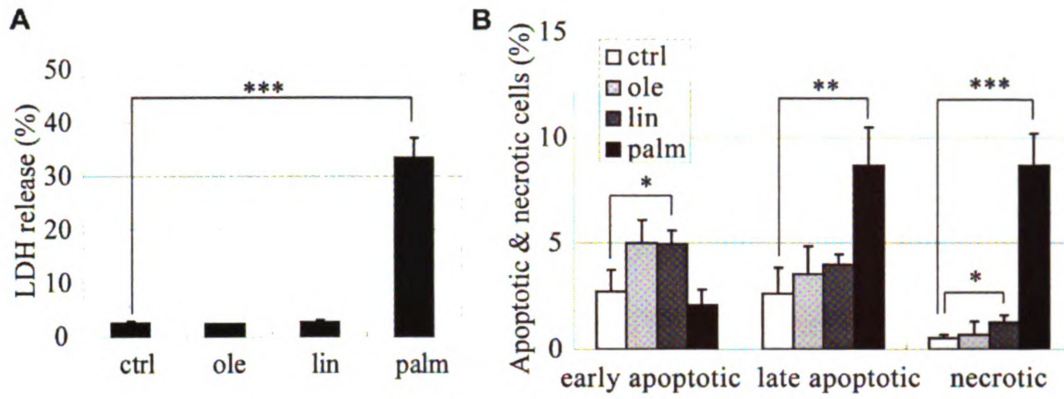

Figure 4.1 LDH release and cell death by FFAs treatment. (A) LDH release from cells in medium/BSA (ctrl), 0.7 mM oleate, linoleate and palmitate for 24 h. (B) Apoptotic and necrotic labeling by PI (propidium iodide) and Alexa Fluor-488 conjugated annexin V for cells in medium/BSA (ctrl), 0.7 mM oleate, linoleate and palmitate for 24 h. *Early apoptotic cells:* PI^- annexin V^+ cells; *late apoptotic cells*: PI^+ annexin V^+ cells; *necrotic cells*: PI^+ annexin V^- cells ($n = 3$). *: $p < 0.05$; **: $p < 0.01$; ***: $p < 0.001$.

4.4.2 Palmitate dose dependently reduces intracellular cAMP levels

Previously we showed that intracellular cAMP levels were reduced by palmitate but not oleate or linoleate in HepG2 cells [163]. The effect of palmitate on cAMP levels was also dependent on the palmitate concentration. cAMP level was increased slightly by 0.2 mM palmitate and significantly by 0.4 mM palmitate, whereas a high concentration of palmitate (0.7 mM) decreased cAMP level significantly (Figure 4.2A). Since the high concentration palmitate caused significant cell death, we assessed whether restoring cAMP level to near control level would prevent cell death. Intracellular cAMP levels were restored by IBMX (phosphodiesterase inhibitor), forskolin (adenylyl cyclase agonist), 8CPT-2Me-cAMP (cell-permeant cAMP analog) and glucagon (a hormone that activates adenylyl cyclase). 100 μM IBMX, 1 μM forsolin, 1 μM 8CPT-2Me-cAMP and 100 nM glucagon restored cAMP levels to near control level in the 0.7 mM palmitate

condition (Figure 4.2B). A combination of 10 μM forskolin and 100 μM IBMX was also evaluated, which achieved an even higher level of cAMP (Figure 4.2B).

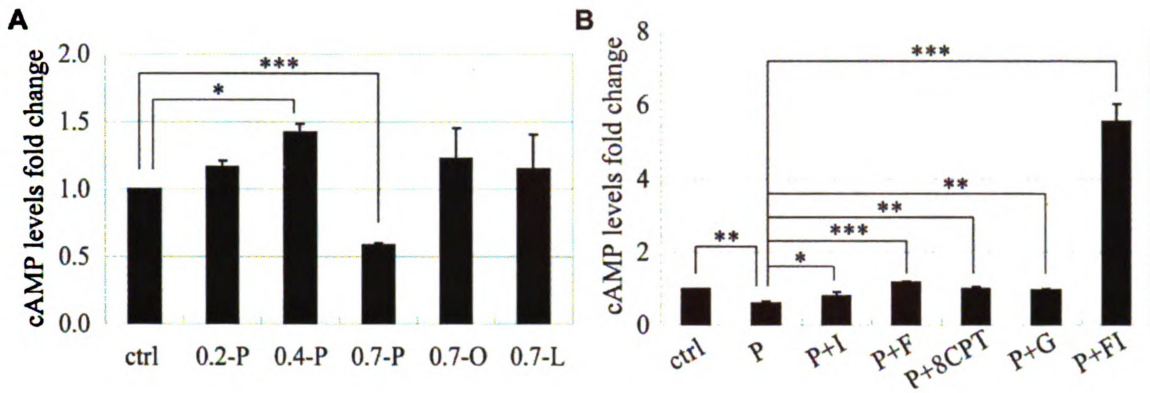

Figure 4.2 Effect of FFAs on cAMP levels. (A) Intracellular cAMP levels of cells in control, 0.2 mM palmitate (0.2-P), 0.4 mM palmitate (0.4-P), 0.7 mM palmitate (0.7-P), 0.7 mM oleate (0.7-O) and 0.7 mM linoleate (0.7-L) for 24 h ($n = 4$). (B) Intracellular cAMP levels of cells in control, 0.7 mM palmitate (P), 0.7 mM palmitate supplemented with 100 μM IBMX (P + I), 0.7 mM palmitate supplemented with 1 μM forskolin (P + F), 0.7 mM palmitate supplemented with 1 μM 8CPT-2Me-cAMP (P + 8CPT), 0.7 mM palmitate supplemented with 100 nM glucagon (P + G) and 0.7 mM palmitate supplemented with 10 μM forskolin and 100 μM IBMX (P + FI) for 24 h ($n = 3$). *: $p < 0.05$; **: $p < 0.01$; ***: $p < 0.001$.

4.4.3 cAMP and palmitate synergistically promote cell death at high concentrations

Studies in pancreatic β-cells indicated that apoptosis was reduced upon supplementation with cAMP increasing agents [14]. However, another study suggested that although apoptosis was reduced, the mode of cell death was switched to necrosis upon cAMP elevation in the palmitate condition [247]. When we used IBMX, forskolin, 8CPT-2Me-cAMP or glucagon to restore cAMP levels to the control level, the mode and level of cell death remained unchanged in the 0.7 mM palmitate conditions (Figure 4.3A). However, when cAMP was increased to a high level by supplementing with forskolin and IBMX (abbreviated as FI), it caused a significant increase in the necrotic cell population (Figure 4.3A). When the same concentration of FI was used to co-treat cells in control,

0.4 mM palmitate or 0.7 mM oleate, the synergistic increase in necrotic cell death was not observed (Figure 4.3B).

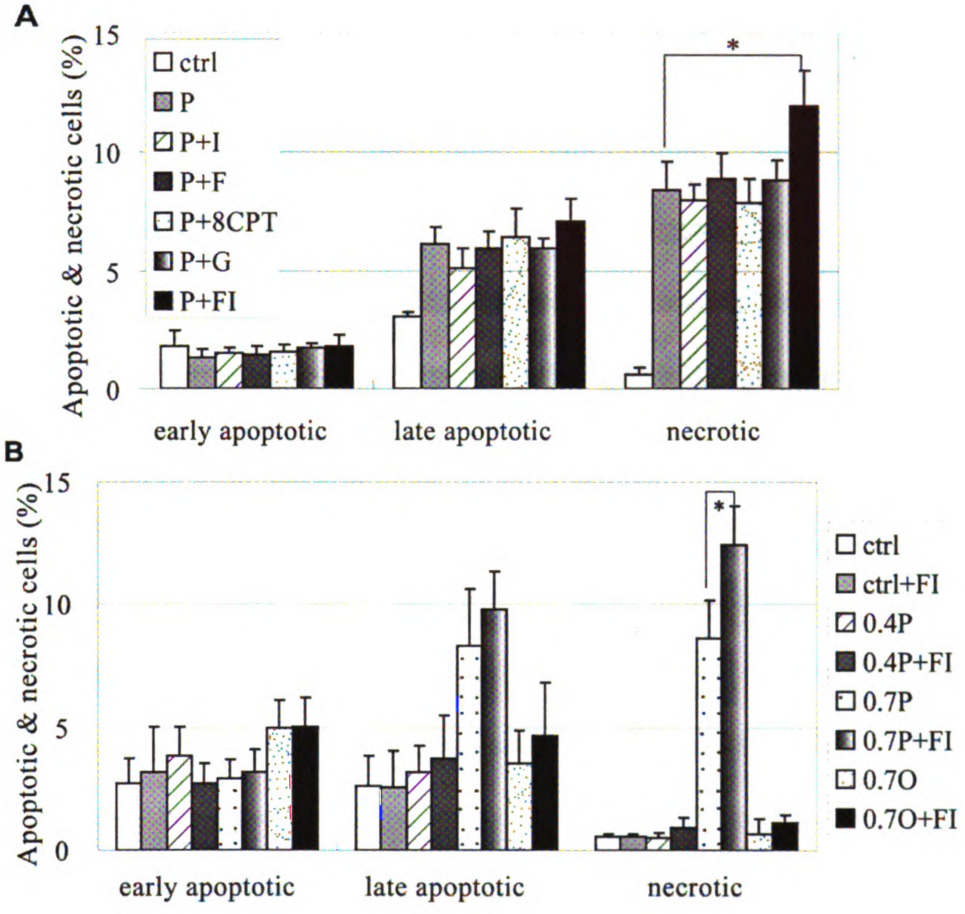

Figure 4.3 Apoptosis and necrosis by FFA treatment in the absence or presence of FI. (A) Apoptotic and necrotic labeling by PI (propidium iodide) and Alexa Fluor-488 conjugated annexin *V* for cells in control, 0.7 mM palmitate (P), 0.7 mM palmitate supplemented with 100 μM IBMX (P + I), 0.7 mM palmitate supplemented with 1 μM forskolin (P + F), 0.7 mM palmitate supplemented with 1 μM 8CPT-2Me-cAMP (P + 8CPT), 0.7 mM palmitate supplemented with 100 nM glucagon (P + G) and 0.7 mM palmitate supplemented with 10 μM forskolin and 100 μM IBMX (P + FI) for 24 h. *Early apoptotic cells:* PI^- annexin V^+ cells; *late apoptotic cells*: PI^+ annexin V^+ cells; ***necrotic cells***: PI^+ annexin V^- cells ($n = 3$). (B) Apoptotic and necrotic labeling by PI (propidium iodide) and Alexa Fluor-488 conjugated annexin *V* for cells in control, control supplemented with FI (ctrl + FI), 0.4 mM palmitate (0.4P), 0.4 mM palmitate supplemented with FI (0.4P + FI), 0.7 mM palmitate (0.7P), 0.7 mM palmitate supplemented with FI (0.7P + FI), 0.7 mM oleate (0.7O) and 0.7 mM oleate supplemented with FI (0.7O + FI) for 24 h ($n = 3$). *: $p < 0.05$.

The increase in the sub-G1 population attests further to the synergistic effect of elevated palmitate concentration and cAMP on cell death. Small fragmented DNA can be washed out from cells, leaving a sub-G1 peak to the left of the G0/G1 peak [262]. Compared with the control cells (Figure 4.4A), cells treated with 0.7mM palmitate had a small population of sub-G1 cells (Figure 4.4C). The addition of FI increased the sub-G1 population (Figure 4.4D), suggestive of further DNA fragmentation, in palmitate but not in the control cells (Figure 4.4B). Cells in different cell cycle phases, including sub-G1 cells, were quantified and shown in Figure 4.4E. Significant increase in sub-G1 phase cells was already observed 12 hours after 0.7mM palmitate treatment. The synergistic or additive effect of cAMP in promoting DNA fragmentation in the palmitate culture was not observed at 12 hours, (Figure 4.4E). However at 24 hours, cAMP increased the sub-G1 fraction significantly in the palmitate condition (Figure 4.4E). Although palmitate alone decreased the G2/M phase cells, the addition of FI did not reduce the S phase or G2/M phase cells but rather increased the G2/M phase cells at 12 hours (Figure 4.4E). Since cAMP did not prevent cell cycle progression, the increase in cell death caused by cAMP in the palmitate condition is not likely the result of DNA-damage induced cell cycle arrest at the checkpoint.

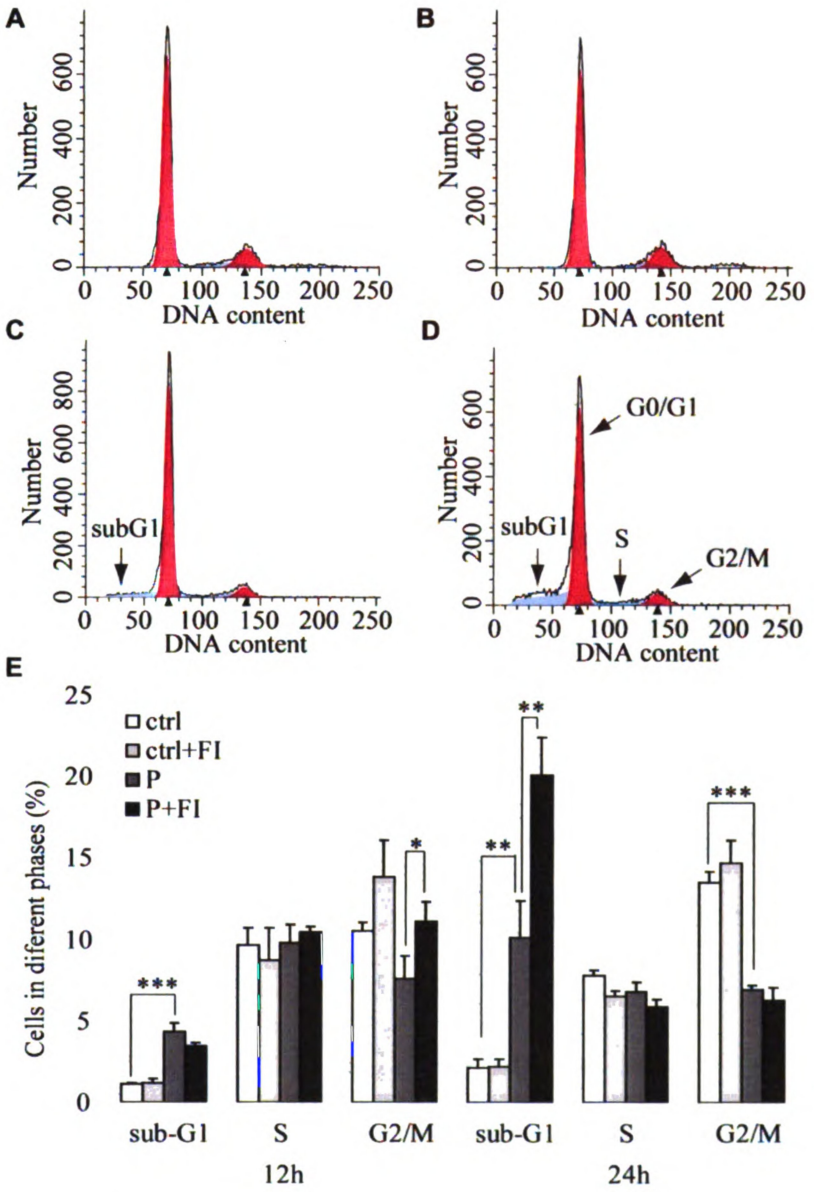

Figure 4.4 Effect of palmitate and FI on cell cycle distribution. (A) In control for 24 h (ctrl). (B) In control supplemented with 10 μM forskolin and 100 μM IBMX (FI) for 24 h (ctrl + FI). (C) In 0.7 mM palmitate for 24 h (P). (D) In 0.7 mM palmitate supplemented with FI for 24 h (P + FI). (E) Quantification of cells in sub-G1, S and G2/M phases 12 h and 24 h after treatment ($n = 3$). *: $p < 0.05$; **: $p < 0.01$; ***: $p < 0.001$.

4.4.4 cAMP and palmitate induced cell death is not caused by palmitate β-oxidation

Mitochondria are the main sites for fatty acid β-oxidation, with acetyl-CoA as one of the primary products. The majority of acetyl-CoA enters the TCA cycle, whereas a small

proportion will undergo ketogenesis in the mitochondria matrix [263]. Unused FFAs can be stored in the form of triglyceride in the cytosol. The capacity of non-adipose cells to store FFAs as triglyceride is limited. A previous study indicated that storage of oleate as triglyceride protected non-adipose cells from lipotoxicity, whereas palmitate was poorly incorporated into triglyceride and therefore led to apoptosis [264]. When we measured the level of triglycerides in HepG2 cells, we found that oleate and linoleate were more likely to be stored as triglyceride than palmitate (Figure 4.5A-D). This is in accordance with our previous finding that oxidation is higher with palmitate than with the unsaturated FFAs [163]. Given that the mitochondria serve as primary sites for FFA β-oxidation, enhanced palmitate oxidation may be related to enhanced mitochondrial biogenesis. Therefore we measured the mitochondria mass and found a significant increase in the 0.7 mM palmitate condition (Figure 4.6A). Although 0.7 mM palmitate greatly enhanced mitochondrial biogenesis in the palmitate treatment, this effect was not observed in the oleate treatment (Figure 4.6A). This could be due to the higher ability of oleate to be stored as triglycerides [37]. However, the addition of FI stimulated mitochondrial biogenesis, regardless of the treatment condition (Figure 4.6A). This effect was most obvious in the co-treatment of FI with 0.7 mM palmitate (Figure 4.6A). Since mitochondria are the primary sites for FFA β-oxidation and cAMP promoted mitochondrial biogenesis to a greater extent in palmitate, we expected that the addition of FI would enhance FFAs β-oxidation and reduce triglyceride storage. However, supplementing FI in the control and the different FFAs did not appear to give a visual difference in triglyceride levels according to Oil Red O staining for triglycerides (Figure 4.5E-H). For further confirmation, we quantified the triglyceride levels. Indeed,

supplementing with FI did not change the triglyceride levels (Figure 4.5I). It appears that mitochondrial biogenesis did not further enhance FFA β-oxidation. The lower triglyceride level in the palmitate condition was already apparent at 5 and 12 hours after treatment (Appendix figure 4.1), whereas mitochondrial biogenesis occurred at a much later time point (Figure 4.6B), indicating that β-oxidation occurred prior to mitochondrial biogenesis.

Palmitate was oxidized to a higher extent than oleate and caused significant cell death in HepG2 cells, therefore we assessed whether inhibiting palmitate β-oxidation would reduce or prevent cell death. When the FFAs oxidation inhibitor etomoxir was employed, it did not affect the cell death observed in palmitate, as reported previously [265]. Etomoxir decreased the necrotic population only slightly in the palmitate supplemented with FI condition (Figure 4.5J), suggesting that cell death induced by palmitate and palmitate supplemented with FI was not due to β-oxidation.

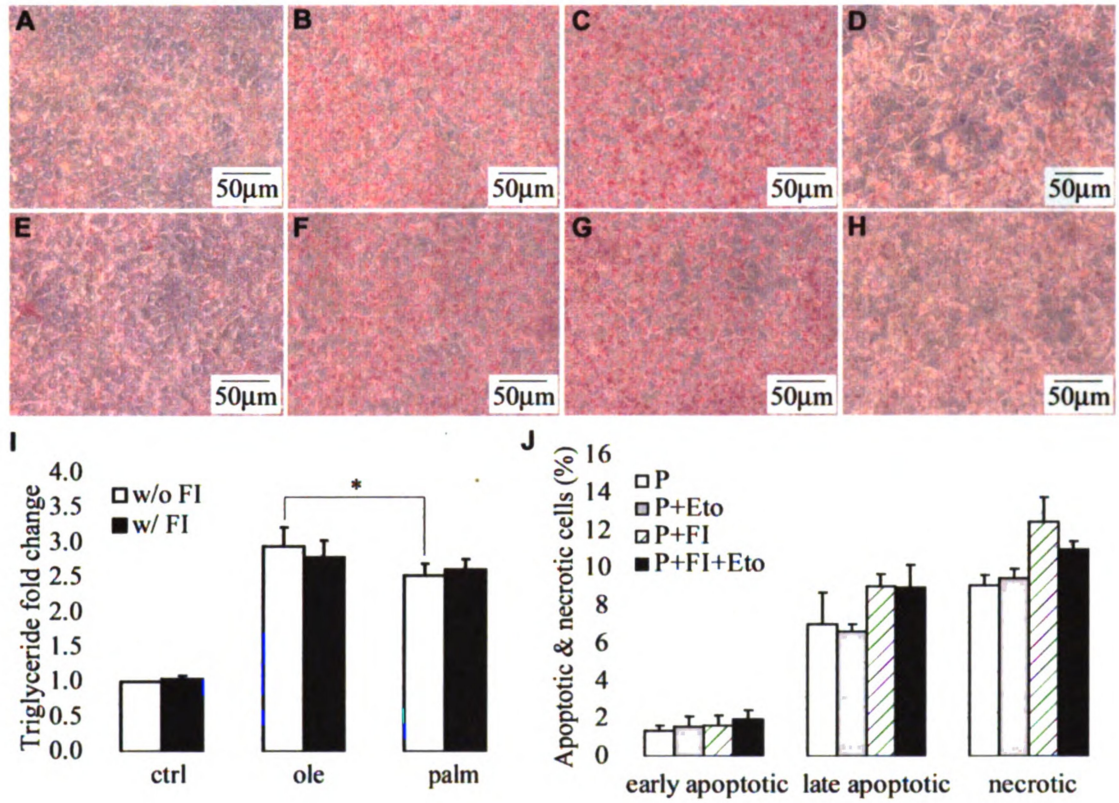

Figure 4.5 Triglyceride storage, palmitate oxidation and cell death. (A–H) Triglyceride storage by Oil Red O staining for cells in (A) control, (B) 0.7 mM oleate, (C) 0.7 mM linoleate, (D) 0.7 mM palmitate, (E) control supplemented with 10 μM forskolin and 100 μM IBMX (FI), (F) 0.7 mM oleate supplemented with FI, (G) 0.7 mM linoleate supplemented with FI and (H) 0.7 mM palmitate supplemented with FI for 24 h ($n = 3$). (I) Quantification of triglyceride levels by an assay for cells in control, 0.7 mM oleate and 0.7 mM palmitate without (w/o) or with (w/) FI for 24 h ($n = 4$). (J) Apoptotic and necrotic labeling by PI (propidium iodide) and Alexa Fluor-488 conjugated annexin V for cells in 0.7 mM palmitate and 0.7 mM palmitate supplemented with FI in the absence or presence of free fatty acid oxidation inhibitor etomoxir ($n = 3$). *: $p<0.05$.

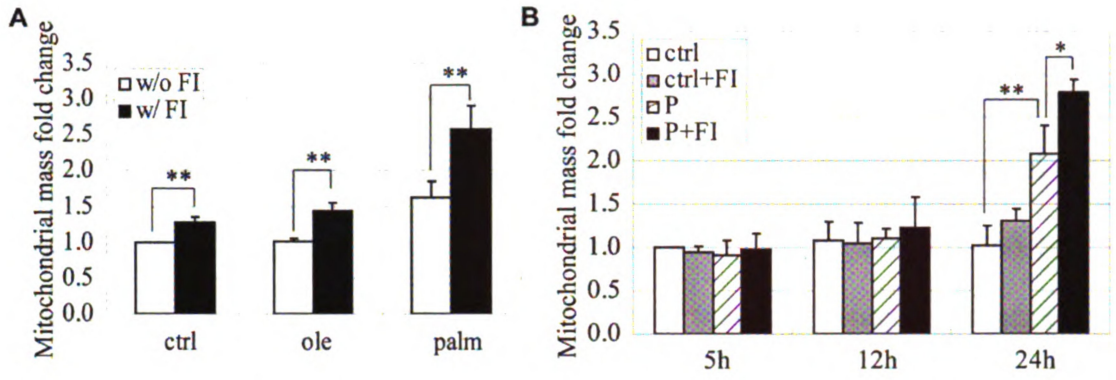

Figure 4.6 Effect of FFAs and FI on mitochondrial mass. (A) Mitochondrial mass fold change of cells in control, 0.7 mM oleate and 0.7 mM palmitate without (w/o) or with (w/) 10 μM forskolin and 100 μM IBMX (FI) for 24 h ($n = 3$). *: $p<0.05$; **: $p<0.01$.

4.4.5 cAMP synergized with palmitate to alter mitochondrial morphology and integrity

Mitochondria are not only primary sites for FFA β-oxidation, but also play an important role in cell death and survival [266]. In healthy cells, mitochondria exhibit elongated and connected morphology. When cells are subjected to apoptotic stimuli, mitochondria fragment into small and disconnected mitochondria [256, 257]. Control HepG2 cells exhibited long and connected thread-like mitochondria structure (Figure 4.7A). When the cells were subjected to 0.7 mM palmitate treatment, the mitochondrial morphology changed dramatically. The interconnected network was disrupted and collapsed into short disconnected morphology (Figure 4.7C). The elongated mitochondrial network also condensed and collapsed to the perinuclear locations (Figure 4.7C, arrow heads). The addition of FI to the control cells did not alter the connectivity of the mitochondrial network (Figure 4.7B, arrows), however supplementing the palmitate medium with FI continued the disconnected and punctuate mitochondria structure (Figure

4.7D, arrow heads) in a higher population of cells (Figure 4.7E). No mitochondrial fragmentation was observed in the 0.2 mM palmitate condition (Appendix figure 4.2B, arrows). When palmitate concentration was increased to 0.4 mM, mitochondrial fragmentation had begun to occur and a number of cells had disconnected and punctate mitochondrial structures (Appendix figure 4.2C, arrow heads), whereas the majority of cells still have elongated mitochondrial network as indicated by the arrow (Appendix figure 4.2C). As the palmitate concentration was further increased to 0.7 mM, more cells showed short and disconnected mitochondrial structures (Appendix figure 4.2D). Fragmentation of mitochondria is associated with cell death and the release of cytotoxic proteins that reside in the intermembrane space [256]. In accordance with the mitochondrial fragmentation observed in the high palmitate condition, we detected less Smac in the mitochondria and relatively more Smac in the cytosol (Appendix figure 4.3). Indeed, Smac colocalized in the mitochondria in the control (Figure 4.7F) and control supplemented with FI conditions (Figure 4.7G), since almost no green fluorescence was observed outside the mitochondria. However more cytosolic Smac (indicated by the green fluorescence) was released into the cytosol in the palmitate (Figure 4.7H) and palmitate supplemented with FI conditions (Figure 4.7I), suggesting that the mitochondrial membrane integrity was compromised. We also observed that the mitochondrial anti-apoptotic protein Bcl2 level was further reduced by FI supplementation (Appendix figure 4.3). Bcl2 is an anti-apoptotic protein that antagonizes pro-apoptotic proteins, such as Bax, thereby preventing the release of cytotoxic proteins from the mitochondria [254]. The significant decrease in mitochondrial Bcl2 protein induced by the addition of FI to palmitate treated cells may disrupt the outer

mitochondria membrane integrity [267]. As a consequence, cytotoxic proteins, such as Smac which promotes caspase activation by inhibiting the inhibitor of apoptosis (IAP), are more likely to be released into the cytosolic compartment [254]. In support of this idea, caspase 3 activity was highest in the palmitate supplemented with FI condition (Figure 4.8A), which had the highest level of mitochondrial fragmentation (Figure 4.7E) and lowest level of mitochondrial Bcl2 (Appendix figure 4.3).

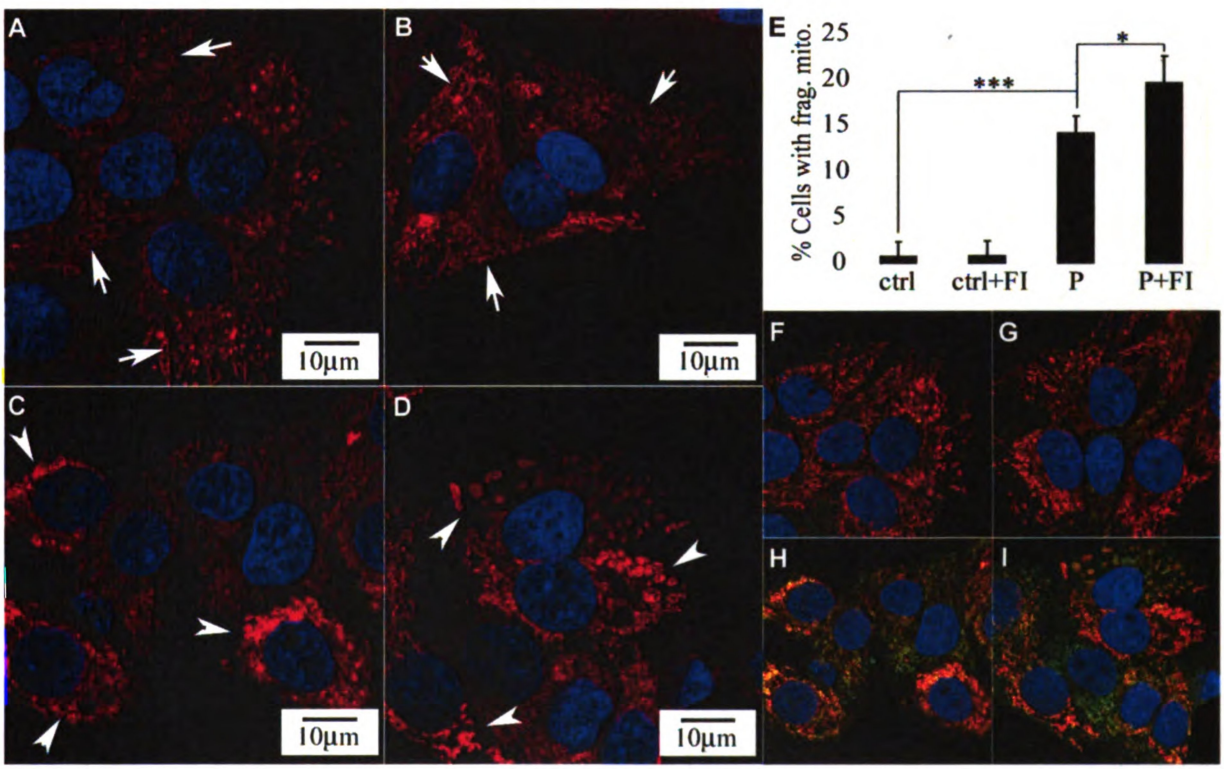

Figure 4.7 Mitochondrial fragmentation and release of cytotoxic protein. (A–D) Mitochondrial morphology of cells in (A) control, (B) control supplemented with 10 μM forskolin and 100 μM IBMX (FI), (C) 0.7 mM palmitate and (D) 0.7 mM palmitate supplemented with FI for 24 h ($n = 3$). Panels A–B exhibited elongated and tubular structure, while panels C–D displayed short and disconnected morphology. (E) Quantification of the percentage of cells with fragmented mitochondria as displayed in panels A–D ($n = 3$). *: $p < 0.05$; ***: $p < 0.001$. (F–I) Immunostaining of mitochondria (red), Smac (green) and nucleus (blue) for cells in (F) control, (G) control supplemented with FI, (H) 0.7 mM palmitate and (I) 0.7 mM palmitate supplemented with FI for 24 h ($n = 3$).

Since caspase 3 activity was activated by 0.7 mM palmitate and significantly increased by FI supplementation (Figure 4.8A), we assessed whether caspase was involved in causing the cell death. When the pan caspase inhibitor Z-VAD-FMK was used to inhibit caspase activity, late apoptosis and necrosis were not reduced (Figure 4.8B), suggesting that the cell death induced by palmitate and cAMP was caspase-independent. This is not too surprising given that the majority of the population under this condition is necrotic as opposed to apoptotic.

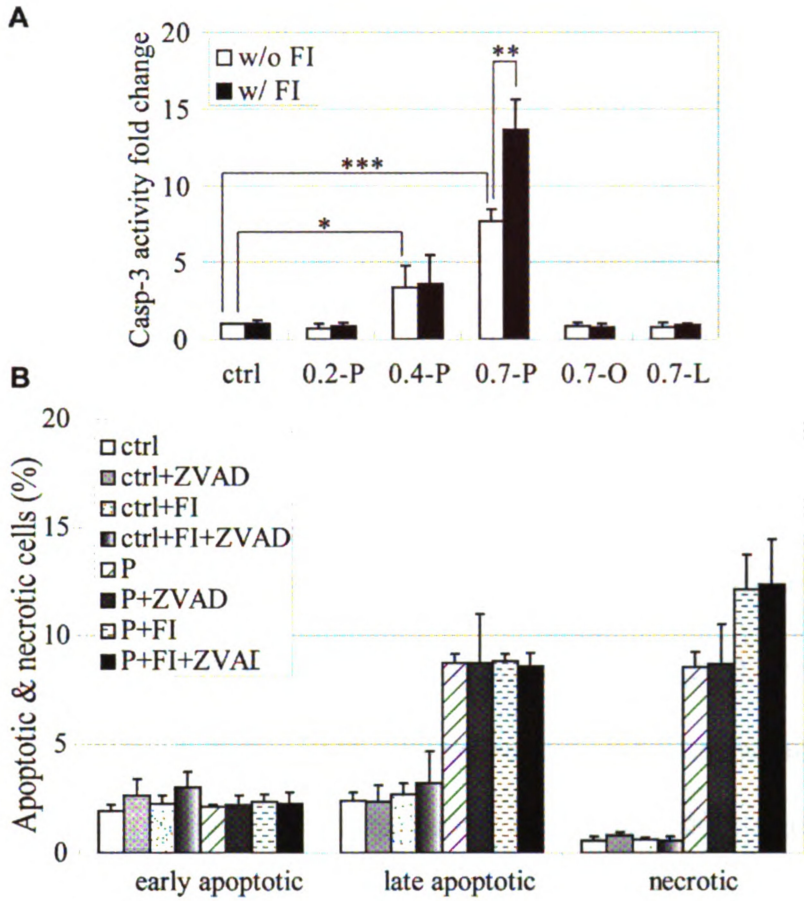

Figure 4.8 Effect of Caspase inhibition on apoptosis and necrosis. (A) Caspase 3 activity of cells in control (ctrl), 0.2 mM palmitate (0.2-P), 0.4 mM palmitate (0.4-P), 0.7 mM palmitate (0.7-P), 0.7 mM oleate (0.7-O) and 0.7 mM linoleate (0.7-L) without (w/o) or with (w/) FI for 24 h ($n = 4$). (B) Apoptotic and necrotic labeling by PI (propidium iodide) and Alexa Fluor-488 conjugated annexin *V* for cells in control (ctrl) and 0.7 mM palmitate (P) in the absence or presence of FI and/or 10 μM pan-caspase inhibitor Z-VAD-FMK (Z-VAD) for 24 h. *Early apoptotic cells:* PI^- annexin V^+ cells; *late apoptotic cells*: PI^+ annexin V^+ cells; *necrotic cells*: PI^+ annexin V^- cells ($n = 3$). *: $p<0.05$; **: $p<0.01$; ***: $p<0.001$.

4.4.6 cAMP synergized with palmitate to enhance ROS generation in mitochondria

Mitochondria are also the primary sites for ROS generation. Although palmitate β-oxidation was not the cause of cell death, generation of ROS at Complex I and Complex III during the process of oxidative phosphorylation through the electron transport chain in the mitochondria can induce cell death [260]. Excessive ROS generation can result in

cellular damage and cell death. Mitochondrial superoxide anion ($O_2^{-}\bullet$) was increased significantly in the palmitate condition after 24 hours (Figure 4.9B) as compared with the control (Figure 4.9A). Moreover, the short, disconnected and perinuclear mitochondria appeared to have higher $O_2^{-}\bullet$ levels (Figure 4.9B, arrow heads). Quantification of mitochondrial $O_2^{-}\bullet$ levels indicated that palmitate did not induce an increase in mitochondrial $O_2^{-}\bullet$ levels at 5 or 12 hour, but a significant increase was observed at 24 hours (Figure 4.9C). Elevating cAMP level by FI synergistically increased the mitochondrial $O_2^{-}\bullet$ levels at 24 hours (Figure 4.9C). $O_2^{-}\bullet$ is the precursor of stronger ROS, such as hydrogen peroxide (H_2O_2) and hydroxyl radical ($HO\bullet$) [260]. When whole cell ROS levels were measured, higher ROS activity was detected in the palmitate condition 24 hours after treatment (Figure 4.9D). Similar to the mitochondrial superoxide levels, the cellular ROS level did not increase at 5 and 12 hours. However at 24 hours, FI induced a slight increase in ROS level in the palmitate condition albeit not significantly (Figure 4.9D).

In order to evaluate whether ROS production contributes to the cell death induced by palmitate and palmitate supplemented with FI, we used several ROS scavengers. The ROS scavengers employed were: DMU for hydroxyl radicals, catalase for hydrogen superoxide, Cu-DIPS and MnTBAP for superoxide. Employing DMU or catalase resulted in a decrease in both late apoptotic cells and necrotic cells caused by palmitate, however, the decrease was not significant (Figure 4.9E). When DMU and catalase were used simultaneously, both late apoptosis and necrosis were reduced significantly in the palmitate condition (Figure 4.9E). Similarly, DMU and catalase together significantly

reduced late apoptosis and necrosis in palmitate supplemented with FI. DMU itself also significantly reduced both late apoptosis and necrosis but catalase only significantly reduced necrosis (Figure 4.9E). The superoxide scavengers Cu-DIPS and MnTBAP did not decrease cell death (data not shown). This is likely due to the reduction of $O_2^{-}\bullet$ by Cu-DIPS and MnTBAP to generate the stronger ROS, H_2O_2 and HO• [260] which would be expected to further continue the damage to the cells. Although the H_2O_2 and HO• scavengers reduced cell death, H_2O_2 and HO• are not likely the reason that cell death was initiated. At 5 and 12 hours of palmitate and palmitate supplemented with FI treatment, cell death had already been initiated (Appendix figure 4.4) but the ROS level did not increase until 24 hours (Figure 4.9D). However, ROS generation may be linked to mitochondrial fragmentation. At 12 hours, some cells already had fragmented mitochondria in the 0.7mM palmitate condition (Appendix figure 4.5A, arrow heads). This is especially the case for the cells with fragmented nucleus (Appendix figure 4.5B, rectangle), their mitochondria were all short and disconnected (Appendix figure 4.5C, arrow heads). The short and disconnected mitochondria tend to have higher ROS levels (Figure 4.9B, arrow heads). Therefore, mitochondria fragmentation precedes ROS generation and may have contributed to the ROS produced.

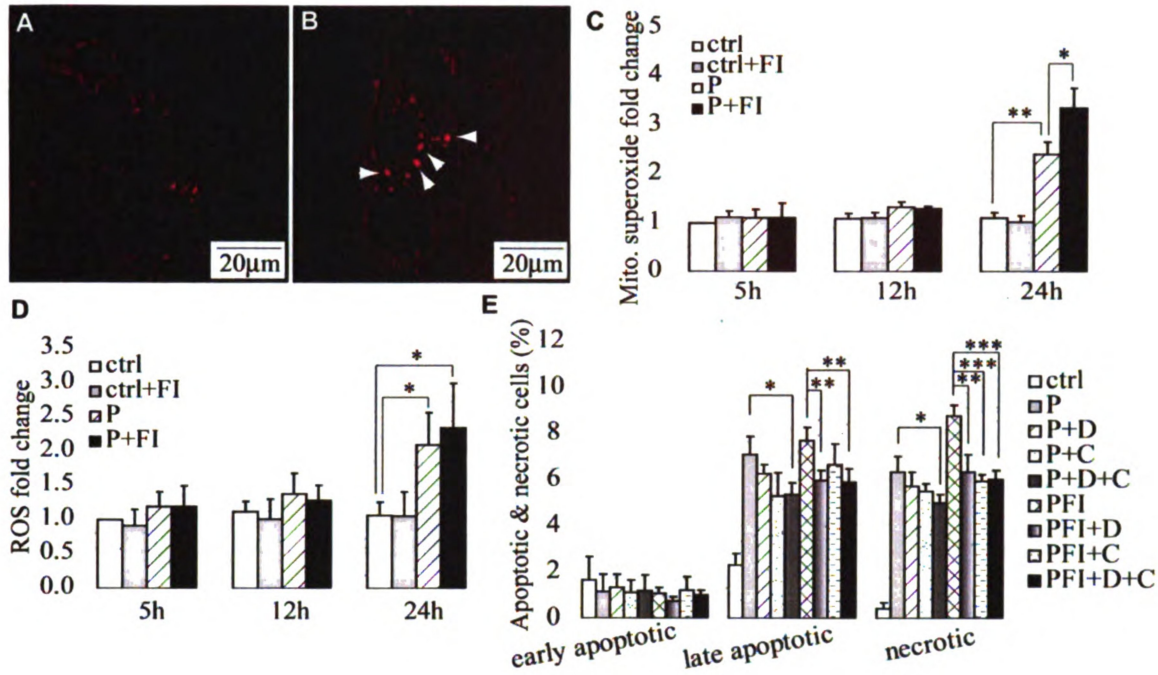

Figure 4.9 ROS and cell death. (A) Mitochondrial superoxide labeling for cells in control and (B) cells treated with 0.7 mM palmitate for 24 h. Arrowheads denote short and disconnected mitochondria which have higher superoxide levels ($n = 3$). (C) Mitochondrial superoxide levels fold change for cells in control and 0.7 mM palmitate without (w/o) or with (w/) 10 μM forskolin and 100 μM IBMX (FI) for 5 h, 12 h and 24 h ($n = 4$). (D) Cellular ROS levels fold change for cells in control and 0.7 mM palmitate without (w/o) or with (w/) 10 μM forskolin and 100 μM IBMX (FI) for 5 h, 12 h and 24 h ($n = 3$). (E) Apoptotic and necrotic labeling by PI (propidium iodide) and Alexa Fluor-488 conjugated annexin V for cells in control, 0.7 mM palmitate (P) and 0.7 mM palmitate supplemented with 10 μM forskolin and 100 μM IBMX (FI) in the presence of ROS inhibitors ($n = 3$). D: hydroxyl radical inhibitor DMU; CA: hydrogen peroxide inhibitor catalase. *: $p<0.05$; **: $p<0.01$; ***: $p<0.001$.

4.5 Discussion

Lipotoxicity induced by palmitate has been demonstrated in a number of different cell types. In human HepG2 cells, both apoptotic behaviors, such as caspase 3 activation (Figure 4.8A) and annexin V labeling for phosphatidylserine (Figure 4.1B), and necrotic behaviors, such as propidium iodide (PI) penetration (Figure 4.1B), have been observed for palmitate-induced cell death. Many obese and diabetic patients have high plasma FFAs levels [250-252]. cAMP has been proposed as a potential drug target for type 2

diabetes [249] due to it ability to stimulate pancreatic β-cell insulin secretion. In light of the fact that elevated FFAs can induce hepatotoxicity, it warrants evaluating the effect of cAMP under the circumstance of high FFAs. In this study, we evaluated the effect of cAMP on hepatotoxicity and cell death under elevated FFAs conditions. A high cAMP level achieved by adding 10 μM forskolin and 100 μM IBMX (abbreviated as FI) promoted palmitate-induced cell death in a synergistic manner (Figure 4.3 and 4.4). The increase in cell death caused by cAMP supplementation was mostly necrotic (Figure 4.3B), without an increase in the early apoptotic population (Appendix figure 4.4), and further appeared to be caspase-independent (Figure 4.8B).

Cell death caused by palmitate may be related to its lower ability to be stored in the form of triglyceride [264]. Reduced cytoxicity and cell death in HepG2 cells were achieved by inhibiting NADH dehydrogenase (complex I), which was accompanied by enhanced triglyceride storage [268]. While oleate and linoleate are more likely to be stored as triglyceride (Figure 4.5B-C), palmitate was less likely to be stored in the form of triglycerides (Figure 4.5D and 4.5I). The lower ability of palmitate to be stored as triglyceride may contribute to its enhanced oxidation in mitochondria. Indeed, our previous study showed that palmitate was oxidized more than oleate and linoleate by the HepG2 cells [163]. The total mitochondrial mass was increased significantly in the palmitate condition but not in the oleate condition (Figure 4.6A). Since mitochondria are the primary sites for FFA β-oxidation, we initially assumed that the induction of mitochondrial biogenesis would allow more palmitate to undergo β-oxidation and therefore have less triglyceride to be stored. cAMP can promote mitochondrial biogenesis by directly regulating mitochondrial related genes or indirectly by inducing the

expression of transcriptional coactivator, PGC-1α [269]. When FI was added to the different conditions, mitochondrial biogenesis was enhanced in all cases, but the extent was much higher in the palmitate condition (Figure 4.6A). However, the addition of FI did not cause a significant change in triglyceride levels (Figure 4.5I). A time-dependent study indicated that mitochondrial biogenesis occurred later than triglyceride storage (Figure 4.6B and Appendix figure 4.1), indicating that mitochondrial biogenesis would not likely contribute to reduced triglyceride storage in the palmitate condition. Therefore, even though FI increased mitochondrial biogenesis (Figure 4.6A), triglyceride levels were not affected (Figure 4.5I). Since the palmitate condition had higher β-oxidation [163] and lower triglyceride storage (Fig. 5I), we assessed whether palmitate β-oxidation is involved in palmitate-induced cell death. When β-oxidation was inhibited by etomoxir, no change in cell death was observed (Figure 4.5J), suggesting that palmitate β-oxidation was not the cause of cell death.

Although β-oxidation was not the cause of cell death, generation of ROS by oxidative phosphorylation through the mitochondrial electron transport chain can damage cells [268]. Indeed, inhibiting NADH dehydrogenase (complex I), one of the primary sites for ROS generation, reduced the cytotoxicity induced by palmitate treatment [268]. Superoxide ($O_2^{-}\bullet$), which is the precursor of most ROS, was much higher in the palmitate condition and further increased upon FI supplementation (Figure 4.9C). In addition to mitochondrial $O_2^{-}\bullet$ levels, total cellular ROS levels were also much higher in the palmitate condition (Figure 4.9D).

Mitochondrial $O_2^{-}\bullet$ levels correlated with mitochondrial biogenesis (Figure 4.6B and 4.9C). Whether mitochondrial biogenesis promote mitochondrial $O_2^{-}\bullet$ generation or

mitochondrial O_2^{-}• generation promote mitochondrial biogenesis still remains a question. From our results, it is unlikely that mitochondrial biogenesis itself promoted mitochondrial O_2^{-}• generation, since FI supplementation promoted mitochondrial biogenesis in the control and oleate conditions (Figure 4.6A) but no increase in mitochondrial O_2^{-}• levels was observed in these two conditions (Appendix figure 4.6). It is possible that O_2^{-}• generation may enhance mitochondrial biogenesis. Previous studies have suggested that ROS can enhance nuclear respiratory factor-1 (NRF-1) and mitochondrial transcription factor A (Tfam), which are involved in regulating mitochondrial biogenesis [270, 271].

Generation of ROS, however, may be linked to mitochondrial fragmentation. A previous study has indicated that changes in mitochondrial morphology resulted in ROS overproduction [272]. We showed that palmitate induced morphology changes in the mitochondria, causing long interconnected networks (Figure 4.7A) to become short disconnected structures located in the perinuclear (Figure 4.7C). When HepG2 cells were subjected to palmitate and FI, mitochondrial fragmentation was further enhanced (Figure 4.7D), judging by the increase in the total number of cells with fragmented mitochondria (Figure 4.7E). Under the conditions of a high percent of mitochondrial fragmentation, mitochondrial O_2^{-}• and total cellular ROS levels were also high (Figure 4.9C-D). The occurrence of mitochondrial fragmentation precedes mitochondrial ROS generation. At 12 hours, mitochondrial fragmentation had already begun to occur in the 0.7 mM palmitate condition (Appendix figure 4.5), while ROS generation was not much higher than control until after 12 hours (Figure 4.9D). In addition, the fragmented mitochondria tend to have higher superoxide (O_2^{-}•) levels as denoted by the arrow heads in Figure 4.9B.

Thus it is likely that mitochondrial fragmentation contributed to ROS overproduction. ROS overproduction, in turn, further damages the mitochondria, and as a self defense mechanism, mitochondrial damage stimulates the synthesis of new mitochondria to ameliorate the damage [273]. However, what regulates mitochondrial fragmentation still remains an open question. Recent work in our lab indicated that endoplasmic reticulum (ER) stress was observed several hours after palmitate treatment (unpublished data). ER stress can induce the release of Ca^{2+} from the ER [274]. Release of Ca^{2+} can activate the Ca^{2+} and calmodulin-dependent phosphatase calcineurin [275]. Calcineurin has been shown to dephosphorylate dynamin-related protein 1 (Drp1), a key protein involved in mitochondria fragmentation, and therefore promote mitochondrial fragmentation [276]. Therefore, it is possible that palmitate, which has been shown to induce ER [277], initiated Ca^{2+} release and activated calcineurin, which subsequently activates Drp1 and leads to mitochondrial fragmentation.

In summary, cAMP promoted cell death in the presence of high level of palmitate in a synergistic or additive manner in HepG2 cells. The many effects exerted by palmitate on the mitochondria, such as mitochondrial fragmentation, mitochondrial ROS generation, and mitochondrial biogenesis, were amplified by cAMP supplementation. Mitochondrial fragmentation appears to precede ROS generation and may have contributed to mitochondrial ROS overproduction, which in turn stimulated mitochondrial biogenesis.

CHAPTER 5. CONCLUSIONS AND FUTURE DIRECTIONS

5.1 Conclusions

The capability of MSCs to differentiate into neural lineage cells, undergo rapid *in vitro* amplification, secrete growth factors, suppress immune cell proliferation as well as their ease of isolation, make them a promising source for treating neuronal diseases. Numerous *in vitro* studies have applied different methods to induce MSCs to differentiate into neural lineages, which include chemicals, growth factors, co-culture with neural lineage cells and transgene expression [4, 119, 138, 139, 144, 147-158, 278]. Various *in vivo* studies also indicate that MSCs can adopt neural lineage cell fates [131, 134, 195-197]. Despite the ongoing research and application of MSCs for clinical applications, a clear understanding of whether MSCs can differentiate into truly functional neurons and the conditions required for generating functional neurons to replace the damaged neurons is still lacking [6].

The ubiquitous second messenger cAMP, which has been shown to elicit neural differentiation in MSCs in 2001 [4] and since then been frequently employed in *in vitro* induction media [148, 153, 155, 156], has been indicated as an important regulator for regeneration of the central nervous system [36, 192, 193]. In particular, a prior report suggested that a combinatorial approach containing cAMP, neurotrophins and MSCs can enhance repair of spinal cord injury [279]. However, it remains unclear whether cAMP has adverse effect on MSCs and if cAMP can convert MSCs into functional neurons and thereby facilitate replacement of damaged neurons. The lack of understanding regarding these questions hinders the potential application of cAMP and MSCs in future therapeutic applications for treating neuronal diseases, such as spinal cord injury. Therefore, the aim

of this thesis work is to investigate the effect of cAMP on MSC differentiation to neural lineage and the potential mechanisms involved.

The present study demonstrates that cAMP induced an early-phase neuron-like morphological changes and a late-phase neural marker expression and function. While the early-phase morphological changes are likely due to cell shrinkage and cause subsequent apoptosis, the late-phase neuron marker expression occurrs gradually and does not rely on the appearance of the morphological changes. Both events are regulated by cAMP activated PKA, however, their regulation diverged downstream of PKA, since the morphological changes do not require transcription and translation while the expression of neural markers does. Moreover, cAMP also enabled MSCs to respond, with a rise in calcium signaling, to neuronal activators, namely, dopamine, glutamate and KCl. The strongest calcium response was observed with dopamine, followed by KCl and then glutamate. While the cells induced with cAMP showed a certain degree of neuronal function, they lacked the neuronal morphology and further, their responses to the three neuronal activators were quite heterogeneous, suggesting cAMP alone is not sufficient to differentiate all the MSCs into mature neurons. These results suggest that cAMP have both positive and negative effects on MSCs. The ability of cAMP to promote MSCs differentiate into neural lineages and obtain some neuronal function may facilitate the replacement of damaged neurons. However, cAMP also resulted in cell shrinkage and correlated apoptosis, which may reduce treatment efficacy and also possibly lead to inflammation.

In light of the fact that activated CREB appears to co-localize with immature neurons and promote their maturation [206, 207], we hypothesized that it is involved in cAMP

induced neural differentiation of MSCs. However, whether CREB can regulate calcium signaling in response to neuronal activators was not known until this current study. To investigate the role of CREB in calcium signaling in MSCs, a stable cell line expressing the dominant-negative CREB (M1-CREB) was established. Introducing the dominant negative CREB greatly decreased the calcium signaling elicited by the neuronal activators but not by the positive control, ATP. Further analysis indicated that downregulating CREB activity reduced the expression of membrane receptors, such as dopamine receptor 1, which may contribute to the reduction in calcium response. Surprisingly, while down-regulating CREB reduced the calcium response, it facilitated the adoption of a neuron-like morphology. It appears that CREB has contrasting effects, encouraging neuronal function while inhibiting neuron-like morphology. It is unclear how CREB manages this; perhaps the timing of CREB activation may be important in achieving both morphological and functional differentiation. Contrasting effects on differentiation were reported for the Wnt/β-catenin signaling pathway. Early activation of Wnt/β-catenin signaling promoted cardiac lineage of embryonic stem cells (ESCs), while late activation of Wnt/β-catenin signaling inhibited cardiac lineage differentiation of ESCs [238, 239]. Therefore, the design of the induction media may need to be optimized in such a way that CREB activity is tuned to allow both functional and morphological neural lineage differentiation of MSCs.

Apart from its role in differentiation, cAMP also initiated apoptosis in MSCs and enhanced palmitate-induced cell death in HepG2 cells. While cAMP itself is not harmful to HepG2 cells, it promoted cell death in the presence of high levels of palmitate in a synergistic manner. The many detrimental effects exerted by palmitate, such as

mitochondrial fragmentation and mitochondrial ROS generation, were significantly amplified by cAMP. Mitochondrial fragmentation appears to precede ROS generation and may have contributed to the mitochondrial ROS overproduction, which is partially responsible for palmitate and cAMP induced cell death. cAMP has been proposed as a potential drug target for type 2 diabetes [249], since it appears to enhance insulin secretion. In light of the fact that palmitate is elevated in obesity and diabetes [250-252] and can induce hepatotoxicity, administering cAMP to type 2 diabetic patients may further the adverse effects on the liver, given that our results suggest that cAMP promotes cell death with palmitate in a synergistic manner in HepG2 cells.

In summary, the current study revealed that cAMP is able to induce MSCs to neural lineage cells with some neuronal function *in vitro*. Its downstream signaling component, CREB, plays a role in the acquisition of neuronal function. The findings from the MSC study shed some light on the application of cAMP and MSCs for treating neuronal diseases which could help better design future *in vitro* differentiation strategies. In addition, the pro-apoptotic affects of cAMP observed in HepG2 cells, i.e. promoting cell death and mitochondrial dysfunction, provides some insights into the potential application of cAMP for treating type II diabetes.

5.2 Future directions

5.2.1 To enhance neural lineage differentiation of MSCs

MSCs are naturally heterogeneous, with varying morphologies and sizes, different growth rates and differentiation abilities [108, 113, 115, 280, 281]. Such heterogeneity introduces uncertainty in cell fate determination and also compromises the differentiation

efficiency. To better control and increase differentiation efficiency, enrichment of a sub-population of cells with high neural differentiation potential is desired.

The most abundant subpopulations in rat MSCs are the rapidly growing spindle-like cells, star-like cells and small round cells. Another subpopulation of cells with flat morphology also appeared frequently in culture. Although these cells are morphologically heterogeneous, they all express the same known markers for MSCs [108]. Currently it is not possible to separate these subpopulations of MSCs with known surface markers. A potential way to enrich MSCs with higher neural lineage differentiation is to select out a sub-population of cells that express certain neural lineage markers, since uninduced MSCs already express several neuronal/glial markers and these cells may have higher ability to differentiate into neural lineage cells [282]. However, all the examined neural lineage markers in the aforementioned study, such as nestin and GFAP [282], are intracellular proteins and cannot be used for live cell sorting. During our study, around 12% of MSCs was observed to express dopamine receptor 1 (D1), which is a membrane bound protein and therefore can be used for live cell sorting. These D1-positive cells are likely to have a higher potential to differentiate into neurons since they already possess some neuronal features.

In addition, to obtain a more amenable sub-population of cells for differentiation, the differentiation induction media needs to be further improved. A good induction protocol may require different components at different stages. For example, development of midbrain dopaminergic neurons includes four stages and different factors are required at the different stages, i.e., Shh and FGF8 for specification of precursors to the dopaminergic fate, and Wnt5a and FGF20 for development of postmitotic dopaminergic

neurons [283]. Therefore, the composition of the induction media may need to be optimized for better differentiation.

5.2.2 Using polymer surfaces and modeling to study the relationship between cell morphology and differentiation capability

While it is unlikely that current known cell surface markers can be used to separate the subpopulations of MSCs with different morphologies, we observed that cell morphology can be tuned by the substrates, with some surfaces favoring a particular morphology, which could affect the selection of a subpopulation of cells [284]. Moreover, it is likely that addition of cAMP may favor further selection of the subpopulation of cells with higher neural lineage differentiation potential. Therefore, another future work is to apply polymer surfaces to enrich cells for neural lineage differentiation. To test if indeed certain subpopulations can be enriched by different culture surfaces and whether cAMP addition can facilitate the selection of cells with higher neural lineage differentiation potential, the following approaches may be taken. 1) Single cell-derived cells can be obtained by cloning cylinders. The subpopulations arising from different single cells can be labeled with cell tracer beads (which comes in different colors and can be retained in cells for several weeks). 2) Different culture substrates, such as agarose, chitosan and polyelectrolyte multilayers (PEMs), can be prepared and tested for the cell cultures. The labeled subpopulations of MSCs can be combined and cultured on the different substrates to evaluate whether a certain population has a better ability to survive. cAMP can then be supplemented to the media and immunostained using neuronal markers to assess which subpopulation have a higher potential to differentiate into neural lineage cells. 3) Finally,

a modeling approach as described in [284] can be used to predict the range of surface stiffness that favors the selection of a certain subpopulation of MSCs with the highest neural lineage differentiation. This study is not limited to neural lineage differentiation, but can also be extended to differentiation of MSCs into other lineages such as osteoblasts, through modulating surface characteristics and induction media. It addition to MSC, the approach could be applied to ESCs and induced pluripotency stem (iPS) cells, which are often highly heterogeneous [285-288]. ESCs and iPS cells have great potential for future cell-based therapies since they can differentiate into all cell types, however, the intrinsic heterogeneity may lead to uncontrolled differentiation and cause teratoma formation. It is likely modulation of culture substrate mechanics may help to reduce heterogeneity in ESCs and iPS cells and thereby restrict their differentiation into specific lineages.

5.2.3 Determine how CREB regulates D1 mRNA and protein levels

It is intriguing that knocking down CREB activity reduced D1 protein level but increased D1 mRNA levels. There are two possible explanations for why knock-down of CREB could result in upregulation of D1 mRNA. First, D1 promoter contains a putative CRE sites and can be potentially regulated by the CREB/ATF family transcription factors. While CREB is an activator for cAMP-responsive genes, it can induced the expression of a transcriptional inhibitor, inducible cAMP early repressor (ICER), which can compete with CREB for binding to the CRE sites and thereby repress transcription of cAMP-responsive genes [34]. Promoter analysis reveals that the D1 promoter contains a half CRE sequence (Appendix figure 3.5A). We have observed that cAMP treatment caused

constant upregulation of ICER (Appendix figure 3.5B). It is possible for ICER to bind to the CRE site and inhibit D1 transcription. When CREB activity is knocked down, expression of ICER would be inhibited, thereby relieving the transcriptional inhibition of D1. Alternatively, CREB may modulate D1 transcription indirectly through regulating other transcription factors. Transcription of D1 is known to be regulated by the Sp family proteins [289, 290] and the D1 promoter contains several Sp binding sites (Appendix figure 3.5A). While Sp1 activates D1 transcription, the other Sp family protein Sp3 inhibits D1 transcription [290]. Transcription of Sp3 was shown to be upregulated by c-fos [291], a transcription factor that is activated by CREB [34], c-fos was observed to be transiently upregulated by cAMP in our study (Appendix Figure 3.5C). Therefore, it could be possible that CREB indirectly inhibits D1 transcription by upregulating c-fos expression, which increases Sp3 expression and thereby represses D1 transcription. While such transcriptional regulation could contribute to the upregulation of the D1 mRNA levels, it does not explain why the D1 protein level decreases. One possible explanation could be posttranscriptional regulation of the D1 protein. microRNAs (miRNAs), which mainly regulates mRNA by binding to the 3'-untranslated (3'-UTR) regions of the mRNA to suppress translation [292], are potential candidates for the reduced D1 protein level. A recent study suggested that expression of D1 can be modulated by the miRNA miR-504 [293]. It is not known how miR-504 expression is regulated. A possible scenario is that knock-down of the CREB activity is due to an upregulation of the miR-504 levels by a yet unknown mechanism, and thereby leading to down-regulation of the D1 protein level.

5.2.4 Combining experiments and modeling to delineate signaling pathways involved in regulating CREB and ATF4 activation of HepG2 cells

Previously, we showed that palmitate down-regulated cAMP [163, 177]. In contrast to the down-regulation of cAMP by palmitate, we observed that its downstream signaling component, CREB, was activated by palmitate. Similarly, the activating transcription factor 4 (ATF4), which also belongs to the CREB/ATF family transcription factors, was elevated by palmitate. While CREB is predominantly anti-apoptotic, regulating the transcription of anti-apoptotic genes such as Bcl2 [294, 295] and Bcl-xL [296], prolonged activation of ATF4 is considered pro-apoptotic, inducing C/EBP homologous protein (CHOP, also known as GADD153), which is a major component of the endoplasmic reticulum (ER) stress-mediated apoptotic pathway [297]. Therefore, the coordinated regulation of CREB and ATF4 may exert an important role in cell fate determination. Accordingly, an approach that integrates both experimental and modeling data may help to delineate the signaling events involved and enhance our understanding of how palmitate reduces cAMP levels while enhancing CREB activation and further explain how cAMP synergizes with palmitate to enhance cell death. While little is known about the transcriptional regulation of ATF4, our preliminary results suggest that ATF4 may be transcriptionally regulated by CREB and vice versa. A Boolean network model is currently being developed to delineate the upstream pathways that lead to CREB and ATF4 activation. Delineation of the upstream signaling network initiated by palmitate that led to CREB and ATF4 activation may facilitate our understanding of how palmitate activates both anti- and pro-apoptotic pathways to elicit a pro-apoptotic cell fate.

5.3 Overall conclusions and impact

Taken together, the work in this thesis suggests that a combinatorial approach of cAMP and MSCs for treating neuronal diseases, such as spinal cord injury, may be appropriate since cAMP is able to guide MSCs to differentiate into neural lineage cells. However, careful attention should also be paid to the fact that cAMP may also result in undesirable effects, such as apoptosis of MSCs. In general, this study advances our understanding regarding the potential of MSCs to differentiate into neural lineage cells and obtain some neuronal function upon stimulation by cAMP. Although the neural lineage differentiation ability of MSCs is not the same as neural stem cells (NSCs), ESCs or iPS cells, MSCs have their own advantages with respect to therapeutic applications. For example, MSCs can be obtained more easily than NSCs and do not have the moral or political issues associated with ESCs. They are also much safer for clinical applications than iPS cells, which are more likely to form tumor and are quite different from ESCs in many ways [298]. Therefore, a better understanding of MSCs is still necessary and could potentially greatly advance the application of stem cells for clinical applications.

Although current studies indicate that the ability of MSCs to repair neuronal damage is mainly related to their ability to secrete growth factors, the ability of MSCs to differentiate into neural lineage cells cannot be denied and would be beneficial to promoting neuronal repair. As such, future work aimed at purifying subpopulations of MSCs to obtain ones with higher ability to differentiate into neural lineages is desirable. Therefore, our ongoing research is to use a multi-prong approach, including optimization of induction media, modification of culture substrate and construction of models, to aid the selection of a subpopulation of MSCs that may have higher neural induction

efficiency. Obtaining an enriched cell source may advance the research regarding neural lineage differentiation of MSCs and facilitate the therapeutic application of MSCs for treating neuronal diseases.

APPENDICES

APPENDIX 1. ISOLATION AND ENRICHMENT OF MSCS AND SEPARATION OF SINGLE-COLONY DERIVED MSCS

This work has been published in Journal of Visualized Experiments
Zhang, L. and Chan, C. Isolation and enrichment of rat mesenchymal stem cells (MSCs) and separation of single-colony derived MSCs. J Vis Exp. 2010 Mar 22;(37). pii: 1852. doi: 10.3791/1852.

Abstract

MSCs are a population of adult stem cells that is a promising source for therapeutic applications. These cells can be isolated from the bone marrow and can be easily separated from the hematopoietic stem cells (HSCs) due to their plastic adherence. This protocol describes how to isolate MSCs from rat femurs and tibias. The isolated cells were further enriched against two MSCs surface markers CD54 and CD90 by magnetic cell sorting. Expression of surface markers CD54 and CD90 were then confirmed by flow cytometry analysis. HSC marker CD45 was also included to check if the sorted MSCs were depleted of HSCs. MSCs are naturally quite heterogenous. There are subpopulations of cells that have different shapes, proliferation and differentiation abilities. These subpopulations all express the known MSCs markers and no unique marker has yet been identified for the different subpopulations. Therefore, an alternative approach to separate out the different subpopulations is using cloning cylinders to separate out single-colony derived cells. The cells derived from the single-colonies can then be cultured and evaluated separately.

Protocol

1. Isolation of rat MSCs

Mesenchymal stem cells were isolated from 6-8 week old Sprague-Dawley female rat as previously described [152, 299]. Isolated MSCs can adhere to plastic surface and easily expand during in vitro culture.

1.1 The animal is put into an anaesthesia chamber and anaesthetized for around five minutes. During the anaesthesia, the rate of blinking, breathing and motor activity of the aminal is observed. Immediately after the animal stops motor activity and its blinking rate became infrequent, remove the animal from the anaesthesia chamber.

1.2 The animal is layed down on an operation station and killed by cervical dislocation. Femurs and tibias are cut off from the back limbs and the attached skin and muscles are removed.

1.3 The dissected femurs and tibias are put in 70% isopropanol for a few seconds and transferred to 1X D-PBS.

1.4 In a biosafety cabinet, the femurs and tibias are transferred to a 10 cm dish containing DMEM. Each bone is then held with tweezers and the two ends are cut open with a scissor. A 22G needle is attached to a 3ml syringe and filled with DMEM, then the marrow is flushed into a 50ml tube by inserting the needle to one open end of the bone. This is repeated 2~3 times for each bone. When all the marrows are obtained, cells are resuspended and the cell suspension is passed through a 70 μm cell strainer to remove the bone debris and blood aggregates.

1.5 Cells are centrifuged at 200g, 4 ^{o}C for 5 minutes and the supernatant is removed by aspiration. After that, cells are resuspended in 25 ml MSC medium (DMEM containing 10% FBS and 1% Pen-Strep). 10 ml cell suspension is seeded into each 10

cm culture dish for a total of two dishes. The culture dishes are kept in a 37 °C and 5% CO_2 incubator for 1~2 weeks. Medium is changed every 2~3 days.

2. Enrichment of rat MSCs

A number of surface proteins have been used to enrich MSCs, including CD54, CD90, CD73, CD105 and CD271 [107-109]. In this study, we used CD54 and CD90 as markers to enrich MSCs by magnetic cell sorting.

2.1 When cells reached around 80% confluency, the medium is aspirated and 4~5ml trypsin-EDTA is added to each dish. The dishes are put back to the incubator for around 5 minutes to allow cell detachment. Once cells are detached, equal amount of culture medium is added to inactivate trypsin. Cell suspension is collected into a 15 ml tube and centrifuged at 200g, 4 °C for 5 minutes.

2.2 The next steps describe how to enrich MSCs by two surface markers CD54 and CD90 according to the manual for cell separation using BD IMagnet. Cell pellet is resuspended in cell staining buffer (3% heat inactivated FBS in 1X D-PBS) at 20 million cells/ml. Biotinylated CD54 antibody (0.25 μg per million cells) and biotinylated CD90 antibody (0.15 μg per million cells) is added and mixed gently with the cell suspension. After incubation on ice for 15 minutes, labeled cells are washed with an excess volume of 1X BD IMag buffer. The labeled cells are spinned down at 200g, 4 °C for 5 minutes.

2.3 The BD IMag streptavidin particles are vortexed thoroughly, and 40 μl particles are added for every 10 million cells. The labled cells are mixed with the particles

thoroughly and incubated at 6~12 °C for 30 minutes. This allows the streptavidin particles to bind to the biotinylated anti-CD54 and anti-CD90, which is bound to the surface proteins CD54 and CD90 respectively.

2.4 During the incubation time, a round-bottom test tube is labled to collect the positive fraction. After incubation, the labeling volume is brought to 20 million cells/ml with 1X BD IMag buffer and the labeled cells are transferred to the positive-fraction collection tube. The positive-fraction tube is placed onto the BD IMagnet for 6 minutes. After that, the supernatant is removed with a glass Pasteur pipette with the positive-fraction tube still on the BD IMagnet.

2.5 The positive-fraction tube is removed from the BD IMagnet and placed on ice. 1ml ice cold 1X BD IMag buffer is added to the tube and cells are resuspended by gentle mixing. The tube is placed back onto the BD IMagnet for 2~4 minutes. The supernant is removed with a new glass Pasteur pipette. This step is repeated one more time.

2.6 The tube is removed from the BD IMagnet and cells are resuspended in culture medium. seed one 75cm^2 flask for maintaining the cells and a 10 cm dish for flow cytometry.

3. Verification of surface marker expression by flow cytometry

Flow cytometry analysis is performed to verify the cells we obtained express CD54 and CD90. The HSC marker CD45 is used to confirm that the MSCs are depleted of HSCs.

3.1 Cells are trypsinized with trypsin-EDTA when they become ~80% confluent.,Trypsinized cells are collected into a 15 ml tube and centrifuged at 200g, 4 ^{o}C for 5 minutes to collect cells.

3.2 After aspirating the supernatant, cells are washed with 1X D-PBS once. Cells are then resuspended in cell staining buffer (1X D-PBS containing 2% FBS and 0.05% sodium azide) to a final concentration of 5~10 million cells/ml and kept on ice. Cell suspension are aliquoted into six labeled tubes (1. cells only; 2. isotype control IgG2a; 3. Isotype control IgG1; 4. CD45; 5. CD54; 6. CD90), with 100 μl each tube.

3.3 Isotype controls and primary antibodies at appropriate concentrations (IgG2a and IgG1: 20 μl per million cells; CD45: 0.5 μg per million cells; CD54: 0.25 μg per million cells; CD90: 0.15 μg per million cells) are added to the cell suspension and incubated at 4 ^{o}C for 30 minutes.

3.4 After washing cells with 1X D-PBS twice, they are resuspended in 100 μl cell staining buffer. SA-PE (streptavidin- phycoerythrin, use 0.15 μg per million cells) is added to every tube and the cell suspensions are incubated at 4 ^{o}C for 30 minutes in dark.

3.5 Labeled cells are washed with 1X D-PBS twice and resuspended in 400 μl cell staining buffer, and then transferred to a falcon tube for flow cytometry analysis.

4. Separation of single-colony derived MSCs

MSCs is a heterogeneous population composed of different subpopulations with different cell shape, growth rate as well as differentiation ability [281]. However, all the subpopulations express the known MSC markers and therefore it is not feasible to use markers to separate out these subpopulations. Therefore, we applied cloning cylinders to separate out the different subpopulations, which are colonies formed by single cells.

4.1 Cells are plated at about 50~100 cells per 10 cm dish and incubated in a 37 ^{o}C and 5% CO_2 incubator for 1~2 weeks. During this period, colonies are examined with an inverted microscope. Once the colonies have reached big enough size (better more than 100 cells in each colony), the well isolated (no surrounding colonies) colonies are marked with a sharpie at the bottom of the dish.

4.2 After aspirating medium and washing with 1X D-PBS, sterile cloning cylinders are gently placed around the marked colonies. The picked colonies should be far away from each other such that every cloning cylinder only contains one colony.

4.3 A volume of 100 μl trypsin-EDTA is added to each cloning cylinder and the dish is put back to the incubator for ~5 minutes. After 5 minutes, cells are checkecd under the microscope to see whether they are rounding up. When the cells have lifted up, an equal amount of culture medium is added to inactivate trypsin. The cell suspension was then transferred to a 60 mm dish containing 3ml prewarmed culture medium. Morphology can be trackedover the next few days.

Representative Results

According to the protocol described in the part for rat MSCs isolation, plastic adherent MSCs should be visible the next day after plating. As cells continue to proliferate, the confluent cells should look like the cells shown in Appendix figure 1.1A. When cells reach ~80% confluency (Appendix figure 1.1B), subculturing can be carried out. During subculture, trypsin-EDTA was used to detach cells and lifted cells are small and round as shown in Appendix figure 1.1C.

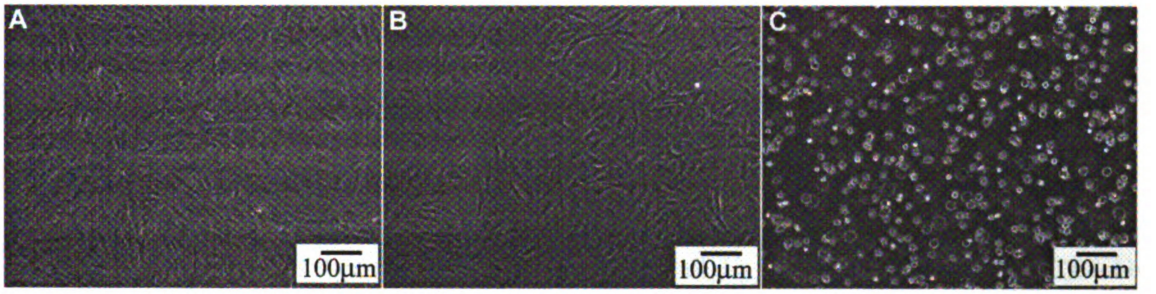

Appendix figure 1.1 Phase contrast images of rat MSCs. (A) Confluent MSCs. The majority of cells are spindle-like or star-like. (B) MSCs around 80% confluency. (C) Lifted cells after trypsinization are small and round.

Once MSCs are enriched by magnetic cell sorting, flow cytometry analysis is performed to verify the surface marker expressions. If the enrichment is good, the cells should show positive staining against MSC markers CD54 and CD90 but negative against the HSC marker CD45 (Appendix figure 1.2). Isotype controls IgG2a and IgG1 are used as negative controls.

When cells are seeded at proper clonal density, colonies should rise from single cells. Appendix figure 1.3A represents a colony formed by a single cell. Cloning cylinders can then be used to separate the colonies and cells derived from the colonies can be cultured separately. Appendix figure 1.3B and 1.3C represents cells derived from two individual colonies. The cells derived from colony 1 are spindle like (Appendix figure 1.3B) whereas the cells derived from colony 2 are round (Appendix figure 1.3C).

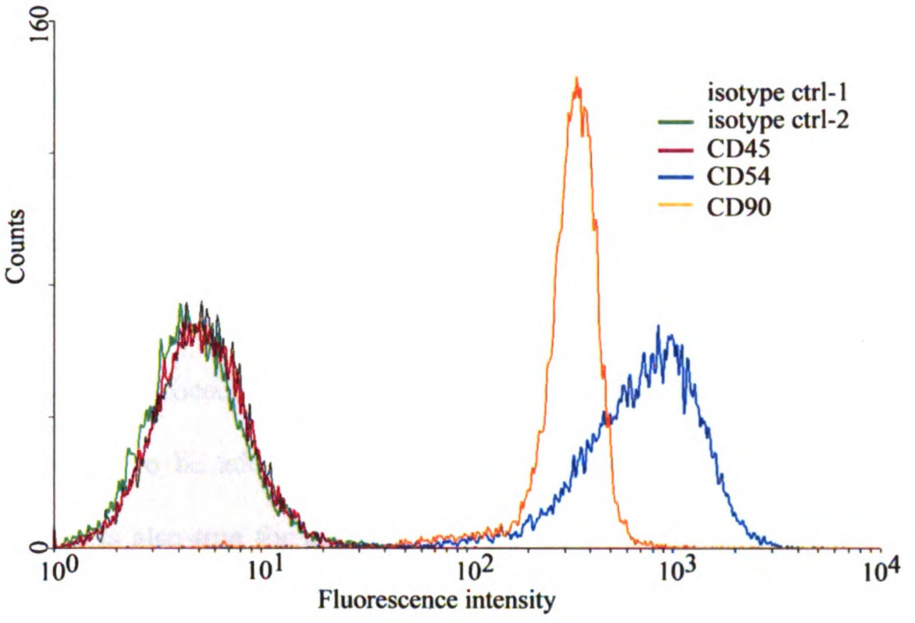

Appendix figure 1.2 Flow cytometry analysis of MSCs for surface markers. MSCs were labeled with antibodies against IgG2a (isotype control 1), IgG1 (isotype control 2), CD45, CD54 and CD90. MSCs expressed CD54 and CD90 but not CD45.

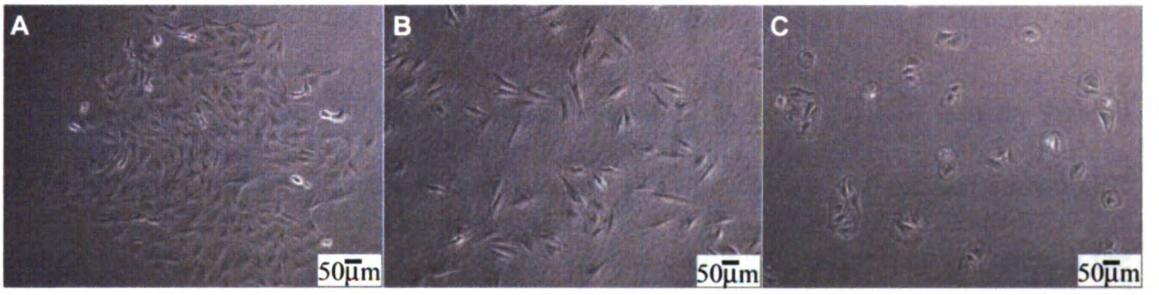

Appendix figure 1.3 Colony formation by MSCs and single-colony derived cells. MSCs cultured at clonal density form individual colonies. These colonies can be separated by cloning cylinders and cells from different colonies can be cultured separately. (A) A representative colony formed by MSCs when plated at clonal density. (B) Spindle-like cells derived from one colony. (C) Round cells derived from another colony.

Discussion

This protocol describes how to isolate and enrich MSCs. A method to separate the single-colony derived cells is also incorporated. There are several steps that are important for a successful isolation, enrichment and colony separation. While doing cell isolation

from rat, it is recommended to filter through a cell strainer or a sterile nylon mesh of similar size to get rid of the blood clots and bone debris. After plating the cells overnight, many dead cells will be floating in the medium and the dead cells are removed by replacing with fresh medium which should help the growth of the attached cells.

The magnetic cell sorting in this protocol describes how to perform a positive selection, and similar procedures can be used to perform a negative selection. The amount of antibodies to be added may differ and optimization is required to achieve better sorting. This is also true for labeling the cells for flow cytometry analysis. If not running flow cytometry analysis for the labeled samples immediately, samples can be fixed with 2% formaldehyde and run later. However, long-term storage is not recommended since this tends to increase the auto-fluorescence and sacrifice sample quality.

The key part for the colony separation is seeding at the right cell density (which should be optimized experimentally) and locating single clones that are not surrounded by other clones. If there are other clones nearby, the cloning cylinder may encompass the nearby clones and the cells obtained will no longer be from one clone. When placing the cloning cylinder over the clone, also be careful not to slide it over the dish surface as this will cause the silicon grease at the bottom of the cloning cylinder to cover the cells and prevent the trypsin from reaching the cells to detach them.

Appendix Table 1.1 Specific reagents and equipment

Name of the reagent	Company	Catalogue number	Comments (optional)
1X D-PBS	Invitrogen	14040-133	
DMEM	Invitrogen	11885-084	
Cell strainer	BD Bioscience	352350	
FBS	Invitrogen	26140-079	
Pen-Strep	Invitrogen	15140	
Trypsin-EDTA	Invitrogen	25200-056	
BD Imagnet	BD Bioscience	552311	
Biotin mouse IgG2a	BD Bioscience	555572	
Biotin mouse IgG1	BD Bioscience	555747	
Biotin anti-rat CD54	Cedarlane Labs	CL054B	
Biotin anti-rat CD90	Cedarlane Labs	CL005B	
Biotin anti-rat CD45	Cedarlane Labs	CL001B	
BD Imag buffer	BD Bioscience	552362	
Round-bottom tube	BD Bioscience	352063	
Streptavidin particles	BD Bioscience	557812	
SA-PE	R&D systems	F0040	
Cloning cylinder	Sigma	C2059	

APPENDIX 2. SUPPLEMENTARY METHODS AND FIGURES FOR CHAPTER 2

Supplementary methods

Quantitative real time polymerase chain reaction (RT-PCR)

Cells were treated as indicated and mRNA was extracted using the RNA extraction kit from Qiagen according to the manufacture's instruction. mRNA was then reverse transcribed into cDNA using the cDNA synthesis kit from Bio-Rad. The following primer sets (Eurofins MWG Operon) were used for PCR: actin (5'-CCCTAGACTTCGAGCAAGAGA-3', 5'- AGGAAGGAAGGCTGG AAGAG-3'), NSE (5'-ACCACATCAACAGCACCATC-3', 5'-TTGTTCTCAGTCCCATCCAA-3'), Tuj1 (5'-TAGTGGAGAACACGGATGAGA-3', 5'-GCAGACACAAGGTGGTTGAG-3'), GFAP (5'-GCTCCAAGATGAAACCAACC-3', 5'-AACCTTCCTCTCCAGATCCA-3'). Amplification of the cDNA templates were detected by SYBR Green Supermix (Bio-Rad) using Real-Time PCR Detection System (Bio-Rad). The cycle threshold (CT) values for each condition were determined by the MyIQ software.

Colony-forming units (CFU) assay

CFU assay was used to assess the self-renewal capability of MSCs [300]. In brief, 50~100 cells were plated in a 10 cm culture dish and the dish is incubated in a 5% CO_2 incubator at 37℃ for 10~14 days. Colonies were stained with 0.5% crystal violet (Sigma) in methanol for 5~10 minutes at room temperature and the number of colonies were scored with a scoring grid.

Adipogenesis induction

Adipogenesis induction was carried out according to the protocol provided on the Millipore website. Cells were induced with adipogenesis induction media (cell culture media supplemented with 10 mM dexamethasone (Sigma), 0.5 M IBMX (Sigma), 10 mg/mL insulin (Sigma) and 20 mM indomethacin (Sigma)) after reaching confluency. This corresponds to differentiation day 1. The induction media was changed on day 3 and day 5. On day 7, the media was changed to adipogenesis maintenance media (cell culture media containing 10 mg/mL insulin) for two days. On days 9, 11 and 13, the media was replaced with fresh adipogenesis induction media. On day 15, the media was replaced with fresh adipogenesis maintenance media. On days 17 and 19, the media was replaced with fresh adipogenesis induction media. On day 21, the cells were fixed and lipid droplets were stained using Oil Red O solution (Sigma).

Osteogenesis induction

Osteogenesis induction was carried out according to the protocol provided on the Millipore website. Confluent cells were induced with osteogenesis induction media (cell culture media supplemented with 1 mM dexamethasone (Sigma), 0.1 M ascorbic acid 2-phosphate (Sigma), 1 M glycerol 2-phosphate (Calbiochem) and 200 mM L-glutamine (Sigma)). Media was changed every two days for a total of 14 days. Calcium deposition can then be visualized by Alizarin Red (Sigma) staining.

Oil Red O staining for lipid droplets

Cells were fixed with 4% formaldehyde for 30 minutes at room temperature. After carefully removing the fixative, the cells were rinsed three times with PBS, and twice with DI water. The cells were then covered with enough Oil Red O solution and incubated for 50 minutes at room temperature. Excess dye was removed and the cells were rinsed three times with DI water. The cells stained with Oil Red O can be visualized using phase contrast imaging (with a color camera).

Alizarin Red staining for calcium deposits

Cells were fixed with 70% ice cold ethanol for 1 hour. After carefully removing the fixative, the cells were washed twice with DI water for 5~10 minutes each. Alizarin Red solution was added to stain the cells for 30 minutes after removing the water. The cells were rinsed four times with DI water before phase contrast imaging (with a color camera).

Supplementary Figures

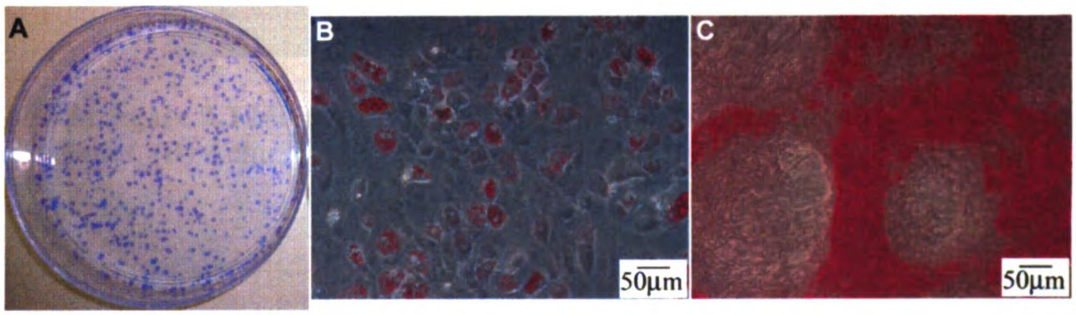

Appendix figure 2.1 Self-renewal and multi-lineage differentiation ability of MSCs. (A) Colony-forming units (CFU) assay indicates that MSCs can form colonies and have self-renewal property. (B) Oil Red O staining for oil droplets indicates MSCs can differentiate into adiocytes. (C) Alizarin Red staining for calcium deposit indicates MSCs can differentiate into osteoblasts.

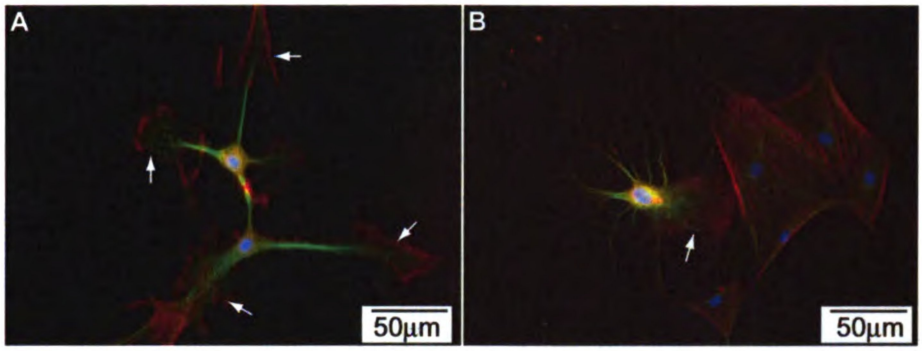

Appendix figure 2.2 Cytoskeleton staining for actin filaments and microtubules. MSCs were treated with 10 μM forskolin and 100 μM IBMX (FI) for 1 hr. Green: microtubules; red: actin filaments; blue: nucleus.

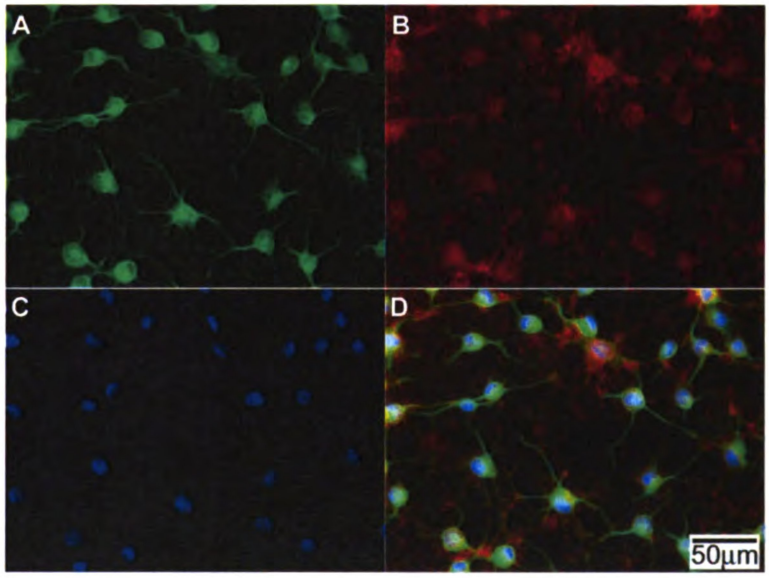

Appendix figure 2.3 Morphology of MSCs treated with staurosporine (1 μM) 1 hour. (A) Microtubules, (B) Actin filaments, (C) Nucleus and (D) Overlaid image of (A-C).

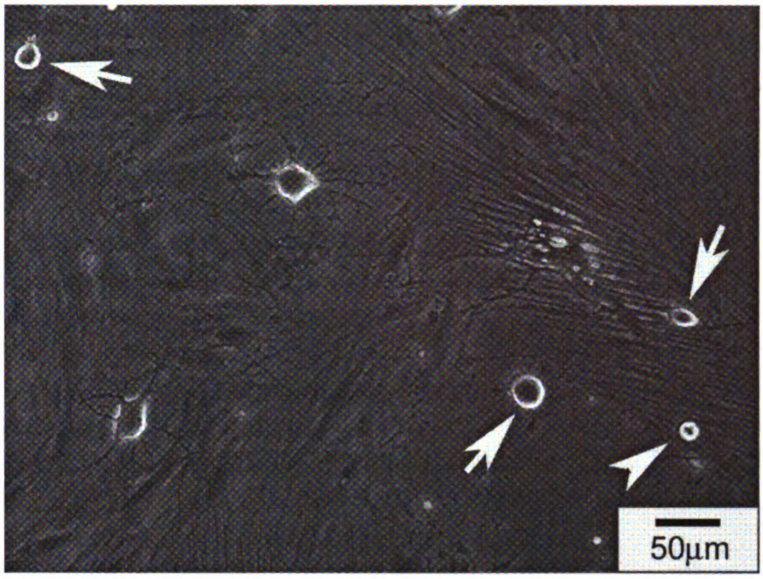

Appendix figure 2.4 Morphology of MSCs treated with 10 μM forskolin and 100 μM IBMX (FI) for 12 hours. The cell denoted by the arrow head has changed morphologically and lifted up from the surface. The cells denoted by the arrows are not as anchored to the surface and eventually may lift up.

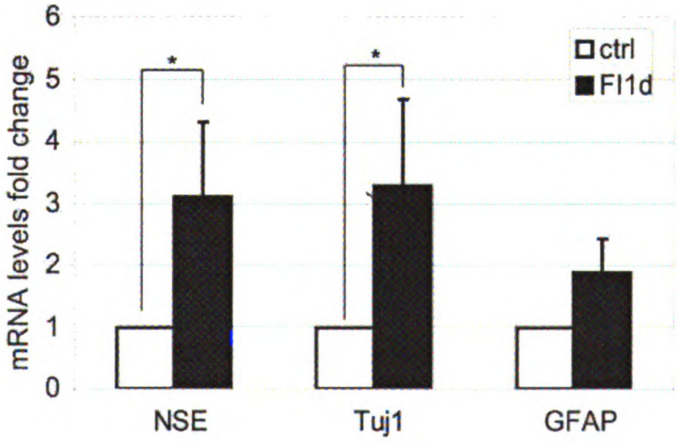

Appendix figure 2.5 mRNA levels of neural markers NSE, Tuj1 and GFAP. MSCs were in control media or induced with 10 μM forskolin and 100 μM IBMX (FI) for one day. (n=3 for NSE and Tuj1, n=2 for GFAP). *: $p<0.05$.

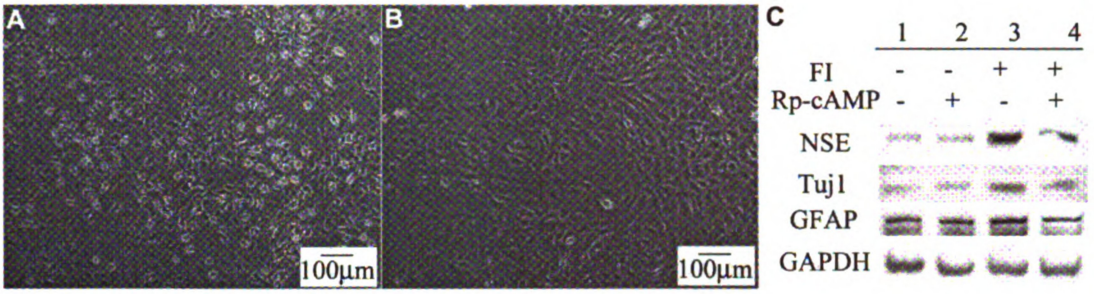

Appendix figure 2.6 PKA regulates morphology and marker expression. (A) MSCs induce with 10 μM forskolin and 100 μM IBMX (FI) for one hour. (B) MSCs pretreated with 10 μM Rp-cAMPS for 30 minutes and induced with FI supplemented with 10 μM Rp-cAMPS for 1 hour. (C) Expression of neural markers NSE, Tuj1 and GFAP. MSCs were treated with FI in the absence or presence of 10 μM Rp-cAMPS for 24 hours.

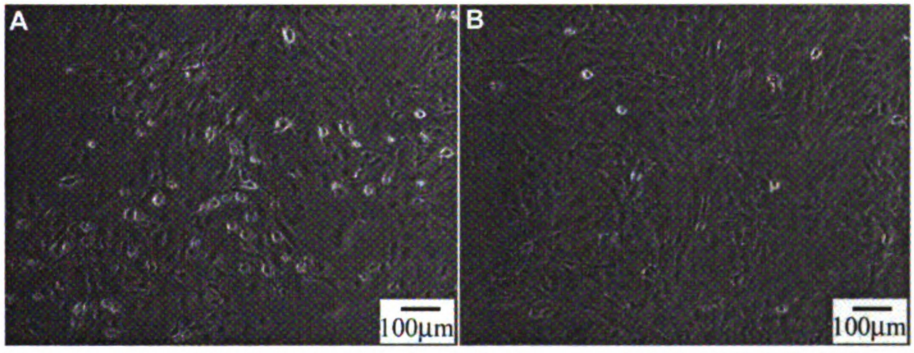

Appendix figure 2.7 Morphology of MSCs treated with FI and paclitaxel. (A) Morphology of MSCs treated with 10 μM forskolin and 100 μM IBMX (FI) for 3 hours followed by fresh FI medium for 1 hour. (B) Morphology of MSCs treated with FI in the presence of 0.4 μM paclitaxel for 3 hours followed by fresh FI medium for 1 hour.

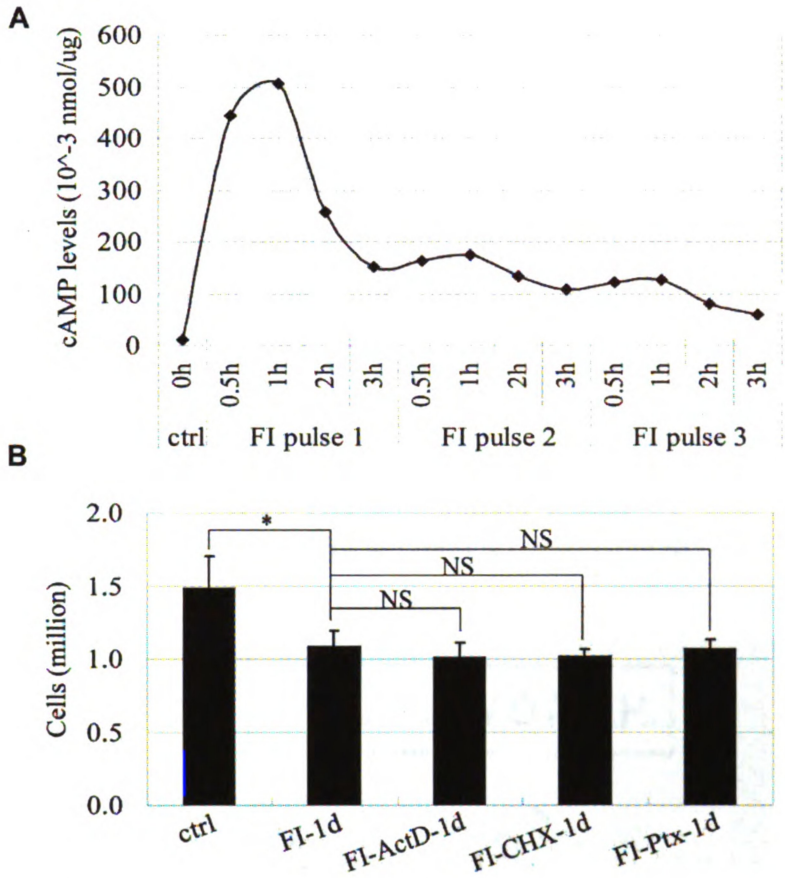

Appendix figure 2.8 cAMP levels and live cells in different treatments (A) Intracellular cAMP levels for untreated cells, or cells treated with 10 μM forskolin and 100 μM IBMX (FI) for 0.5, 1, 2 and 3 hours (FI pulse 1), or after the first pulse treated again with FI for 0.5, 1, 2 and 3 hours (FI pulse 2), or after the second pulse treated again with FI for 0.5, 1, 2 and 3 hours. (B) Number of viable cells in control and FI treated culture, in the absence or presence of 1 μg/ml actinomycin D (ActD), 10 μg/ml cycloheximide (CHX) or 0.4 μM paclitaxel (Ptx) for 3 hours followed by fresh FI medium for another 21 hours (n=3). *: $p<0.05$, NS: not significant.

APPENDIX 3. SUPPLEMENTARY FIGURES FOR CHAPTER 3

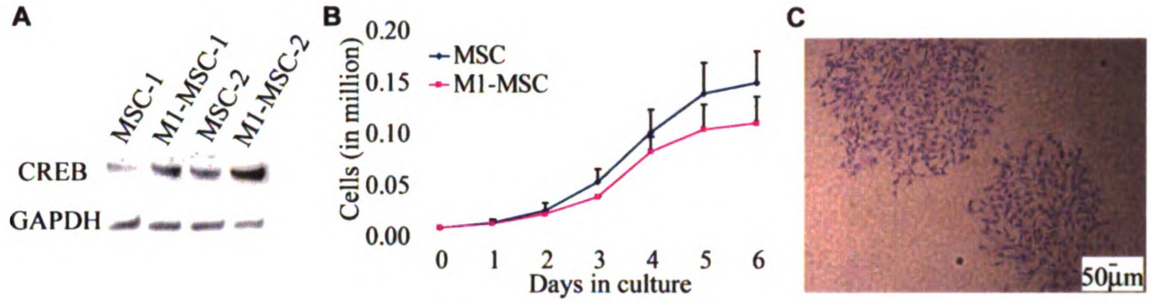

Appendix figure 3.1 Evaluation of MSCs expressing M1-CREB. (A) Expression of CREB for MSCs expressing the control vector and MSCs expressing the dominant negative M1-CREB (M1-MSCs). (B) Proliferation curves for MSCs and M1-MSCs during culture. (C) Colony formation of M1-MSCs (expressing M1-CREB).

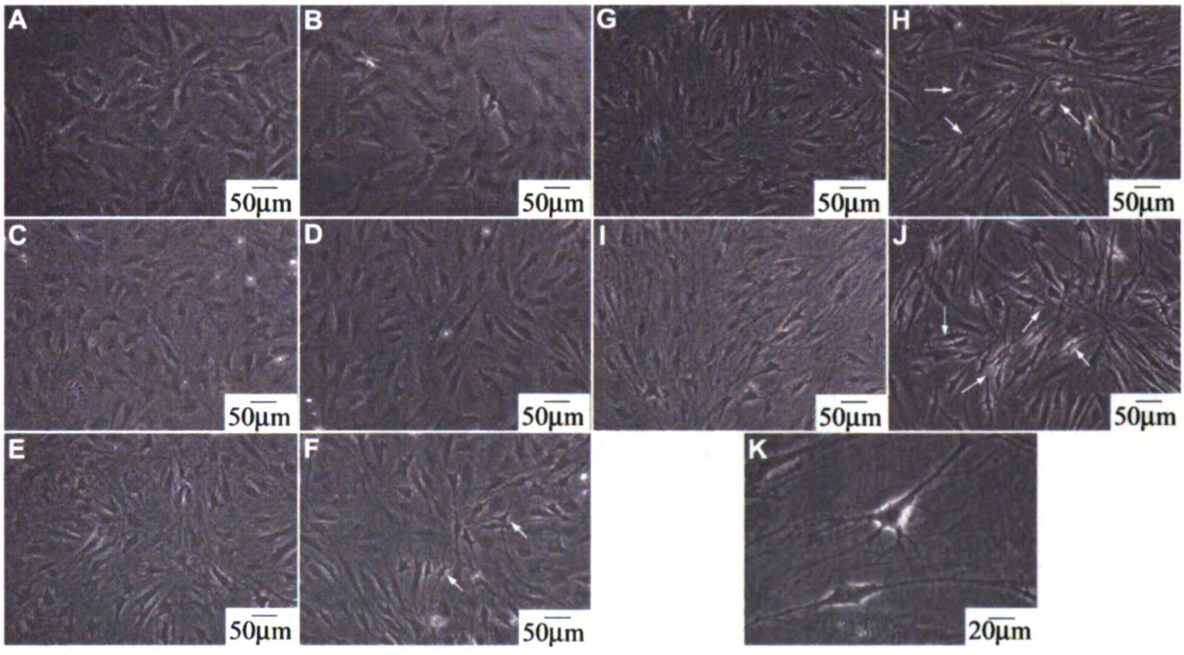

Appendix figure 3.2 Time-dependent morphological changes upon 10 μM forskolin and 100 μM IBMX (FI) induction of MSCs (expressing control vector) and M1-MSCs (expressing M1-CREB). (A-B) MSCs and M1-MSCs in control medium (left: MSCs; right: M1-MSCs). (C-D) MSCs and M1-MSCs induced with FI for 2 days. (E-F) MSCs and M1-MSCs induced with FI for 4 days. (G-H) MSCs and M1-MSCs induced with FI for 6 days. (I-J) MSCs and M1-MSCs induced with FI for 8 days. (K) Magnified view of M1-MSCs induced with FI for 8 days. Arrows denote a typical cell (M1-MSCs) that adopted a distinct morphology.

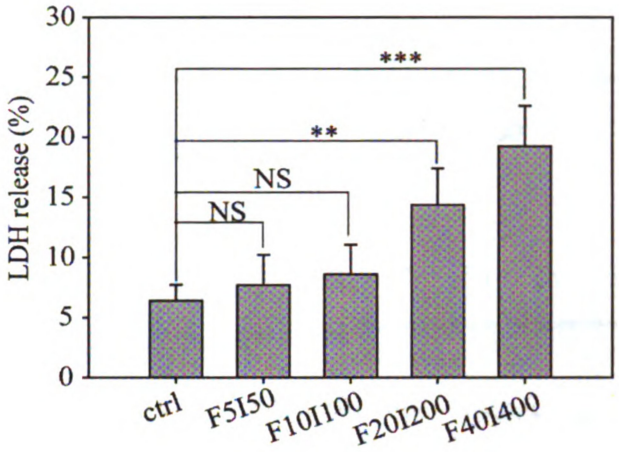

Appendix figure 3.3 LDH release as indication of toxicity of treatment. Cells were incubated in control media, media containing 5 μM forskolin and 50 μM IBMX (F5I50), 10 μM forskolin and 100 μM IBMX (F10I100), 20 μM forskolin and 200 μM IBMX (F20I200) and 40 μM forskolin and 400 μM IBMX (F40I400) for 24 hours. NS: not significant; **: $p<0.01$; ***: $p<0.001$.

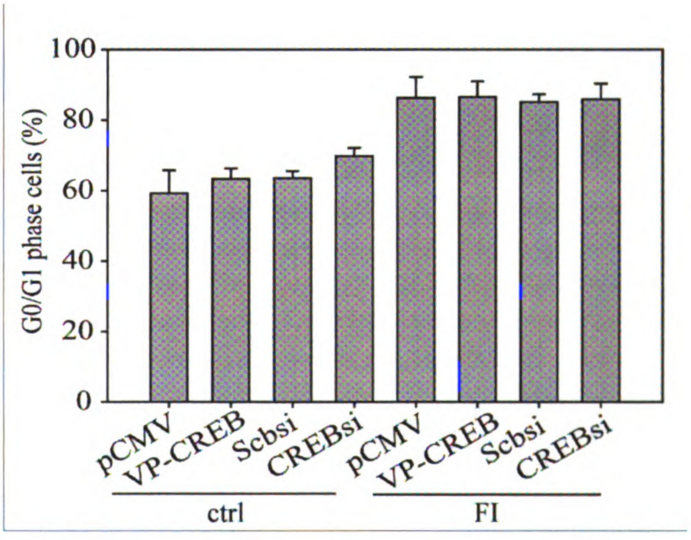

Appendix figure 3.4 CREB and G0/G1 phase cells. MSCs were transfected with the control vector pCMV, the constitutively active CREB (VP16-CREB), the negative control scramble siRNA and CREB siRNA. Transfected cells were incubated in medium in the absence (ctrl) or presence of 10 μM forskolin and 100 μM IBMX (FI) for 20 hours and cell cycle distribution was assessed after that (n=3). *: $p<0.05$; **: $p<0.01$.

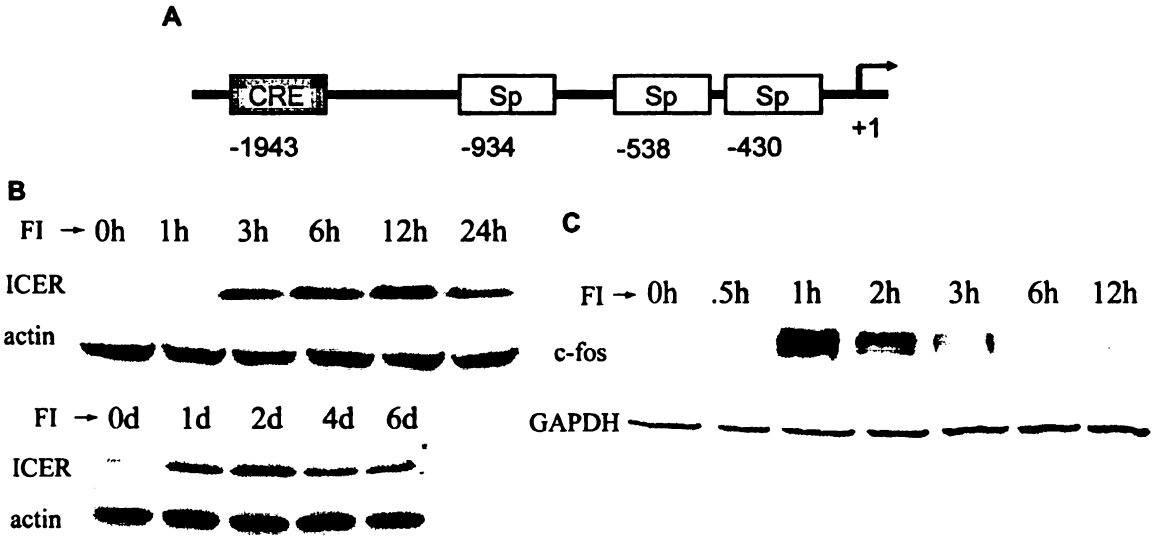

Appendix figure 3.5 D1 promoter and expression of ICER and c-fos. (A) D1 promoter contains a CRE site and several Sp sites. (B) ICER expression upon 10 μM forskolin and 100 μM IBMX (FI) treatment for the indicated time. (C) c-fos expression upon FI treatment for the indicated time.

APPENDIX 4. SUPPLEMENTARY FIGURES FOR CHAPTER 4

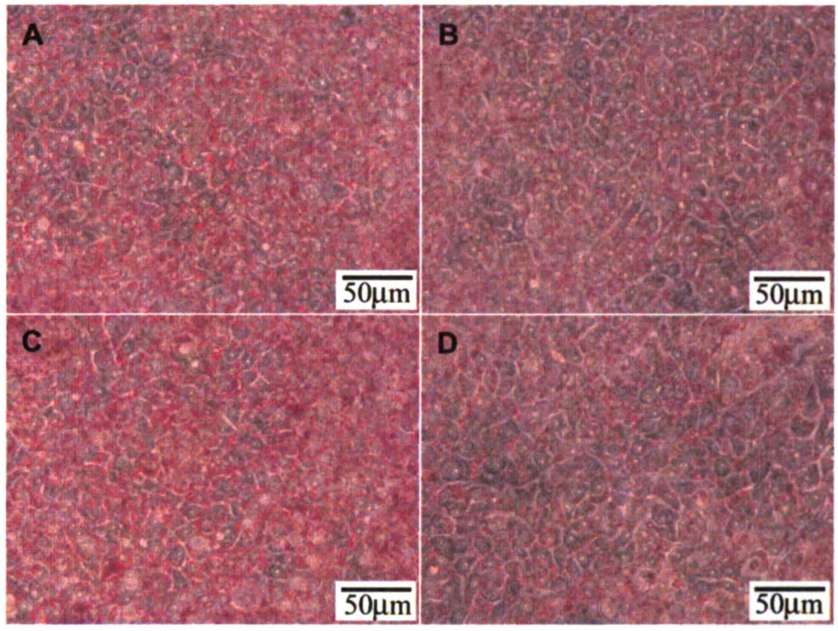

Appendix figure 4.1 Oil Red O staining for triglyceride. (A) cells treated with 0.7 mM oleate for 5 h, (B) cells treated with 0.7 mM palmitate for 5 h, (C) cells treated with 0.7 mM oleate for 12 h, and (D) cells treated with 0.7 mM palmitate for 12 h.

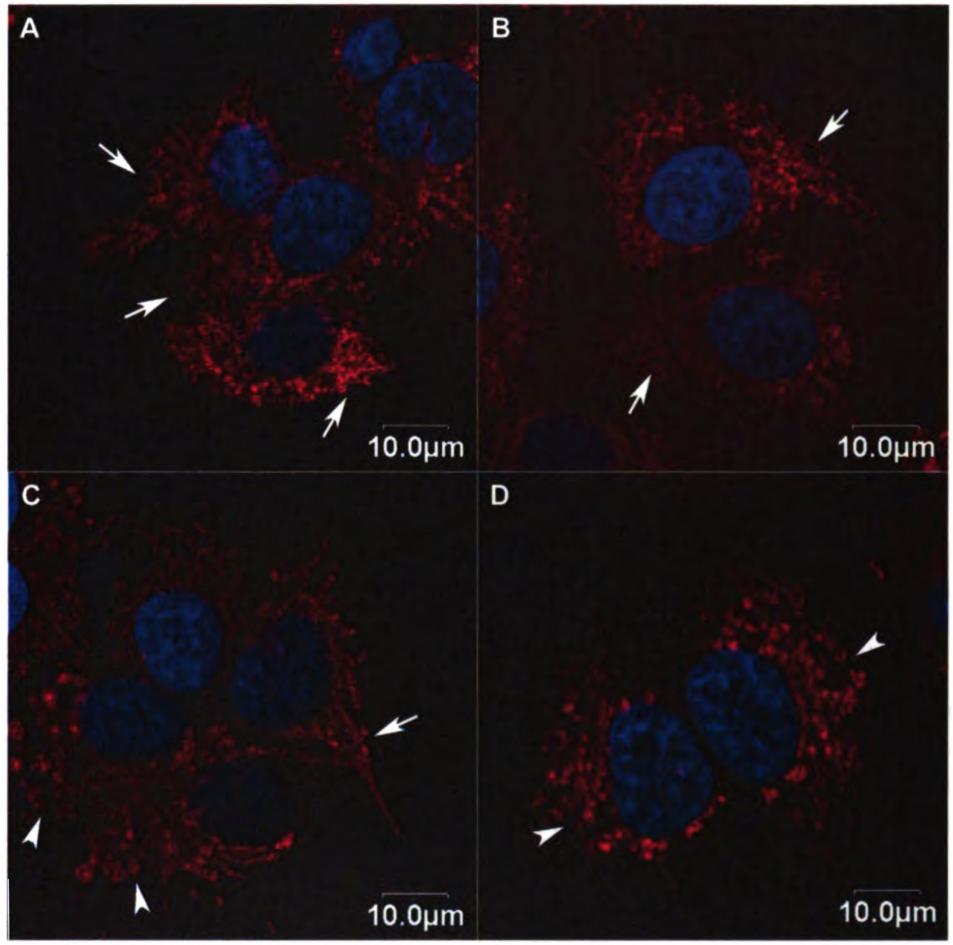

Appendix figure 4.2 Mitochondrial morphology. (A) control cells in medium/BSA, (B) cells treated with 0.2 mM palmitate for 24 h, (C) cells treated with 0.4 mM palmitate for 24 h, (D) and cells treated with 0.7 mM palmitate for 24 h.

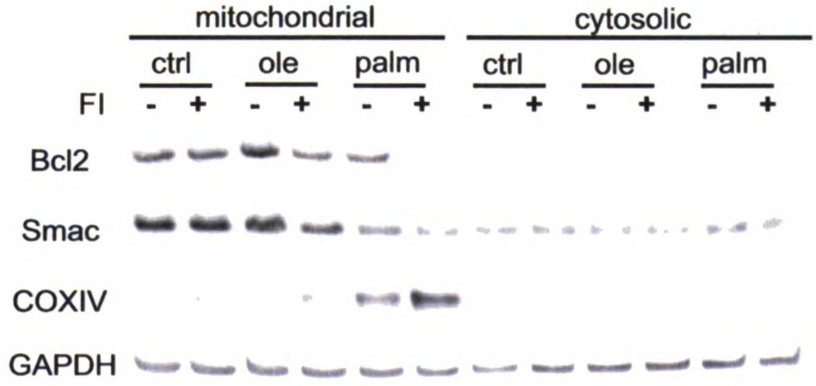

Appendix figure 4.3 Western blot of mitochondrial and cytosolic fractions. Cells were in control, 0.7 mM oleate and 0.7 mM palmitate in the absence or presence of 10 µM forskolin and 100 µM IBMX (FI) for 24 h ($n = 3$).

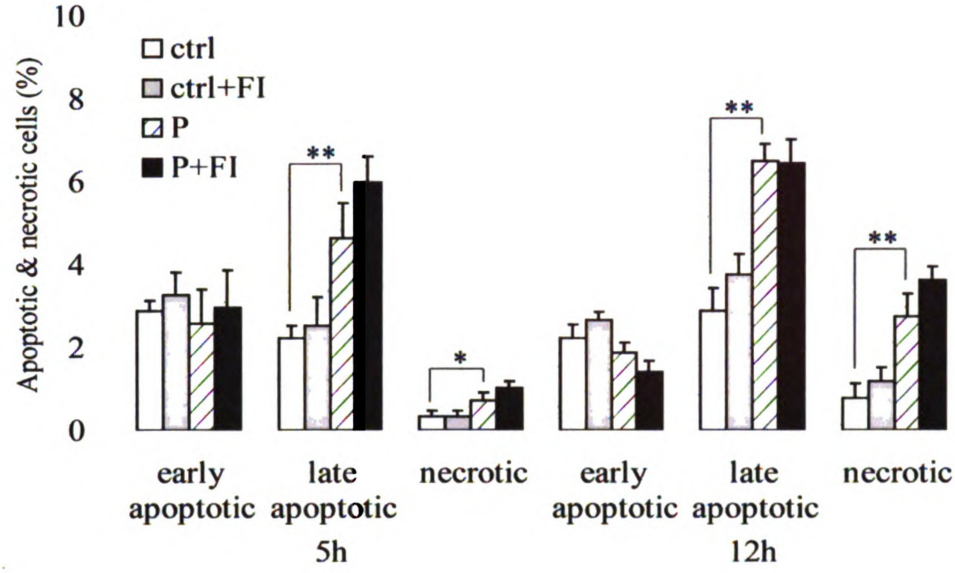

Appendix figure 4.4 Apoptotic and necrotic labeling by PI (propidium iodide) and Alexa Fluor-488 conjugated annexin V. Cells were in control (ctrl) and 0.7 mM palmitate (P) without (w/o) or with (w/) 10 μM forskolin and 100 μM IBMX (FI) for 5 h and 12 h. *Early apoptotic cells:* PI^- annexin V^+ cells; *late apoptotic cells*: PI^+ annexin V^+ cells; *necrotic cells*: PI^+ annexin V^- cells ($n = 3$).*: $p < 0.05$; **: $p < 0.01$.

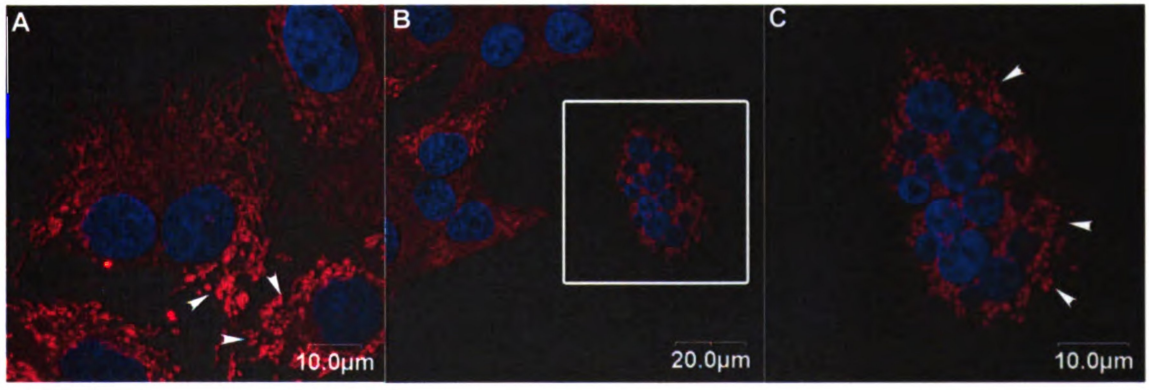

Appendix figure 4.5 Mitochondrial morphology of cells treated with 0.7 mM palmitate for 12 h. (A) Some cells already had fragmented mitochondria, as indicated by the arrowheads. (B) Some cell had both fragmented mitochondria and fragmented nucleus, as indicated by the rectangle. (C) Enlargement of the rectangle area in panel B.

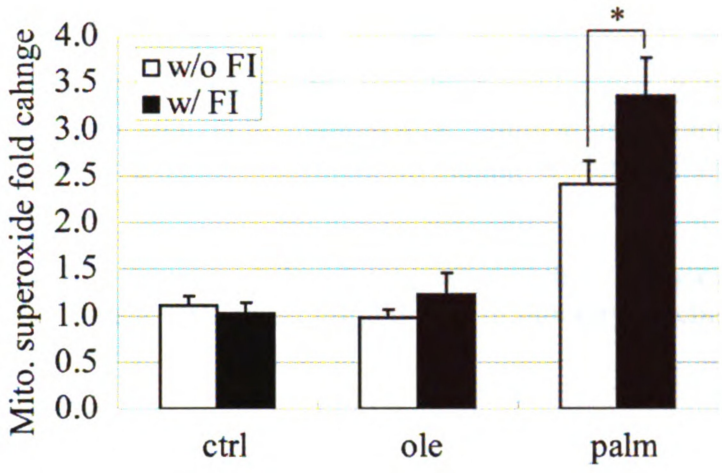

Appendix figure 4.6 Mitochondrial superoxide levels. Cells were in control, 0.7 mM oleate and 0.7 mM palmitate without (w/o) or with (w/) FI for 24 h ($n = 3$). *: $p < 0.05$; **: $p < 0.01$.

BIBILIOGRAPHY

[1] Hanna, J., Cheng, A.W., Saha, K., Kim, J., Lengner, C.J., Soldner, F., Cassady, J.P., Muffat, J., Carey, B.W., Jaenisch, R., Human embryonic stem cells with biological and epigenetic characteristics similar to those of mouse ESCs, *Proc Natl Acad Sci U S A* **107** 9222-9227.

[2] Mackay, A.V., Iversen, L.L., Increased tyrosine hydroxylase activity of sympathetic ganglia cultured in the presence of dibutyryl cyclic AMP, *Brain Res* **48** (1972) 424-426.

[3] Prasad, K.N., Hsie, A.W., Morphologic differentiation of mouse neuroblastoma cells induced in vitro by dibutyryl adenosine 3':5'-cyclic monophosphate, *Nature: New biology* **233** (1971) 141-142.

[4] Deng, W., Obrocka, M., Fischer, I., Prockop, D.J., In vitro differentiation of human marrow stromal cells into early progenitors of neural cells by conditions that increase intracellular cyclic AMP, *Biochem Biophys Res Commun* **282** (2001) 148-152.

[5] Schwarz, E.J., Alexander, G.M., Prockop, D.J., Azizi, S.A., Multipotential marrow stromal cells transduced to produce L-DOPA: engraftment in a rat model of Parkinson disease, *Human gene therapy* **10** (1999) 2539-2549.

[6] Parr, A.M., Tator, C.H., Keating, A., Bone marrow-derived mesenchymal stromal cells for the repair of central nervous system injury, *Bone Marrow Transplant* **40** (2007) 609-619.

[7] Webster, C.R., Anwer, M.S., Cyclic adenosine monophosphate-mediated protection against bile acid-induced apoptosis in cultured rat hepatocytes, *Hepatology (Baltimore, Md* **27** (1998) 1324-1331.

[8] Webster, C.R., Usechak, P., Anwer, M.S., cAMP inhibits bile acid-induced apoptosis by blocking caspase activation and cytochrome c release, *American journal of physiology* **283** (2002) G727-738.

[9] Graf, D., Reinehr, R., Kurz, A.K., Fischer, R., Haussinger, D., Inhibition of taurolithocholate 3-sulfate-induced apoptosis by cyclic AMP in rat hepatocytes involves protein kinase A-dependent and -independent mechanisms, *Archives of biochemistry and biophysics* **415** (2003) 34-42.

[10] Reinehr, R., Haussinger, D., Inhibition of bile salt-induced apoptosis by cyclic AMP involves serine/threonine phosphorylation of CD95, *Gastroenterology* **126** (2004) 249-262.

[11] Li, J., Yang, S., Billiar, T.R., Cyclic nucleotides suppress tumor necrosis factor alpha-mediated apoptosis by inhibiting caspase activation and cytochrome c release in primary hepatocytes via a mechanism independent of Akt activation, *J Biol Chem* **275** (2000) 13026-13034.

[12] Wang, Y., Kim, P.K., Peng, X., Loughran, P., Vodovotz, Y., Zhang, B., Billiar, T.R., Cyclic AMP and cyclic GMP suppress TNFalpha-induced hepatocyte apoptosis by inhibiting FADD up-regulation via a protein kinase A-dependent pathway, *Apoptosis* **11** (2006) 441-451.

[13] Fladmark, K.E., Gjertsen, B.T., Doskeland, S.O., Vintermyr, O.K., Fas/APO-1(CD95)-induced apoptosis of primary hepatocytes is inhibited by cAMP, *Biochemical and biophysical research communications* **232** (1997) 20-25.

[14] Kwon, G., Pappan, K.L., Marshall, C.A., Schaffer, J.E., McDaniel, M.L., cAMP Dose-dependently prevents palmitate-induced apoptosis by both protein kinase A- and cAMP-guanine nucleotide exchange factor-dependent pathways in beta-cells, *The Journal of biological chemistry* **279** (2004) 8938-8945.

[15] Montminy, M., Transcriptional regulation by cyclic AMP, *Annual review of biochemistry* **66** (1997) 807-822.

[16] Daniel, P.B., Walker, W.H., Habener, J.F., Cyclic AMP signaling and gene regulation, *Annu Rev Nutr* **18** (1998) 353-383.

[17] Serezani, C.H., Ballinger, M.N., Aronoff, D.M., Peters-Golden, M., Cyclic AMP: master regulator of innate immune cell function, *American journal of respiratory cell and molecular biology* **39** (2008) 127-132.

[18] Huang, C., Hepler, J.R., Chen, L.T., Gilman, A.G., Anderson, R.G., Mumby, S.M., Organization of G proteins and adenylyl cyclase at the plasma membrane, *Mol Biol Cell* **8** (1997) 2365-2378.

[19] Simonds, W.F., G protein regulation of adenylate cyclase, *Trends Pharmacol Sci* **20** (1999) 66-73.

[20] Cooper, D.M., Crossthwaite, A.J., Higher-order organization and regulation of adenylyl cyclases, *Trends Pharmacol Sci* **27** (2006) 426-431.

[21] Willoughby, D., Cooper, D.M., Organization and Ca2+ regulation of adenylyl cyclases in cAMP microdomains, *Physiological reviews* **87** (2007) 965-1010.

[22] Bender, A.T., Beavo, J.A., Cyclic nucleotide phosphodiesterases: molecular regulation to clinical use, *Pharmacological reviews* **58** (2006) 488-520.

[23] Francis, S.H., Corbin, J.D., Structure and function of cyclic nucleotide-dependent protein kinases, *Annual review of physiology* **56** (1994) 237-272.

[24] Taylor, S.S., Buechler, J.A., Yonemoto, W., cAMP-dependent protein kinase: framework for a diverse family of regulatory enzymes, *Annual review of biochemistry* **59** (1990) 971-1005.

[25] Wong, W., Scott, J.D., AKAP signalling complexes: focal points in space and time, *Nature reviews* **5** (2004) 959-970.

[26] Michel, J.J., Scott, J.D., AKAP mediated signal transduction, *Annual review of pharmacology and toxicology* **42** (2002) 235-257.

[27] Sassone-Corsi, P., Transcription factors responsive to cAMP, *Annual review of cell and developmental biology* **11** (1995) 355-377.

[28] Sands, W.A., Palmer, T.M., Regulating gene transcription in response to cyclic AMP elevation, *Cell Signal* **20** (2008) 460-466.

[29] Servillo, G., Della Fazia, M.A., Sassone-Corsi, P., Coupling cAMP signaling to transcription in the liver: pivotal role of CREB and CREM, *Experimental cell research* **275** (2002) 143-154.

[30] Johannessen, M., Delghandi, M.P., Moens, U., What turns CREB on?, *Cell Signal* **16** (2004) 1211-1227.

[31] Kwok, R.P., Lundblad, J.R., Chrivia, J.C., Richards, J.P., Bachinger, H.P., Brennan, R.G., Roberts, S.G., Green, M.R., Goodman, R.H., Nuclear protein CBP is a coactivator for the transcription factor CREB, *Nature* **370** (1994) 223-226.

[32] Lundblad, J.R., Kwok, R.P., Laurance, M.E., Harter, M.L., Goodman, R.H., Adenoviral E1A-associated protein p300 as a functional homologue of the transcriptional co-activator CBP, *Nature* **374** (1995) 85-88.

[33] Shaywitz, A.J., Greenberg, M.E., CREB: a stimulus-induced transcription factor activated by a diverse array of extracellular signals, *Annu Rev Biochem* **68** (1999) 821-861.

[34] Mayr, B., Montminy, M., Transcriptional regulation by the phosphorylation-dependent factor CREB, *Nat Rev Mol Cell Biol* **2** (2001) 599-609.

[35] Carlezon, W.A., Jr., Duman, R.S., Nestler, E.J., The many faces of CREB, *Trends in neurosciences* **28** (2005) 436-445.

[36] Rydel, R.E., Greene, L.A., cAMP analogs promote survival and neurite outgrowth in cultures of rat sympathetic and sensory neurons independently of nerve growth factor, *Proceedings of the National Academy of Sciences of the United States of America* **85** (1988) 1257-1261.

[37] Hanson, M.G., Jr., Shen, S., Wiemelt, A.P., McMorris, F.A., Barres, B.A., Cyclic AMP elevation is sufficient to promote the survival of spinal motor neurons in vitro, *J Neurosci* **18** (1998) 7361-7371.

[38] D'Mello, S.R., Galli, C., Ciotti, T., Calissano, P., Induction of apoptosis in cerebellar granule neurons by low potassium: inhibition of death by insulin-like growth factor I and cAMP, *Proceedings of the National Academy of Sciences of the United States of America* **90** (1993) 10989-10993.

[39] Li, M., Wang, X., Meintzer, M.K., Laessig, T., Birnbaum, M.J., Heidenreich, K.A., Cyclic AMP promotes neuronal survival by phosphorylation of glycogen synthase kinase 3beta, *Molecular and cellular biology* **20** (2000) 9356-9363.

[40] Parvathenani, L.K., Buescher, E.S., Chacon-Cruz, E., Beebe, S.J., Type I cAMP-dependent protein kinase delays apoptosis in human neutrophils at a site upstream of caspase-3, *J Biol Chem* **273** (1998) 6736-6743.

[41] Ottonello, L., Gonella, R., Dapino, P., Sacchetti, C., Dallegri, F., Prostaglandin E2 inhibits apoptosis in human neutrophilic polymorphonuclear leukocytes: role of intracellular cyclic AMP levels, *Exp Hematol* **26** (1998) 895-902.

[42] Niwa, M., Hara, A., Kanamori, Y., Matsuno, H., Kozawa, O., Yoshimi, N., Mori, H., Uematsu, T., Inhibition of tumor necrosis factor-alpha induced neutrophil apoptosis by cyclic AMP: involvement of caspase cascade, *European journal of pharmacology* **371** (1999) 59-67.

[43] Martin, M.C., Dransfield, I., Haslett, C., Rossi, A.G., Cyclic AMP regulation of neutrophil apoptosis occurs via a novel protein kinase A-independent signaling pathway, *The Journal of biological chemistry* **276** (2001) 45041-45050.

[44] Boucher, M.J., Duchesne, C., Laine, J., Morisset, J., Rivard, N., cAMP protection of pancreatic cancer cells against apoptosis induced by ERK inhibition, *Biochem Biophys Res Commun* **285** (2001) 207-216.

[45] Hui, H., Nourparvar, A., Zhao, X., Perfetti, R., Glucagon-like peptide-1 inhibits apoptosis of insulin-secreting cells via a cyclic 5'-adenosine monophosphate-dependent protein kinase A- and a phosphatidylinositol 3-kinase-dependent pathway, *Endocrinology* **144** (2003) 1444-1455.

[46] Hoshino, T., Tsutsumi, S., Tomisato, W., Hwang, H.J., Tsuchiya, T., Mizushima, T., Prostaglandin E2 protects gastric mucosal cells from apoptosis via EP2 and EP4 receptor activation, *J Biol Chem* **278** (2003) 12752-12758.

[47] Goetzl, E.J., An, S., Zeng, L., Specific suppression by prostaglandin E2 of activation-induced apoptosis of human CD4+CD8+ T lymphoblasts, *J Immunol* **154** (1995) 1041-1047.

[48] Negrotto, S., Pacienza, N., D'Atri, L.P., Pozner, R.G., Malaver, E., Torres, O., Lazzari, M.A., Gomez, R.M., Schattner, M., Activation of cyclic AMP pathway prevents CD34(+) cell apoptosis, *Experimental hematology* **34** (2006) 1420-1428.

[49] Pozner, R.G., Negrotto, S., D'Atri, L.P., Kotler, M.L., Lazzari, M.A., Gomez, R.M., Schattner, M., Prostacyclin prevents nitric oxide-induced megakaryocyte apoptosis, *British journal of pharmacology* **145** (2005) 283-292.

[50] Nishihara, H., Kizaka-Kondoh, S., Insel, P.A., Eckmann, L., Inhibition of apoptosis in normal and transformed intestinal epithelial cells by cAMP through induction of inhibitor of apoptosis protein (IAP)-2, *Proceedings of the National Academy of Sciences of the United States of America* **100** (2003) 8921-8926.

[51] Polte, T., Schroder, H., Cyclic AMP mediates endothelial protection by nitric oxide, *Biochem Biophys Res Commun* **251** (1998) 460-465.

[52] Orlov, S.N., Thorin-Trescases, N., Dulin, N.O., Dam, T.V., Fortuno, M.A., Tremblay, J., Hamet, P., Activation of cAMP signaling transiently inhibits apoptosis in vascular smooth muscle cells in a site upstream of caspase-3, *Cell death and differentiation* **6** (1999) 661-672.

[53] Saavedra, A.P., Tsygankova, O.M., Prendergast, G.V., Dworet, J.H., Cheng, G., Meinkoth, J.L., Role of cAMP, PKA and Rap1A in thyroid follicular cell survival, *Oncogene* **21** (2002) 778-788.

[54] Garcia-Bermejo, L., Perez, C., Vilaboa, N.E., de Blas, E., Aller, P., cAMP increasing agents attenuate the generation of apoptosis by etoposide in promonocytic leukemia cells, *Journal of cell science* **111 (Pt 5)** (1998) 637-644.

[55] Jun, C.D., Pae, H.O., Yoo, J.C., Kwak, H.J., Park, R.K., Chung, H.T., Cyclic adenosine monophosphate inhibits nitric oxide-induced apoptosis in human leukemic HL-60 cells, *Cellular immunology* **183** (1998) 13-21.

[56] Anderson, K.L., Anderson, G., Michell, R.H., Jenkinson, E.J., Owen, J.J., Intracellular signaling pathways involved in the induction of apoptosis in immature thymic T lymphocytes, *J Immunol* **156** (1996) 4083-4091.

[57] McConkey, D.J., Orrenius, S., Okret, S., Jondal, M., Cyclic AMP potentiates glucocorticoid-induced endogenous endonuclease activation in thymocytes, *Faseb J* **7** (1993) 580-585.

[58] Naderi, S., Blomhoff, H.K., Activation of cAMP signaling enhances Fas-mediated apoptosis and activation-induced cell death through potentiation of caspase 8 activation, *Hum Immunol* (2008).

[59] Myklebust, J.H., Josefsen, D., Blomhoff, H.K., Levy, F.O., Naderi, S., Reed, J.C., Smeland, E.B., Activation of the cAMP signaling pathway increases apoptosis in

human B-precursor cells and is associated with downregulation of Mcl-1 expression, *J Cell Physiol* **180** (1999) 71-80.

[60] Ji, Z., Mei, F.C., Johnson, B.H., Thompson, E.B., Cheng, X., Protein kinase A, not Epac, suppresses hedgehog activity and regulates glucocorticoid sensitivity in acute lymphoblastic leukemia cells, *J Biol Chem* **282** (2007) 37370-37377.

[61] Ji, Z., Mei, F.C., Miller, A.L., Thompson, E.B., Cheng, X., Protein kinase A (PKA) isoform RIIbeta mediates the synergistic killing effect of cAMP and glucocorticoid in acute lymphoblastic leukemia cells, *J Biol Chem* **283** (2008) 21920-21925.

[62] Pastan, I.H., Johnson, G.S., Anderson, W.B., Role of cyclic nucleotides in growth control, *Annual review of biochemistry* **44** (1975) 491-522.

[63] Kato, J.Y., Matsuoka, M., Polyak, K., Massague, J., Sherr, C.J., Cyclic AMP-induced G1 phase arrest mediated by an inhibitor (p27Kip1) of cyclin-dependent kinase 4 activation, *Cell* **79** (1994) 487-496.

[64] Gutzkow, K.B., Naderi, S., Blomhoff, H.K., Forskolin-mediated G1 arrest in acute lymphoblastic leukaemia cells: phosphorylated pRB sequesters E2Fs, *J Cell Sci* **115** (2002) 1073-1082.

[65] Kim, T.Y., Kim, W.I., Smith, R.E., Kay, E.D., Role of p27(Kip1) in cAMP- and TGF-beta2-mediated antiproliferation in rabbit corneal endothelial cells, *Investigative ophthalmology & visual science* **42** (2001) 3142-3149.

[66] L'Allemain, G., Lavoie, J.N., Rivard, N., Baldin, V., Pouyssegur, J., Cyclin D1 expression is a major target of the cAMP-induced inhibition of cell cycle entry in fibroblasts, *Oncogene* **14** (1997) 1981-1990.

[67] Naderi, S., Wang, J.Y., Chen, T.T., Gutzkow, K.B., Blomhoff, H.K., cAMP-mediated inhibition of DNA replication and S phase progression: involvement of Rb, p21Cip1, and PCNA, *Mol Biol Cell* **16** (2005) 1527-1542.

[68] Vadiveloo, P.K., Filonzi, E.L., Stanton, H.R., Hamilton, J.A., G1 phase arrest of human smooth muscle cells by heparin, IL-4 and cAMP is linked to repression of cyclin D1 and cdk2, *Atherosclerosis* **133** (1997) 61-69.

[69] van Oirschot, B.A., Stahl, M., Lens, S.M., Medema, R.H., Protein kinase A regulates expression of p27(kip1) and cyclin D3 to suppress proliferation of leukemic T cell lines, *The Journal of biological chemistry* **276** (2001) 33854-33860.

[70] Sherr, C.J., G1 phase progression: cycling on cue, *Cell* **79** (1994) 551-555.

[71] Johnson, D.G., Walker, C.L., Cyclins and cell cycle checkpoints, *Annu Rev Pharmacol Toxicol* **39** (1999) 295-312.

[72] Cook, S.J., McCormick, F., Inhibition by cAMP of Ras-dependent activation of Raf, *Science (New York, N.Y* **262** (1993) 1069-1072.

[73] Wu, J., Dent, P., Jelinek, T., Wolfman, A., Weber, M.J., Sturgill, T.W., Inhibition of the EGF-activated MAP kinase signaling pathway by adenosine 3',5'-monophosphate, *Science (New York, N.Y* **262** (1993) 1065-1069.

[74] Dumaz, N., Marais, R., Integrating signals between cAMP and the RAS/RAF/MEK/ERK signalling pathways. Based on the anniversary prize of the Gesellschaft fur Biochemie und Molekularbiologie Lecture delivered on 5 July 2003 at the Special FEBS Meeting in Brussels, *The FEBS journal* **272** (2005) 3491-3504.

[75] Schmitt, J.M., Stork, P.J., Cyclic AMP-mediated inhibition of cell growth requires the small G protein Rap1, *Molecular and cellular biology* **21** (2001) 3671-3683.

[76] Schmitt, J.M., Stork, P.J., PKA phosphorylation of Src mediates cAMP's inhibition of cell growth via Rap1, *Molecular cell* **9** (2002) 85-94.

[77] Sevetson, B.R., Kong, X., Lawrence, J.C., Jr., Increasing cAMP attenuates activation of mitogen-activated protein kinase, *Proceedings of the National Academy of Sciences of the United States of America* **90** (1993) 10305-10309.

[78] Hafner, S., Adler, H.S., Mischak, H., Janosch, P., Heidecker, G., Wolfman, A., Pippig, S., Lohse, M., Ueffing, M., Kolch, W., Mechanism of inhibition of Raf-1 by protein kinase A, *Mol Cell Biol* **14** (1994) 6696-6703.

[79] Mischak, H., Seitz, T., Janosch, P., Eulitz, M., Steen, H., Schellerer, M., Philipp, A., Kolch, W., Negative regulation of Raf-1 by phosphorylation of serine 621, *Mol Cell Biol* **16** (1996) 5409-5418.

[80] Prasad, K.N., Cole, W.C., Yan, X.D., Nahreini, P., Kumar, B., Hanson, A., Prasad, J.E., Defects in cAMP-pathway may initiate carcinogenesis in dividing nerve cells: a review, *Apoptosis* **8** (2003) 579-586.

[81] Lazarovici, P., Jiang, H., Fink, D., Jr., The 38-amino-acid form of pituitary adenylate cyclase-activating polypeptide induces neurite outgrowth in PC12 cells that is dependent on protein kinase C and extracellular signal-regulated kinase but not on protein kinase A, nerve growth factor receptor tyrosine kinase, p21(ras) G protein, and pp60(c-src) cytoplasmic tyrosine kinase, *Mol Pharmacol* **54** (1998) 547-558.

[82] Sanchez, S., Jimenez, C., Carrera, A.C., Diaz-Nido, J., Avila, J., Wandosell, F., A cAMP-activated pathway, including PKA and PI3K, regulates neuronal differentiation, *Neurochem Int* **44** (2004) 231-242.

[83] Ravni, A., Vaudry, D., Gerdin, M.J., Eiden, M.V., Falluel-Morel, A., Gonzalez, B.J., Vaudry, H., Eiden, L.E., A cAMP-dependent, protein kinase A-independent signaling pathway mediating neuritogenesis through Egr1 in PC12 cells, *Mol Pharmacol* **73** (2008) 1688-1708.

[84] Hansen, T.O., Rehfeld, J.F., Nielsen, F.C., Cyclic AMP-induced neuronal differentiation via activation of p38 mitogen-activated protein kinase, *Journal of neurochemistry* **75** (2000) 1870-1877.

[85] Vesanen, M., Salminen, M., Wessman, M., Lankinen, H., Sistonen, P., Vaheri, A., Morphological differentiation of human SH-SY5Y neuroblastoma cells inhibits human immunodeficiency virus type 1 infection, *The Journal of general virology* **75 (Pt 1)** (1994) 201-206.

[86] Lando, M., Abemayor, E., Verity, M.A., Sidell, N., Modulation of intracellular cyclic adenosine monophosphate levels and the differentiation response of human neuroblastoma cells, *Cancer research* **50** (1990) 722-727.

[87] Stachowiak, E.K., Fang, X., Myers, J., Dunham, S., Stachowiak, M.K., cAMP-induced differentiation of human neuronal progenitor cells is mediated by nuclear fibroblast growth factor receptor-1 (FGFR1), *Journal of neurochemistry* **84** (2003) 1296-1312.

[88] Sarkar, D.K., Boyadjieva, N.I., Chen, C.P., Ortiguela, M., Reuhl, K., Clement, E.M., Kuhn, P., Marano, J., Cyclic adenosine monophosphate differentiated beta-endorphin neurons promote immune function and prevent prostate cancer growth, *Proc Natl Acad Sci U S A* **105** (2008) 9105-9110.

[89] Beyer, C., Karolczak, M., Estrogenic stimulation of neurite growth in midbrain dopaminergic neurons depends on cAMP/protein kinase A signalling, *Journal of neuroscience research* **59** (2000) 107-116.

[90] Cibelli, G., Corsi, P., Diana, G., Vitiello, F., Thiel, G., Corticotropin-releasing factor triggers neurite outgrowth of a catecholaminergic immortalized neuron via cAMP and MAP kinase signalling pathways, *The European journal of neuroscience* **13** (2001) 1339-1348.

[91] Fields, R.D., Stevens-Graham, B., New insights into neuron-glia communication, *Science (New York, N.Y* **298** (2002) 556-562.

[92] McManus, M.F., Chen, L.C., Vallejo, I., Vallejo, M., Astroglial differentiation of cortical precursor cells triggered by activation of the cAMP-dependent signaling pathway, *J Neurosci* **19** (1999) 9004-9015.

[93] Vallejo, I., Vallejo, M., Pituitary adenylate cyclase-activating polypeptide induces astrocyte differentiation of precursor cells from developing cerebral cortex, *Molecular and cellular neurosciences* **21** (2002) 671-683.

[94] Messens, J., Slegers, H., Synthesis of glial fibrillary acidic protein in rat C6 glioma in chemically defined medium: cyclic AMP-dependent transcriptional and translational regulation, *Journal of neurochemistry* **58** (1992) 2071-2080.

[95] Yoshimura, S., Sakai, H., Nakashima, S., Nozawa, Y., Shinoda, J., Sakai, N., Yamada, H., Differential expression of Rho family GTP-binding proteins and protein kinase C isozymes during C6 glial cell differentiation, *Brain research* **45** (1997) 90-98.

[96] Takanaga, H., Yoshitake, T., Hara, S., Yamasaki, C., Kunimoto, M., cAMP-induced astrocytic differentiation of C6 glioma cells is mediated by autocrine interleukin-6, *J Biol Chem* **279** (2004) 15441-15447.

[97] Raible, D.W., McMorris, F.A., Oligodendrocyte differentiation and progenitor cell proliferation are independently regulated by cyclic AMP, *Journal of neuroscience research* **34** (1993) 287-294.

[98] Shiga, H., Asou, H., Ito, E., Advancement of differentiation of oligodendrocyte progenitor cells by a cascade including protein kinase A and cyclic AMP-response element binding protein, *Neuroscience research* **53** (2005) 436-441.

[99] Mutoh, T., Li, M., Yamamoto, M., Mitsuma, T., Sobue, G., Differential signaling cascade of MAP kinase and S6 kinase depends on 3',5'-monophosphate concentration in schwann cells: correlation to cellular differentiation and proliferation, *Brain Res* **810** (1998) 274-278.

[100] Friedenstein, A.J., Piatetzky, S., II, Petrakova, K.V., Osteogenesis in transplants of bone marrow cells, *J Embryol Exp Morphol* **16** (1966) 381-390.

[101] Friedenstein, A.J., Chailakhjan, R.K., Lalykina, K.S., The development of fibroblast colonies in monolayer cultures of guinea-pig bone marrow and spleen cells, *Cell Tissue Kinet* **3** (1970) 393-403.

[102] Castro-Malaspina, H., Gay, R.E., Resnick, G., Kapoor, N., Meyers, P., Chiarieri, D., McKenzie, S., Broxmeyer, H.E., Moore, M.A., Characterization of human bone marrow fibroblast colony-forming cells (CFU-F) and their progeny, *Blood* **56** (1980) 289-301.

[103] Owen, M., Marrow stromal stem cells, *J Cell Sci Suppl* **10** (1988) 63-76.

[104] Tuan, R.S., Boland, G., Tuli, R., Adult mesenchymal stem cells and cell-based tissue engineering, *Arthritis Res Ther* **5** (2003) 32-45.

[105] Minguell, J.J., Erices, A., Conget, P., Mesenchymal stem cells, *Exp Biol Med (Maywood)* **226** (2001) 507-520.

[106] da Silva Meirelles, L., Chagastelles, P.C., Nardi, N.B., Mesenchymal stem cells reside in virtually all post-natal organs and tissues, *J Cell Sci* **119** (2006) 2204-2213.

[107] Abdallah, B.M., Kassem, M., Human mesenchymal stem cells: from basic biology to clinical applications, *Gene Ther* **15** (2008) 109-116.

[108] Chamberlain, G., Fox, J., Ashton, B., Middleton, J., Concise review: mesenchymal stem cells: their phenotype, differentiation capacity, immunological features, and potential for homing, *Stem Cells* **25** (2007) 2739-2749.

[109] Erica L. Herzog, L.C., and Diane S. Krause Plasticity of marrow-derived stem cells, *Blood* **102** (2003) 3483-3493.

[110] Jones, E., McGonagle, D., Human bone marrow mesenchymal stem cells in vivo, *Rheumatology (Oxford)* **47** (2008) 126-131.

[111] Uccelli, A., Moretta, L., Pistoia, V., Mesenchymal stem cells in health and disease, *Nat Rev Immunol* **8** (2008) 726-736.

[112] Satomura, K., Krebsbach, P., Bianco, P., Gehron Robey, P., Osteogenic imprinting upstream of marrow stromal cell differentiation, *J Cell Biochem* **78** (2000) 391-403.

[113] Herbertson, A., Aubin, J.E., Cell sorting enriches osteogenic populations in rat bone marrow stromal cell cultures, *Bone* **21** (1997) 491-500.

[114] Kuznetsov, S.A., Krebsbach, P.H., Satomura, K., Kerr, J., Riminucci, M., Benayahu, D., Robey, P.G., Single-colony derived strains of human marrow stromal fibroblasts form bone after transplantation in vivo, *J Bone Miner Res* **12** (1997) 1335-1347.

[115] Berry, L., Grant, M.E., McClure, J., Rooney, P., Bone-marrow-derived chondrogenesis in vitro, *J Cell Sci* **101 (Pt 2)** (1992) 333-342.

[116] Bianco, P., Riminucci, M., Gronthos, S., Robey, P.G., Bone marrow stromal stem cells: nature, biology, and potential applications, *Stem Cells* **19** (2001) 180-192.

[117] Lee, K.D., Kuo, T.K., Whang-Peng, J., Chung, Y.F., Lin, C.T., Chou, S.H., Chen, J.R., Chen, Y.P., Lee, O.K., In vitro hepatic differentiation of human mesenchymal stem cells, *Hepatology* **40** (2004) 1275-1284.

[118] Wakitani, S., Saito, T., Caplan, A.I., Myogenic cells derived from rat bone marrow mesenchymal stem cells exposed to 5-azacytidine, *Muscle Nerve* **18** (1995) 1417-1426.

[119] Wislet-Gendebien, S., Leprince, P., Moonen, G., Rogister, B., Regulation of neural markers nestin and GFAP expression by cultivated bone marrow stromal cells, *J Cell Sci* **116** (2003) 3295-3302.

[120] Bossolasco, P., Cova, L., Calzarossa, C., Rimoldi, S.G., Borsotti, C., Deliliers, G.L., Silani, V., Soligo, D., Polli, E., Neuro-glial differentiation of human bone marrow stem cells in vitro, *Exp Neurol* **193** (2005) 312-325.

[121] Caplan, A.I., Dennis, J.E., Mesenchymal stem cells as trophic mediators, *J Cell Biochem* **98** (2006) 1076-1084.

[122] Horwitz, E.M., Prockop, D.J., Fitzpatrick, L.A., Koo, W.W., Gordon, P.L., Neel, M., Sussman, M., Orchard, P., Marx, J.C., Pyeritz, R.E., Brenner, M.K., Transplantability and therapeutic effects of bone marrow-derived mesenchymal cells in children with osteogenesis imperfecta, *Nat Med* **5** (1999) 309-313.

[123] Koc, O.N., Day, J., Nieder, M., Gerson, S.L., Lazarus, H.M., Krivit, W., Allogeneic mesenchymal stem cell infusion for treatment of metachromatic leukodystrophy (MLD) and Hurler syndrome (MPS-IH), *Bone Marrow Transplant* **30** (2002) 215-222.

[124] Bruder, S.P., Fink, D.J., Caplan, A.I., Mesenchymal stem cells in bone development, bone repair, and skeletal regeneration therapy, *J Cell Biochem* **56** (1994) 283-294.

[125] Bianchi, G., Muraglia, A., Daga, A., Corte, G., Cancedda, R., Quarto, R., Microenvironment and stem properties of bone marrow-derived mesenchymal cells, *Wound Repair Regen* **9** (2001) 460-466.

[126] Lee, M.S., Makkar, R.R., Stem-cell transplantation in myocardial infarction: a status report, *Ann Intern Med* **140** (2004) 729-737.

[127] Horwitz, E.M., Prockop, D.J., Gordon, P.L., Koo, W.W., Fitzpatrick, L.A., Neel, M.D., McCarville, M.E., Orchard, P.J., Pyeritz, R.E., Brenner, M.K., Clinical responses to bone marrow transplantation in children with severe osteogenesis imperfecta, *Blood* **97** (2001) 1227-1231.

[128] Koc, O.N., Gerson, S.L., Cooper, B.W., Dyhouse, S.M., Haynesworth, S.E., Caplan, A.I., Lazarus, H.M., Rapid hematopoietic recovery after coinfusion of

autologous-blood stem cells and culture-expanded marrow mesenchymal stem cells in advanced breast cancer patients receiving high-dose chemotherapy, *J Clin Oncol* **18** (2000) 307-316.

[129] Stamm, C., Westphal, B., Kleine, H.D., Petzsch, M., Kittner, C., Klinge, H., Schumichen, C., Nienaber, C.A., Freund, M., Steinhoff, G., Autologous bone-marrow stem-cell transplantation for myocardial regeneration, *Lancet* **361** (2003) 45-46.

[130] Ringden, O., Uzunel, M., Rasmusson, I., Remberger, M., Sundberg, B., Lonnies, H., Marschall, H.U., Dlugosz, A., Szakos, A., Hassan, Z., Omazic, B., Aschan, J., Barkholt, L., Le Blanc, K., Mesenchymal stem cells for treatment of therapy-resistant graft-versus-host disease, *Transplantation* **81** (2006) 1390-1397.

[131] Kopen, G.C., Prockop, D.J., Phinney, D.G., Marrow stromal cells migrate throughout forebrain and cerebellum, and they differentiate into astrocytes after injection into neonatal mouse brains, *Proc Natl Acad Sci U S A* **96** (1999) 10711-10716.

[132] Brazelton, T.R., Rossi, F.M., Keshet, G.I., Blau, H.M., From marrow to brain: expression of neuronal phenotypes in adult mice, *Science* **290** (2000) 1775-1779.

[133] Mezey, E., Chandross, K.J., Harta, G., Maki, R.A., McKercher, S.R., Turning blood into brain: cells bearing neuronal antigens generated in vivo from bone marrow, *Science* **290** (2000) 1779-1782.

[134] Mezey, E., Key, S., Vogelsang, G., Szalayova, I., Lange, G.D., Crain, B., Transplanted bone marrow generates new neurons in human brains, *Proc Natl Acad Sci U S A* **100** (2003) 1364-1369.

[135] Kohyama, J., Abe, H., Shimazaki, T., Koizumi, A., Nakashima, K., Gojo, S., Taga, T., Okano, H., Hata, J., Umezawa, A., Brain from bone: efficient "meta-differentiation" of marrow stroma-derived mature osteoblasts to neurons with Noggin or a demethylating agent, *Differentiation* **68** (2001) 235-244.

[136] P. Bossolasco, L.C., C. Calzarossa, S.G. Rimoldi, C. Borsotti, G. Lambertenghi Deliliers, V. Silani, D. Soligo and E. Polli, Neuro-glial differentiation of human bone marrow stem cells in vitro, *Exp Neurol* **193** (2005) 312-325.

[137] Philippe Tropel, N.P., Jean-Claude Platel, Danièle Noël, Mireille Albrieux, Alim-Louis Benabid, François Berger Functional neuronal differentiation of bone marrow-derived mesenchymal stem cells., *Stem Cells* **24** (2006) 2868-2876.

[138] Sanchez-Ramos, J., Song, S., Cardozo-Pelaez, F., Hazzi, C., Stedeford, T., Willing, A., Freeman, T.B., Saporta, S., Janssen, W., Patel, N., Cooper, D.R.,

Sanberg, P.R., Adult bone marrow stromal cells differentiate into neural cells in vitro, *Exp Neurol* **164** (2000) 247-256.

[139] Woodbury, D., Schwarz, E.J., Prockop, D.J., Black, I.B., Adult rat and human bone marrow stromal cells differentiate into neurons, *J Neurosci Res* **61** (2000) 364-370.

[140] Azizi, S.A., Stokes, D., Augelli, B.J., DiGirolamo, C., Prockop, D.J., Engraftment and migration of human bone marrow stromal cells implanted in the brains of albino rats--similarities to astrocyte grafts, *Proc Natl Acad Sci U S A* **95** (1998) 3908-3913.

[141] Kennea, N.L., Waddington, S.N., Chan, J., O'Donoghue, K., Yeung, D., Taylor, D.L., Al-Allaf, F.A., Pirianov, G., Themis, M., Edwards, A.D., Fisk, N.M., Mehmet, H., Differentiation of human fetal mesenchymal stem cells into cells with an oligodendrocyte phenotype, *Cell Cycle* **8** (2009) 1069-1079.

[142] Chen, Y., Teng, F.Y., Tang, B.L., Coaxing bone marrow stromal mesenchymal stem cells towards neuronal differentiation: progress and uncertainties, *Cell Mol Life Sci* **63** (2006) 1649-1657.

[143] Hellmann, M.A., Panet, H., Barhum, Y., Melamed, E., Offen, D., Increased survival and migration of engrafted mesenchymal bone marrow stem cells in 6-hydroxydopamine-lesioned rodents, *Neurosci Lett* **395** (2006) 124-128.

[144] Dezawa, M., Kanno, H., Hoshino, M., Cho, H., Matsumoto, N., Itokazu, Y., Tajima, N., Yamada, H., Sawada, H., Ishikawa, H., Mimura, T., Kitada, M., Suzuki, Y., Ide, C., Specific induction of neuronal cells from bone marrow stromal cells and application for autologous transplantation, *J Clin Invest* **113** (2004) 1701-1710.

[145] Dezawa, M., Takahashi, I., Esaki, M., Takano, M., Sawada, H., Sciatic nerve regeneration in rats induced by transplantation of in vitro differentiated bone-marrow stromal cells, *The European journal of neuroscience* **14** (2001) 1771-1776.

[146] Hofstetter, C.P., Schwarz, E.J., Hess, D., Widenfalk, J., El Manira, A., Prockop, D.J., Olson, L., Marrow stromal cells form guiding strands in the injured spinal cord and promote recovery, *Proc Natl Acad Sci U S A* **99** (2002) 2199-2204.

[147] Jin, K., Mao, X.O., Batteur, S., Sun, Y., Greenberg, D.A., Induction of neuronal markers in bone marrow cells: differential effects of growth factors and patterns of intracellular expression, *Exp Neurol* **184** (2003) 78-89.

[148] Levy, Y.S., Merims, D., Panet, H., Barhum, Y., Melamed, E., Offen, D., Induction of neuron-specific enolase promoter and neuronal markers in

differentiated mouse bone marrow stromal cells, *J Mol Neurosci* **21** (2003) 121-132.

[149] Munoz-Elias, G., Woodbury, D., Black, I.B., Marrow stromal cells, mitosis, and neuronal differentiation: stem cell and precursor functions, *Stem Cells* **21** (2003) 437-448.

[150] Rismanchi, N., Floyd, C.L., Berman, R.F., Lyeth, B.G., Cell death and long-term maintenance of neuron-like state after differentiation of rat bone marrow stromal cells: a comparison of protocols, *Brain Res* **991** (2003) 46-55.

[151] Hermann, A., Gastl, R., Liebau, S., Popa, M.O., Fiedler, J., Boehm, B.O., Maisel, M., Lerche, H., Schwarz, J., Brenner, R., Storch, A., Efficient generation of neural stem cell-like cells from adult human bone marrow stromal cells, *J Cell Sci* **117** (2004) 4411-4422.

[152] de Hemptinne, I., Vermeiren, C., Maloteaux, J.M., Hermans, E., Induction of glial glutamate transporters in adult mesenchymal stem cells, *J Neurochem* **91** (2004) 155-166.

[153] Jori, F.P., Napolitano, M.A., Melone, M.A., Cipollaro, M., Cascino, A., Altucci, L., Peluso, G., Giordano, A., Galderisi, U., Molecular pathways involved in neural in vitro differentiation of marrow stromal stem cells, *J Cell Biochem* **94** (2005) 645-655.

[154] Yaghoobi, M.M., Mowla, S.J., Differential gene expression pattern of neurotrophins and their receptors during neuronal differentiation of rat bone marrow stromal cells, *Neurosci Lett* **397** (2006) 149-154.

[155] Kondo, T., Johnson, S.A., Yoder, M.C., Romand, R., Hashino, E., Sonic hedgehog and retinoic acid synergistically promote sensory fate specification from bone marrow-derived pluripotent stem cells, *Proc Natl Acad Sci U S A* **102** (2005) 4789-4794.

[156] Chu, M.S., Chang, C.F., Yang, C.C., Bau, Y.C., Ho, L.L., Hung, S.C., Signalling pathway in the induction of neurite outgrowth in human mesenchymal stem cells, *Cell Signal* **18** (2006) 519-530.

[157] Mauro Kramperaa, S.M., Annalisa Pasinia, Mirco Galièc, Gino Rigottid, Federico Mosnaa, Martina Tinellia, Laura Lovatob, Elena Anghilerib, Angelo Andreinia, Giovanni Pizzoloa, Andrea Sbarbatic and Bruno Bonetti, Induction of neural-like differentiation in human mesenchymal stem cells derived from bone marrow, fat, spleen and thymus., *Bone* **40** (2007) 382-390.

[158] Tropel, P., Platet, N., Platel, J.C., Noel, D., Albrieux, M., Benabid, A.L., Berger, F., Functional neuronal differentiation of bone marrow-derived mesenchymal stem cells, *Stem Cells* **24** (2006) 2868-2876.

[159] Lu, P., Blesch, A., Tuszynski, M.H., Induction of bone marrow stromal cells to neurons: differentiation, transdifferentiation, or artifact?, *J Neurosci Res* **77** (2004) 174-191.

[160] Eitel, K., Staiger, H., Brendel, M.D., Brandhorst, D., Bretzel, R.G., Haring, H.U., Kellerer, M., Different role of saturated and unsaturated fatty acids in beta-cell apoptosis, *Biochem Biophys Res Commun* **299** (2002) 853-856.

[161] Borradaile, N.M., Han, X., Harp, J.D., Gale, S.E., Ory, D.S., Schaffer, J.E., Disruption of endoplasmic reticulum structure and integrity in lipotoxic cell death, *J Lipid Res* **47** (2006) 2726-2737.

[162] Srivastava, S., Chan, C., Hydrogen peroxide and hydroxyl radicals mediate palmitate-induced cytotoxicity to hepatoma cells: relation to mitochondrial permeability transition, *Free Radic Res* **41** (2007) 38-49.

[163] Srivastava, S., Zhang, L., Jin, R., Chan, C., A novel method incorporating gene ontology information for unsupervised clustering and feature selection, *PLoS ONE* **3** (2008) e3860.

[164] Makino, S., Fukuda, K., Miyoshi, S., Konishi, F., Kodama, H., Pan, J., Sano, M., Takahashi, T., Hori, S., Abe, H., Hata, J., Umezawa, A., Ogawa, S., Cardiomyocytes can be generated from marrow stromal cells in vitro, *J Clin Invest* **103** (1999) 697-705.

[165] Deng, J., Petersen, B.E., Steindler, D.A., Jorgensen, M.L., Laywell, E.D., Mesenchymal stem cells spontaneously express neural proteins in culture and are neurogenic after transplantation, *Stem Cells* **24** (2006) 1054-1064.

[166] McBeath, R., Pirone, D.M., Nelson, C.M., Bhadriraju, K., Chen, C.S., Cell shape, cytoskeletal tension, and RhoA regulate stem cell lineage commitment, *Dev Cell* **6** (2004) 483-495.

[167] Kilian, K.A., Bugarija, B., Lahn, B.T., Mrksich, M., Geometric cues for directing the differentiation of mesenchymal stem cells, *Proc Natl Acad Sci U S A.*

[168] Engler, A.J., Sen, S., Sweeney, H.L., Discher, D.E., Matrix elasticity directs stem cell lineage specification, *Cell* **126** (2006) 677-689.

[169] Krampera, M., Marconi, S., Pasini, A., Galie, M., Rigotti, G., Mosna, F., Tinelli, M., Lovato, L., Anghileri, E., Andreini, A., Pizzolo, G., Sbarbati, A., Bonetti, B., Induction of neural-like differentiation in human mesenchymal stem cells derived from bone marrow, fat, spleen and thymus, *Bone* **40** (2007) 382-390.

[170] Dohi, T., Xia, F., Altieri, D.C., Compartmentalized phosphorylation of IAP by protein kinase A regulates cytoprotection, *Mol Cell* **27** (2007) 17-28.

[171] Park, S.Y., Cho, S.J., Kwon, H.C., Lee, K.R., Rhee, D.K., Pyo, S., Caspase-independent cell death by allicin in human epithelial carcinoma cells: involvement of PKA, *Cancer Lett* **224** (2005) 123-132.

[172] Howe, A.K., Regulation of actin-based cell migration by cAMP/PKA, *Biochim Biophys Acta* **1692** (2004) 159-174.

[173] Yang, Q., Mu, J., Li, Q., Li, A., Zeng, Z., Yang, J., Zhang, X., Tang, J., Xie, P., A simple and efficient method for deriving neurospheres from bone marrow stromal cells, *Biochem Biophys Res Commun* **372** (2008) 520-524.

[174] Wang, T.T., Tio, M., Lee, W., Beerheide, W., Udolph, G., Neural differentiation of mesenchymal-like stem cells from cord blood is mediated by PKA, *Biochem Biophys Res Commun* **357** (2007) 1021-1027.

[175] Patil, S., Melrose, J., Chan, C., Involvement of astroglial ceramide in palmitic acid-induced Alzheimer-like changes in primary neurons, *Eur J Neurosci* **26** (2007) 2131-2141.

[176] Bell, P.B., Jr., Safiejko-Mroczka, B., Improved methods for preserving macromolecular structures and visualizing them by fluorescence and scanning electron microscopy, *Scanning Microsc* **9** (1995) 843-857; discussion 858-860.

[177] Zhang, L., Chan, C., Isolation and enrichment of rat mesenchymal stem cells (MSCs) and separation of single-colony derived MSCs, *J Vis Exp.* **http://www.jove.com/index/Details.stp?ID=1852** (2010).

[178] Chen, C.S., Mrksich, M., Huang, S., Whitesides, G.M., Ingber, D.E., Geometric control of cell life and death, *Science* **276** (1997) 1425-1428.

[179] Flusberg, D.A., Numaguchi, Y., Ingber, D.E., Cooperative control of Akt phosphorylation, bcl-2 expression, and apoptosis by cytoskeletal microfilaments and microtubules in capillary endothelial cells, *Mol Biol Cell* **12** (2001) 3087-3094.

[180] Gilmore, A.P., Anoikis, *Cell Death Differ* **12 Suppl 2** (2005) 1473-1477.

[181] Bergson, C., Levenson, R., Goldman-Rakic, P.S., Lidow, M.S., Dopamine receptor-interacting proteins: the Ca(2+) connection in dopamine signaling, *Trends Pharmacol Sci* **24** (2003) 486-492.

[182] Chen, G., Greengard, P., Yan, Z., Potentiation of NMDA receptor currents by dopamine D1 receptors in prefrontal cortex, *Proc Natl Acad Sci U S A* **101** (2004) 2596-2600.

[183] Wulff, H., Castle, N.A., Pardo, L.A., Voltage-gated potassium channels as therapeutic targets, *Nat Rev Drug Discov* **8** (2009) 982-1001.

[184] Tikhonov, D.B., Magazanik, L.G., Origin and molecular evolution of ionotropic glutamate receptors, *Neurosci Behav Physiol* **39** (2009) 763-773.

[185] Bunemann, M., Lee, K.B., Pals-Rylaarsdam, R., Roseberry, A.G., Hosey, M.M., Desensitization of G-protein-coupled receptors in the cardiovascular system, *Annu Rev Physiol* **61** (1999) 169-192.

[186] Steinberg, R.A., Cauthron, R.D., Symcox, M.M., Shuntoh, H., Autoactivation of catalytic (C alpha) subunit of cyclic AMP-dependent protein kinase by phosphorylation of threonine 197, *Mol Cell Biol* **13** (1993) 2332-2341.

[187] Cauthron, R.D., Carter, K.B., Liauw, S., Steinberg, R.A., Physiological phosphorylation of protein kinase A at Thr-197 is by a protein kinase A kinase, *Mol Cell Biol* **18** (1998) 1416-1423.

[188] Desai, A., Mitchison, T.J., Microtubule polymerization dynamics, *Annu Rev Cell Dev Biol* **13** (1997) 83-117.

[189] Xiao, H., Verdier-Pinard, P., Fernandez-Fuentes, N., Burd, B., Angeletti, R., Fiser, A., Horwitz, S.B., Orr, G.A., Insights into the mechanism of microtubule stabilization by Taxol, *Proc Natl Acad Sci U S A* **103** (2006) 10166-10173.

[190] Yvon, A.M., Wadsworth, P., Jordan, M.A., Taxol suppresses dynamics of individual microtubules in living human tumor cells, *Mol Biol Cell* **10** (1999) 947-959.

[191] Ofir, R., Seidman, R., Rabinski, T., Krup, M., Yavelsky, V., Weinstein, Y., Wolfson, M., Taxol-induced apoptosis in human SKOV3 ovarian and MCF7 breast carcinoma cells is caspase-3 and caspase-9 independent, *Cell Death Differ* **9** (2002) 636-642.

[192] Cai, D., Qiu, J., Cao, Z., McAtee, M., Bregman, B.S., Filbin, M.T., Neuronal cyclic AMP controls the developmental loss in ability of axons to regenerate, *J Neurosci* **21** (2001) 4731-4739.

[193] Goldberg, J.L., Barres, B.A., The relationship between neuronal survival and regeneration, *Annu Rev Neurosci* **23** (2000) 579-612.

[194] Pearse, D.D., Pereira, F.C., Marcillo, A.E., Bates, M.L., Berrocal, Y.A., Filbin, M.T., Bunge, M.B., cAMP and Schwann cells promote axonal growth and functional recovery after spinal cord injury, *Nat Med* **10** (2004) 610-616.

[195] Mahmood, A., Lu, D., Wang, L., Li, Y., Lu, M., Chopp, M., Treatment of traumatic brain injury in female rats with intravenous administration of bone marrow stromal cells, *Neurosurgery* **49** (2001) 1196-1203; discussion 1203-1194.

[196] Mahmood, A., Lu, D., Lu, M., Chopp, M., Treatment of traumatic brain injury in adult rats with intravenous administration of human bone marrow stromal cells, *Neurosurgery* **53** (2003) 697-702; discussion 702-693.

[197] Bae, J.S., Han, H.S., Youn, D.H., Carter, J.E., Modo, M., Schuchman, E.H., Jin, H.K., Bone marrow-derived mesenchymal stem cells promote neuronal networks with functional synaptic transmission after transplantation into mice with neurodegeneration, *Stem cells (Dayton, Ohio)* **25** (2007) 1307-1316.

[198] Weimann, J.M., Charlton, C.A., Brazelton, T.R., Hackman, R.C., Blau, H.M., Contribution of transplanted bone marrow cells to Purkinje neurons in human adult brains, *Proc Natl Acad Sci U S A* **100** (2003) 2088-2093.

[199] Rocchi, S., Gaillard, I., van Obberghen, E., Chambaz, E.M., Vilgrain, I., Adrenocorticotrophic hormone stimulates phosphotyrosine phosphatase SHP2 in bovine adrenocortical cells: phosphorylation and activation by cAMP-dependent protein kinase, *The Biochemical journal* **352 Pt 2** (2000) 483-490.

[200] Han, J.D., Rubin, C.S., Regulation of cytoskeleton organization and paxillin dephosphorylation by cAMP. Studies on murine Y1 adrenal cells, *J Biol Chem* **271** (1996) 29211-29215.

[201] Jaffe, A.B., Hall, A., Rho GTPases: biochemistry and biology, *Annu Rev Cell Dev Biol* **21** (2005) 247-269.

[202] Palazzo, A.F., Cook, T.A., Alberts, A.S., Gundersen, G.G., mDia mediates Rho-regulated formation and orientation of stable microtubules, *Nat Cell Biol* **3** (2001) 723-729.

[203] Busca, R., Bertolotto, C., Abbe, P., Englaro, W., Ishizaki, T., Narumiya, S., Boquet, P., Ortonne, J.P., Ballotti, R., Inhibition of Rho is required for cAMP-induced melanoma cell differentiation, *Mol Biol Cell* **9** (1998) 1367-1378.

[204] Dong, J.M., Leung, T., Manser, E., Lim, L., cAMP-induced morphological changes are counteracted by the activated RhoA small GTPase and the Rho kinase ROKalpha, *J Biol Chem* **273** (1998) 22554-22562.

[205] Lang, P., Gesbert, F., Delespine-Carmagnat, M., Stancou, R., Pouchelet, M., Bertoglio, J., Protein kinase A phosphorylation of RhoA mediates the morphological and functional effects of cyclic AMP in cytotoxic lymphocytes, *EMBO J* **15** (1996) 510-519.

[206] Nakagawa, S., Kim, J.E., Lee, R., Chen, J., Fujioka, T., Malberg, J., Tsuji, S., Duman, R.S., Localization of phosphorylated cAMP response element-binding protein in immature neurons of adult hippocampus, *J Neurosci* **22** (2002) 9868-9876.

[207] Nakagawa, S., Kim, J.E., Lee, R., Malberg, J.E., Chen, J., Steffen, C., Zhang, Y.J., Nestler, E.J., Duman, R.S., Regulation of neurogenesis in adult mouse hippocampus by cAMP and the cAMP response element-binding protein, *J Neurosci* **22** (2002) 3673-3682.

[208] Sordella, R., Classon, M., Hu, K.Q., Matheson, S.F., Brouns, M.R., Fine, B., Zhang, L., Takami, H., Yamada, Y., Settleman, J., Modulation of CREB activity by the Rho GTPase regulates cell and organism size during mouse embryonic development, *Dev Cell* **2** (2002) 553-565.

[209] Haus-Seuffert, P., Meisterernst, M., Mechanisms of transcriptional activation of cAMP-responsive element-binding protein CREB, *Mol Cell Biochem* **212** (2000) 5-9.

[210] Giachino, C., De Marchis, S., Giampietro, C., Parlato, R., Perroteau, I., Schutz, G., Fasolo, A., Peretto, P., cAMP response element-binding protein regulates differentiation and survival of newborn neurons in the olfactory bulb, *J Neurosci* **25** (2005) 10105-10118.

[211] Palmer, T.D., Takahashi, J., Gage, F.H., The adult rat hippocampus contains primordial neural stem cells, *Mol Cell Neurosci* **8** (1997) 389-404.

[212] Zhang, L., Seitz, L., Abramczyk, A., Liu, L., Chan, C., cAMP initiates early phase neuron-like morphology changes and late phase neural differentiation and function in mesenchymal stem cells, *In Press* (2010).

[213] Parekh, A.B., Putney, J.W., Jr., Store-operated calcium channels, *Physiol Rev* **85** (2005) 757-810.

[214] Catterall, W.A., Structure and regulation of voltage-gated Ca2+ channels, *Annual review of cell and developmental biology* **16** (2000) 521-555.

[215] Dingledine, R., Borges, K., Bowie, D., Traynelis, S.F., The glutamate receptor ion channels, *Pharmacol Rev* **51** (1999) 7-61.

[216] Conn, P.J., Battaglia, G., Marino, M.J., Nicoletti, F., Metabotropic glutamate receptors in the basal ganglia motor circuit, *Nat Rev Neurosci* **6** (2005) 787-798.

[217] Rousseaux, C.G., A Review of Glutamate Receptors I: Current Understanding of Their Biology, *J Toxicol Pathol* **21** (2008) 25-51.

[218] Missale, C., Nash, S.R., Robinson, S.W., Jaber, M., Caron, M.G., Dopamine receptors: from structure to function, *Physiol Rev* **78** (1998) 189-225.

[219] Nicola, S.M., Surmeier, J., Malenka, R.C., Dopaminergic modulation of neuronal excitability in the striatum and nucleus accumbens, *Annu Rev Neurosci* **23** (2000) 185-215.

[220] Lee, K., Zerivitz, K. and Akusjarvi, G., Small-Scale preparation of nuclear extracts from mammalian cells, *Cell Biology: A Laboratory Handbook. Academic Press. London* (1994) 668-673.

[221] Berridge, M.J., Lipp, P., Bootman, M.D., The versatility and universality of calcium signalling, *Nat Rev Mol Cell Biol* **1** (2000) 11-21.

[222] Berridge, M.J., Bootman, M.D., Roderick, H.L., Calcium signalling: dynamics, homeostasis and remodelling, *Nat Rev Mol Cell Biol* **4** (2003) 517-529.

[223] Vassort, G., Adenosine 5'-triphosphate: a P2-purinergic agonist in the myocardium, *Physiol Rev* **81** (2001) 767-806.

[224] Dubyak, G.R., el-Moatassim, C., Signal transduction via P2-purinergic receptors for extracellular ATP and other nucleotides, *Am J Physiol* **265** (1993) C577-606.

[225] Montminy, M., CREB Target Gene Database, http://natural.salk.edu/CREB/, 2005.

[226] Trzaska, K.A., King, C.C., Li, K.Y., Kuzhikandathil, E.V., Nowycky, M.C., Ye, J.H., Rameshwar, P., Brain-derived neurotrophic factor facilitates maturation of mesenchymal stem cell-derived dopamine progenitors to functional neurons, *J Neurochem* **110** (2009) 1058-1069.

[227] Callier, S., Snapyan, M., Le Crom, S., Prou, D., Vincent, J.D., Vernier, P., Evolution and cell biology of dopamine receptors in vertebrates, *Biol Cell* **95** (2003) 489-502.

[228] Pasuit, J.B., Li, Z., Kuzhikandathil, E.V., Multi-modal regulation of endogenous D1 dopamine receptor expression and function in the CAD catecholaminergic cell line, *Journal of neurochemistry* **89** (2004) 1508-1519.

[229] Saeki, K., Saeki, K., Yuo, A., Distinct involvement of cAMP-response element-dependent transcriptions in functional and morphological maturation during retinoid-mediated human myeloid differentiation, *Journal of leukocyte biology* **73** (2003) 673-681.

[230] Mimeault, M., Batra, S.K., Concise review: recent advances on the significance of stem cells in tissue regeneration and cancer therapies, *Stem Cells* **24** (2006) 2319-2345.

[231] He, S., Nakada, D., Morrison, S.J., Mechanisms of stem cell self-renewal, *Annu Rev Cell Dev Biol* **25** (2009) 377-406.

[232] Singh, A.M., Dalton, S., The cell cycle and Myc intersect with mechanisms that regulate pluripotency and reprogramming, *Cell Stem Cell* **5** (2009) 141-149.

[233] Borges, K., Dingledine, R., Functional organization of the GluR1 glutamate receptor promoter, *J Biol Chem* **276** (2001) 25929-25938.

[234] Olson, V.G., Zabetian, C.P., Bolanos, C.A., Edwards, S., Barrot, M., Eisch, A.J., Hughes, T., Self, D.W., Neve, R.L., Nestler, E.J., Regulation of drug reward by cAMP response element-binding protein: evidence for two functionally distinct subregions of the ventral tegmental area, *J Neurosci* **25** (2005) 5553-5562.

[235] McClung, C.A., Nestler, E.J., Regulation of gene expression and cocaine reward by CREB and DeltaFosB, *Nature neuroscience* **6** (2003) 1208-1215.

[236] Zhang, L., Seitz, L., Abramczyk, A., Liu, L., Chan, C., cAMP initiates early-phase neuron-like morphological changes and late-phase neural differentiation and function in mesenchymal stem cells, *Cell Mol Life Sci* **Epub ahead of print** (2010).

[237] Fujioka, T., Fujioka, A., Duman, R.S., Activation of cAMP signaling facilitates the morphological maturation of newborn neurons in adult hippocampus, *J Neurosci* **24** (2004) 319-328.

[238] Naito, A.T., Shiojima, I., Akazawa, H., Hidaka, K., Morisaki, T., Kikuchi, A., Komuro, I., Developmental stage-specific biphasic roles of Wnt/beta-catenin signaling in cardiomyogenesis and hematopoiesis, *Proc Natl Acad Sci U S A* **103** (2006) 19812-19817.

[239] Ueno, S., Weidinger, G., Osugi, T., Kohn, A.D., Golob, J.L., Pabon, L., Reinecke, H., Moon, R.T., Murry, C.E., Biphasic role for Wnt/beta-catenin signaling in cardiac specification in zebrafish and embryonic stem cells, *Proc Natl Acad Sci U S A* **104** (2007) 9685-9690.

[240] Morgan, N.G., Dhayal, S., Diakogiannaki, E., Welters, H.J., The cytoprotective actions of long-chain mono-unsaturated fatty acids in pancreatic beta-cells, *Biochem Soc Trans* **36** (2008) 905-908.

[241] Kong, J.Y., Rabkin, S.W., Palmitate-induced apoptosis in cardiomyocytes is mediated through alterations in mitochondria: prevention by cyclosporin A, *Biochim Biophys Acta* **1485** (2000) 45-55.

[242] Ostrander, D.B., Sparagna, G.C., Amoscato, A.A., McMillin, J.B., Dowhan, W., Decreased cardiolipin synthesis corresponds with cytochrome c release in palmitate-induced cardiomyocyte apoptosis, *J Biol Chem* **276** (2001) 38061-38067.

[243] Wei, Y., Wang, D., Topczewski, F., Pagliassotti, M.J., Saturated fatty acids induce endoplasmic reticulum stress and apoptosis independently of ceramide in liver cells, *Am J Physiol Endocrinol Metab* **291** (2006) E275-281.

[244] Feldstein, A.E., Werneburg, N.W., Canbay, A., Guicciardi, M.E., Bronk, S.F., Rydzewski, R., Burgart, L.J., Gores, G.J., Free fatty acids promote hepatic lipotoxicity by stimulating TNF-alpha expression via a lysosomal pathway, *Hepatology* **40** (2004) 185-194.

[245] Ji, J., Zhang, L., Wang, P., Mu, Y.M., Zhu, X.Y., Wu, Y.Y., Yu, H., Zhang, B., Chen, S.M., Sun, X.Z., Saturated free fatty acid, palmitic acid, induces apoptosis in fetal hepatocytes in culture, *Exp Toxicol Pathol* **56** (2005) 369-376.

[246] Malhi, H., Bronk, S.F., Werneburg, N.W., Gores, G.J., Free fatty acids induce JNK-dependent hepatocyte lipoapoptosis, *J Biol Chem* **281** (2006) 12093-12101.

[247] Welters, H.J., Diakogiannaki, E., Mordue, J.M., Tadayyon, M., Smith, S.A., Morgan, N.G., Differential protective effects of palmitoleic acid and cAMP on caspase activation and cell viability in pancreatic beta-cells exposed to palmitate, *Apoptosis* **11** (2006) 1231-1238.

[248] Cullen, K.A., McCool, J., Anwer, M.S., Webster, C.R., Activation of cAMP-guanine exchange factor confers PKA-independent protection from hepatocyte apoptosis, *Am J Physiol Gastrointest Liver Physiol* **287** (2004) G334-343.

[249] Furman, B., Pyne, N., Flatt, P., O'Harte, F., Targeting beta-cell cyclic 3'5' adenosine monophosphate for the development of novel drugs for treating type 2 diabetes mellitus. A review, *J Pharm Pharmacol* **56** (2004) 1477-1492.

[250] Woerle, H.J., Popa, E., Dostou, J., Welle, S., Gerich, J., Meyer, C., Exogenous insulin replacement in type 2 diabetes reverses excessive hepatic glucose release, but not excessive renal glucose release and impaired free fatty acid clearance, *Metabolism* **51** (2002) 1494-1500.

[251] Boden, G., Chen, X., Capulong, E., Mozzoli, M., Effects of free fatty acids on gluconeogenesis and autoregulation of glucose production in type 2 diabetes, *Diabetes* **50** (2001) 810-816.

[252] Skowronski, R., Hollenbeck, C.B., Varasteh, B.B., Chen, Y.D., Reaven, G.M., Regulation of non-esterified fatty acid and glycerol concentration by insulin in normal individuals and patients with type 2 diabetes, *Diabet Med* **8** (1991) 330-333.

[253] Goldenthal, M.J., Marin-Garcia, J., Mitochondrial signaling pathways: a receiver/integrator organelle, *Mol Cell Biochem* **262** (2004) 1-16.

[254] Newmeyer, D.D., Ferguson-Miller, S., Mitochondria: releasing power for life and unleashing the machineries of death, *Cell* **112** (2003) 481-490.

[255] Saelens, X., Festjens, N., Vande Walle, L., van Gurp, M., van Loo, G., Vandenabeele, P., Toxic proteins released from mitochondria in cell death, *Oncogene* **23** (2004) 2861-2874.

[256] Cereghetti, G.M., Scorrano, L., The many shapes of mitochondrial death, *Oncogene* **25** (2006) 4717-4724.

[257] Perfettini, J.L., Roumier, T., Kroemer, G., Mitochondrial fusion and fission in the control of apoptosis, *Trends Cell Biol* **15** (2005) 179-183.

[258] Golstein, P., Kroemer, G., Cell death by necrosis: towards a molecular definition, *Trends Biochem Sci* **32** (2007) 37-43.

[259] Zong, W.X., Thompson, C.B., Necrotic death as a cell fate, *Genes Dev* **20** (2006) 1-15.

[260] Orrenius, S., Gogvadze, V., Zhivotovsky, B., Mitochondrial oxidative stress: implications for cell death, *Annual review of pharmacology and toxicology* **47** (2007) 143-183.

[261] Turrens, J.F., Mitochondrial formation of reactive oxygen species, *The Journal of physiology* **552** (2003) 335-344.

[262] Darzynkiewicz, Z., Juan, G., Li, X., Gorczyca, W., Murakami, T., Traganos, F., Cytometry in cell necrobiology: analysis of apoptosis and accidental cell death (necrosis), *Cytometry* **27** (1997) 1-20.

[263] Garrett, R.H., Grisham, C.M., Biochemistry, Brooks/Cole-Thomson Learning, Pacific Grove, CA, 1999.

[264] Listenberger, L.L., Han, X., Lewis, S.E., Cases, S., Farese, R.V., Jr., Ory, D.S., Schaffer, J.E., Triglyceride accumulation protects against fatty acid-induced lipotoxicity, *Proc Natl Acad Sci U S A* **100** (2003) 3077-3082.

[265] Srivastava, S., Chan, C., Application of metabolic flux analysis to identify the mechanisms of free fatty acid toxicity to human hepatoma cell line, *Biotechnology and bioengineering* **99** (2008) 399-410.

[266] Green, D.R., Reed, J.C., Mitochondria and apoptosis, *Science* **281** (1998) 1309-1312.

[267] Cory, S., Adams, J.M., The Bcl2 family: regulators of the cellular life-or-death switch, *Nat Rev Cancer* **2** (2002) 647-656.

[268] Srivastava, S., Li, Z., Yang, X., Yedwabnick, M., Shaw, S., Chan, C., Identification of genes that regulate multiple cellular processes/responses in the context of lipotoxicity to hepatoma cells, *BMC genomics* **8** (2007) 364.

[269] Hock, M.B., Kralli, A., Transcriptional control of mitochondrial biogenesis and function, *Annual review of physiology* **71** (2009) 177-203.

[270] Perez-de-Arce, K., Foncea, R., Leighton, F., Reactive oxygen species mediates homocysteine-induced mitochondrial biogenesis in human endothelial cells: modulation by antioxidants, *Biochemical and biophysical research communications* **338** (2005) 1103-1109.

[271] Miranda, S., Foncea, R., Guerrero, J., Leighton, F., Oxidative stress and upregulation of mitochondrial biogenesis genes in mitochondrial DNA-depleted HeLa cells, *Biochemical and biophysical research communications* **258** (1999) 44-49.

[272] Yu, T., Robotham, J.L., Yoon, Y., Increased production of reactive oxygen species in hyperglycemic conditions requires dynamic change of mitochondrial morphology, *Proc Natl Acad Sci U S A* **103** (2006) 2653-2658.

[273] Shen, X., Zheng, S., Thongboonkerd, V., Xu, M., Pierce, W.M., Jr., Klein, J.B., Epstein, P.N., Cardiac mitochondrial damage and biogenesis in a chronic model of type 1 diabetes, *American journal of physiology* **287** (2004) E896-905.

[274] Deniaud, A., Sharaf el dein, O., Maillier, E., Poncet, D., Kroemer, G., Lemaire, C., Brenner, C., Endoplasmic reticulum stress induces calcium-dependent permeability transition, mitochondrial outer membrane permeabilization and apoptosis, *Oncogene* **27** (2008) 285-299.

[275] Rusnak, F., Mertz, P., Calcineurin: form and function, *Physiol Rev* **80** (2000) 1483-1521.

[276] Cribbs, J.T., Strack, S., Reversible phosphorylation of Drp1 by cyclic AMP-dependent protein kinase and calcineurin regulates mitochondrial fission and cell death, *EMBO Rep* **8** (2007) 939-944.

[277] Karaskov, E., Scott, C., Zhang, L., Teodoro, T., Ravazzola, M., Volchuk, A., Chronic palmitate but not oleate exposure induces endoplasmic reticulum stress, which may contribute to INS-1 pancreatic beta-cell apoptosis, *Endocrinology* **147** (2006) 3398-3407.

[278] Wislet-Gendebien, S., Hans, G., Leprince, P., Rigo, J.M., Moonen, G., Rogister, B., Plasticity of cultured mesenchymal stem cells: switch from nestin-positive to excitable neuron-like phenotype, *Stem Cells* **23** (2005) 392-402.

[279] Lu, P., Yang, H., Jones, L.L., Filbin, M.T., Tuszynski, M.H., Combinatorial therapy with neurotrophins and cAMP promotes axonal regeneration beyond sites of spinal cord injury, *J Neurosci* **24** (2004) 6402-6409.

[280] Friedenstein, A.J., Latzinik, N.W., Grosheva, A.G., Gorskaya, U.F., Marrow microenvironment transfer by heterotopic transplantation of freshly isolated and cultured cells in porous sponges, *Exp Hematol* **10** (1982) 217-227.

[281] Colter, D.C., Sekiya, I., Prockop, D.J., Identification of a subpopulation of rapidly self-renewing and multipotential adult stem cells in colonies of human marrow stromal cells, *Proc Natl Acad Sci U S A* **98** (2001) 7841-7845.

[282] Tondreau, T., Lagneaux, L., Dejeneffe, M., Massy, M., Mortier, C., Delforge, A., Bron, D., Bone marrow-derived mesenchymal stem cells already express specific neural proteins before any differentiation, *Differentiation* **72** (2004) 319-326.

[283] Abeliovich, A., Hammond, R., Midbrain dopamine neuron differentiation: factors and fates, *Dev Biol* **304** (2007) 447-454.

[284] Mehrotra, S., Hunley, S.C., Pawelec, K.M., Zhang, L., Lee, I., Baek, S., Chan, C., Cell adhesive behavior on thin polyelectrolyte multilayers: cells attempt to achieve homeostasis of its adhesion energy, *Langmuir* **26** (2010) 12794-12802.

[285] Singh, A.M., Hamazaki, T., Hankowski, K.E., Terada, N., A heterogeneous expression pattern for Nanog in embryonic stem cells, *Stem cells (Dayton, Ohio)* **25** (2007) 2534-2542.

[286] Toyooka, Y., Shimosato, D., Murakami, K., Takahashi, K., Niwa, H., Identification and characterization of subpopulations in undifferentiated ES cell culture, *Development (Cambridge, England)* **135** (2008) 909-918.

[287] Singh, A.M., Terada, N., Bypassing heterogeneity: the road to embryonic stem cell-derived cardiomyocyte specification, *Trends in cardiovascular medicine* **17** (2007) 96-101.

[288] Masaki, H., Ishikawa, T., Takahashi, S., Okumura, M., Sakai, N., Haga, M., Kominami, K., Migita, H., McDonald, F., Shimada, F., Sakurada, K., Heterogeneity of pluripotent marker gene expression in colonies generated in human iPS cell induction culture, *Stem cell research* **1** (2007) 105-115.

[289] Minowa, M.T., Minowa, T., Mouradian, M.M., Activator region analysis of the human D1A dopamine receptor gene, *The Journal of biological chemistry* **268** (1993) 23544-23551.

[290] Yang, Y., Hwang, C.K., Junn, E., Lee, G., Mouradian, M.M., ZIC2 and Sp3 repress Sp1-induced activation of the human D1A dopamine receptor gene, *The Journal of biological chemistry* **275** (2000) 38863-38869.

[291] Tapias, A., Ciudad, C.J., Noe, V., Transcriptional regulation of the 5'-flanking region of the human transcription factor Sp3 gene by NF-1, c-Myb, B-Myb, AP-1 and E2F, *Biochimica et biophysica acta* **1779** (2008) 318-329.

[292] Pillai, R.S., Bhattacharyya, S.N., Filipowicz, W., Repression of protein synthesis by miRNAs: how many mechanisms?, *Trends in cell biology* **17** (2007) 118-126.

[293] Huang, W., Li, M.D., Differential allelic expression of dopamine D1 receptor gene (DRD1) is modulated by microRNA miR-504, *Biological psychiatry* **65** (2009) 702-705.

[294] Bonni, A., Brunet, A., West, A.E., Datta, S.R., Takasu, M.A., Greenberg, M.E., Cell survival promoted by the Ras-MAPK signaling pathway by transcription-dependent and -independent mechanisms, *Science* **286** (1999) 1358-1362.

[295] Tokunou, T., Shibata, R., Kai, H., Ichiki, T., Morisaki, T., Fukuyama, K., Ono, H., Iino, N., Masuda, S., Shimokawa, H., Egashira, K., Imaizumi, T., Takeshita, A., Apoptosis induced by inhibition of cyclic AMP response element-binding protein in vascular smooth muscle cells, *Circulation* **108** (2003) 1246-1252.

[296] Eliseev, R.A., Vanwinkle, B., Rosier, R.N., Gunter, T.E., Diazoxide-mediated preconditioning against apoptosis involves activation of cAMP-response element-binding protein (CREB) and NFkappaB, *J Biol Chem* **279** (2004) 46748-46754.

[297] Oyadomari, S., Mori, M., Roles of CHOP/GADD153 in endoplasmic reticulum stress, *Cell death and differentiation* **11** (2004) 381-389.

[298] Amabile, G., Meissner, A., Induced pluripotent stem cells: current progress and potential for regenerative medicine, *Trends in molecular medicine* **15** (2009) 59-68.

[299] Porter, R.M., Huckle, W.R., Goldstein, A.S., Effect of dexamethasone withdrawal on osteoblastic differentiation of bone marrow stromal cells, *J Cell Biochem* **90** (2003) 13-22.

[300] Pochampally, R., Colony forming unit assays for MSCs, *Methods in molecular biology (Clifton, N.J* **449** (2008) 83-91.